Technische Universität Braunschweig

pvz Zentrum für Pharmaverfahrenstechnik

3rd International Symposium on Pharmaceutical Engineering Research

SPhERe

PROCEEDINGS

CONFERENCE DATE
25 – 27 September 2019

TU Braunschweig • Center of Pharmaceutical Engineering

Welcome Note

On behalf of the Center of Pharmaceutical Engineering of Technische Universität Braunschweig and the Scientific Committee it is my great pleasure to welcome you to the 3rd International Symposium on Pharmaceutical Engineering Research – SPhERe. The conference is held from September 25 – 27, 2019 in Braunschweig, Germany.

The Center of Pharmaceutical Engineering (PVZ) has been established in 2017 as an interdisciplinary research center at the Technische Universität Braunschweig offering excellent working and research conditions for approx. 100 scientists from pharmacy, process engineering, and microtechnology. Altogether scientists of over 20 different research groups of TU Braunschweig, Leibniz University of Hannover and TU Clausthal conduct joint research programmes at PVZ.

Working together in mixed, interdisciplinary teams under a common roof provides a unique environment to develop, test and apply new methods and technologies for pharmaceutical production. These beneficial surroundings emphasize our vision on cost-efficient production of medicinal products and customized drug supply.

SPhERe 2019 is our third conference on Pharmaceutical Engineering Research. SPhERe addresses major topics of innovative production methods and processes to develop low-cost, effective and customized drugs. Bringing together pharmacists, process engineers, production engineers as well as microtechnologists from academia and industry facilitates discussions and the exchange of ideas between representatives of different research disciplines and strengthens the community of pharmaceutical engineering.

The symposium features renowned speakers who share, discuss, and dissect significant new developments and scientific advancements with relevance to the future of pharmaceutical engineering and related fields.

Our first-time *Hot Topic Session* highlights different aspects of cannabis production for medicinal use. This special session focuses on the current debate and addresses the challenges on the way to safe and effective cannabis products that best serve patients' health and meet the legal requirements.

We very much welcome you to Braunschweig, the Lion City! Enjoy SPhERe 2019 and your stay.

Prof. Dr.-Ing. Stephan Scholl
Conference Chair SPhERe 2019

Notes on Content of SPhERe Conference Proceedings

Conference abstracts authorised for Open Access publication are listed alphabetically according to the surname of the presenting author. The name of the presenting author is underlined in each conference presentation.

INFLUENCE OF GLYCEROL ON THE POLYMORPHIC BEHAVIOR OF SOLID TRIGLYCERIDE NANOPARTICLES STABILIZED WITH POLY(VINYL ALCOHOL)

N. Bauer[1,2], H.Bunjes[1,2]

[1]TU Braunschweig; Institut für Pharmazeutische Technologie; Mendelssohnstraße 1, 38106 Braunschweig;
[2]PVZ - Zentrum für Pharmaverfahrenstechnik; Franz-Liszt-Straße 35A, 38106 Braunschweig;
n.bauer@tu-braunschweig.de; heike.bunjes@tu-braunschweig.de

ABSTRACT

Colloidal dispersions of lipids, e.g. triglycerides, are under intensive investigation as drug delivery systems. Solid triglyceride nanoparticles exist in different polymorphic modifications. The aim of this study was to investigate the effects of the addition of glycerol, which can be used for the isotonization of such dispersions, on the polymorphic behavior of poly(vinyl alcohol)-stabilized tripalmitin nanoparticles. Glycerol was added to the nanoparticle dispersions at different concentrations in the heat.

The dispersions were investigated for their thermal behavior and storage stability with regard to particle size and polymorphic transitions of the triglyceride matrix, using photon correlation spectroscopy, differential scanning calorimetry and X-ray diffraction. The addition of glycerol led to a decreasing crystallization temperature of the nanoparticles and slowed down the polymorphic transition into the stable β-modification.

Keywords: Triglyceride nanodispersions, crystallization, polymorphism.

INTRODUCTION

Lipid nanoparticles are under intensive investigation as drug delivery systems for poorly-water soluble drugs [Bunjes, 2010]. Many of the lipids used for the preparation, for example triglycerides, are polymorphic substances. Triglycerides occur in three different crystal modifications: the metastable α- and β'-modification and the stable β-modification. These modifications differ from each other in their physicochemical properties, which might have an influence on the drug loading capacity [Westesen, 1997].

After crystallization, triglyceride nanoparticles undergo polymorphic transitions from the metastable α- into the stable β-modification, sometimes via the β'-modification. These transitions are monotropic and depend on several factors, like matrix composition as well as the type of emulsifier used, additives or storage conditions.

The aim of this study was to investigate the influence of the additive glycerol, which is often used for isotonization of triglyceride nanodispersions, on the polymorphic behavior of the lipid nanoparticles.

RESEARCH CONCEPT

A dispersion consisting of 10 % tripalmitin (Dynasan 116®, Condea), 10 % PVA (Mowiol® 3-83, Clariant), and bidestilled water in which PVA was dissolved (all concentrations w/w) was prepared by melt homogenization. First, the lipid and the aqueous phase were heated at ~80 °C separately. Both phases were combined and prehomogenized with an ultra-turrax (IKA T25 digital Ultra-Turrax; S25N-10G, Ika-Werke) at 13.000 rpm for 4 min. The predispersion was homogenized in a Microfluidizer M110S instrument (Microfluidics) for 10 cycles at 800 bar and ~80 °C. The hot dispersion was divided into 10 ml fractions which were allowed to cool to 40 °C. In order to set the glycerol content, the fractions were combined with 10 ml of a glycerol-containing solution and incubated at

40 °C for 30 min. The dispersions were cooled to 5 °C for 30 min to crystallize the nanoparticles and subsequently stored at 20 °C. The final dispersions contained 5 % triglyceride, 5 % PVA and 0 %, 1 %, 2 %, 5 %, 10 %, 15 % and 20 % glycerol, respectively.
Particle size was measured by photon correlation spectroscopy (PCS) with a Zetasizer Nano ZS instrument (Malvern) at 25 °C and an angle of 173 °. The dispersions were diluted with purified and particle-free water. The z-average diameter and PDI were given as mean of three measurements of 5 min each after 5 min of equilibration.

Differential scanning calorimetry (DSC) measurements were performed in a DSC 1 Star^e System with a full range sensor (FRS 5) and a sample robot (Mettler Toledo GmbH). About 15 µl of the dispersions were accurately weighed into aluminum crucibles that were cold sealed. The samples were heated to 85 °C with a heating rate of 10 °C/min, held at that temperature for 5 min, cooled to -5 °C (10 °C/min) and heated again to 85 °C (10 °C/min). All measurements were performed against an empty reference crucible and under nitrogen purge. The enthalpies observed were normalized for the weight of the samples.
The melting enthalpies were used to approximate the fraction of particles in the different polymorphic forms. To determine the fraction of particles in the stable β-modification, the enthalpy values of the β-form melting transition were calculated according to [Joseph, 2015]. A small amount of the dispersions was tempered at 37 °C for 96 h to obtain a β-reference dispersion. The complete transition of this sample into the β-polymorph was confirmed with X-ray diffraction.

X-ray measurements were performed with a small- and wide-angle X-ray diffraction setup (SAXSess, Anton Paar), equipped with a copper anode (λ = 1.54 nm). The sample was measured in a quartz capillary sample holder in 25 runs of 30 s each at 20 °C.

RESULTS

All dispersions had a milky white appearance with a z-average diameter of about 80 nm and a narrow particle size distribution with PDI values between 0.10 and 0.12. DSC investigations revealed that all nanoparticles were in the metastable α-polymorph directly after preparation. Almost no differences were observed for the different samples during the first heating step. X-ray diffraction patterns confirmed that all particles were present in the metastable α-polymorph with only marginal differences in the diffractograms for samples with different glycerol content. During cooling in the DSC, the samples displayed a linearly decreasing crystallization temperature with increasing glycerol content (Fig. 1).

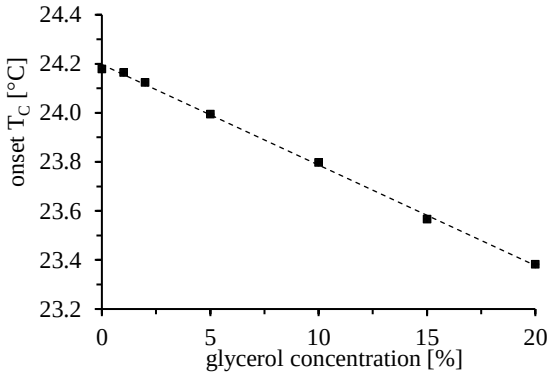

Fig. 1: Onset of crystallization events for dispersions with increasing glycerol concentration.

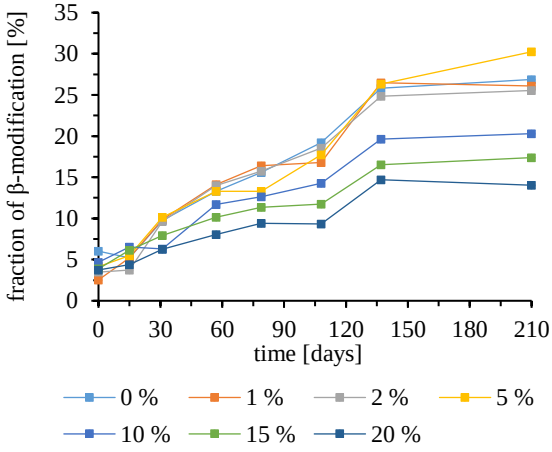

Fig. 2: Fraction of nanoparticles in the β-modification after storage at 20 °C as determined by DSC.

Over a storage time of about 7 months at 20 °C, the transition of nanoparticles into the stable β-modification distinctly slowed down with increasing glycerol content (Fig. 2). After storage, the fraction of particles in the stable β-modification varied from 25 % (0 % glycerol) to 15 % (20 % glycerol).

DISCUSSION

The use of PVA as emulsifier in solid triglyceride nanoparticles led to the formation of the α-modification with a remarkable stability in agreement with previous studies with tristearin nanodispersions [Rosenblatt, 2008; Joseph, 2015]. The addition of glycerol after homogenization did not change the particle size of the dispersions noticeably but influenced the crystallization temperature as well as the polymorphic behavior of the lipid nanoparticles.

The decrease in crystallization temperature may indicate a change of the composition of the nanoparticles as it is, for example, obsorved upon drug loading of triglyceride nanoparticles [Roese, 2017]. As the polarity of glycerol is very high it is unlikely that it interacts with the matrix lipid itself. Instead, it may modify the interaction between PVA and the lipid. The assumed increase in interaction could be an explanation for the higher stability of the metastable α-polymorph in samples containing a high concentration of glycerol.

CONCLUSIONS

In dispersions of PVA-stabilized tripalmitin nanoparticles, the addition of glycerol leads to a decrease in crystallization temperature and slows down the polymorphic transition into the stable β-modification. It is unlikely that glycerol molecules are distributed into the particles due to their high polarity. A possible cause for the observed phenomena could be a specific interaction between glycerol and PVA which affects the composition of the nanoparticles. However, the exact mechanism is still unclear and remains to be elucidated.

ACKNOWLEDGMENT

The Ministry of Science and Culture (MWK) of Lower Saxony, Germany, is acknowledged for financial support within the Smart BioTecs alliance.

REFERENCES

[Bunjes, 2010] Bunjes, H., 2010, Lipid nanoparticles for the delivery of poorly water-soluble drugs, *J. Pharm. Pharmacol*., Vol. 62, pp. 1637-1645.

[Joseph, 2015] Joseph, S., Rappolt, M., Schoenitz, M., Huzhalska, V., Augustin, W., Scholl, S., Bunjes, H., 2015, Stability of the metastable α-polymorph in solid triglyceride drug-carrier nanoparticles, *Langmuir*, Vol. 31, pp. 6663-6674.

[Roese, 2017] Roese, E., Bunjes, H., 2017, Drug release studies from lipid nanoparticles in physiological media by a new DSC method, *J. Control. Release*, Vol. 256, pp. 92-100.

[Rosenblatt, 2008] Rosenblatt, K., Bunjes, H., 2008, Poly(vinyl alcohol) as emulsifier stabilizes solid triglyceride drug carrier nanoparticles in the α-modification, *Mol. Pharm.*, Vol. 6, pp. 105-120.

[Westesen, 1997] Westesen, K., Bunjes, H., Koch, M.H.J., 1997, Physicochemical characterization of lipid nanoparticles and evaluation of their drug loading capacity and sustained release potential, *J. Control. Release*, Vol. 48, pp. 223-236.

SELF-IMMOBILIZING BIOCATALYSTS FOR FLUIDIC REACTION CASCADES

Patrick Bitterwolf[1], Theo Peschke[1], Manfred Maier[1], Sabrina Gallus[1], Teresa Burgahn[1], Esther Mittmann[1], Martin Peng[1], Kersten S. Rabe[1], Christof M. Niemeyer[1]

[1]Institute for Biological Interfaces (IBG 1), Karlsruhe Institute of Technology, Karlsruhe, Germany

ABSTRACT

The industrial implementation of whole-cells and enzymes in flow biocatalysis microreactors is essential for the emergence of a biobased circular economy. Major challenges concern the efficient immobilization of delicate enzymes inside miniaturized reactors without compromising their catalytic activity. We describe the design and application of four different immobilization techniques including self-immobilizing whole-cells and purified enzymes on magnetic microbeads, as well as reactor modules manufactured by 3D printing of bioinks containing thermostable enzymes. To increase the volumetric activity of our microreactors we furthermore developed and applied self-assembling all-enzyme hydrogels with cofactor-regenerating capabilities. The resulting reactor formats have excellent operational stability times of > 14 days and maximum space-time yields of > 450 g product/$L^{-1}day^{-1}$ paving the way for mild and effective immobilization techniques of biocatalysts in microfluidic systems.

Keywords: self-immobilizing, enzymes, continuous flow biocatalysis, cascade reactions, stereoselective

INTRODUCTION

Biocatalysis is currently being transformed by the use of biomimetic fluidic approaches enabling compartmentalized multiple enzyme cascades for the sustainable and continuous production of fine- and value-added chemicals in the industrial "white" biotechnology sector.[1, 2] Apart from optimizing the biocatalysts by protein engineering, effective immobilization techniques are essential to enable precise temporal and spatial reaction control in fluidic microreactors. Thus for the establishment of artificial fluidic cascades new approaches for the immobilization of accessible and active biocatalysts are needed.

RESEARCH CONCEPT

In order to retain the active biocatalysts under continuous flow conditions, we developed different "self-immobilizing" biocatalysts including from whole-cells[3] or pure enzymes[4] in combination with superparamagnetic microparticles as well as reactor modules manufactured by 3D printing of bioinks containing thermostable enzymes.[5] To further increase the volumetric activity of our microreactors, we developed self-assembling and cofactor-regenerating all-enzyme hydrogels, consisting of either an (*R*)- or an (*S*)-enantiospecific ketoreductase and the nicotinamide adenine dinucleotide phosphate regenerating glucose 1-dehydrogenase.[6, 7]

RESULTS & DISCUSSION

For the design of "self-immobilizing" whole-cells we generated bacterial strains that can selectively bind to solid substrates containing an appropriate binding tag,. In an initial work, we employed the cell-surface display of the strepatividin-binding peptide (SBP), the SpyTag/SpyCatcher (ST/SC) system or a HaloTag variant based on the outer membrane protein Lpp-ompA , which led to a spontaneous covalent coupling of magnetic microbeads carrying streptavidin (STV), a ST/SC component or a chlorohexyl (CH) -moiety.[3] At the same time functional content could be expressed in the cytosol of the immobilized cells, as we demonstrated

employing fluorescent proteins or stereoselective ketoreductase enzymes. The latter strains gave high selectivities for specific immobilization onto complementary surfaces and also in the whole-cell stereospecific transformation of a prochiral C_S-symmetric nitrodiketone.

Implementing enzyme cascades into future biocatalytic processes enables the use of compartmentalized microfluidic reactors. However, a major challenge in the establishment of microfluidic enzyme cascades concerns the immobilization of isolated enzymes. To this end we developed "self-immobilizing" enzyme biocatalysts based on (*R*)- and (*S*)-selective ketoreductases in combination with an NADPH regenerating glucose-1-dehydrogenase anchored on magnetic microbeads.[4] The enzymes were tagged with SBP, ST or halo-based oligonucleotide binder (HOB), respectively, and bound to the corresponding streptavidin (STV), SC or chlorohexyl (CH) coated microbeads. The enzyme-modified beads were loaded in four-channel microfluidic chips to create compartments that have the capability for either (*R*)- or (*S*)-selective reduction of the prochiral C_S-symmetrical substrate 5-nitrononane-2,8-dione (NDK). Analysis of the isomeric hydroxyketone and diol products by chiral HPLC was used to quantitatively characterize the performance of reactors configured with different amounts of the enzymes. Long operating times of up to 14 days indicated stable enzyme immobilization and the general robustness of the reactor. Even more important, by fine-tuning of compartment size and loading, the overall product distribution could be controlled to selectively produce a single meso diol with nearly quantitative conversion (>95%) and excellent stereoselectivity (d.r. > 99:1) in a continuous flow process.

In a parallel approach we demonstrate the utility of thermostable enzymes in the generation of biocatalytic agarose-based inks for a simple temperature-controlled 3D printing process.[5] As examples we utilized an esterase and an alcohol dehydrogenase from thermophilic organisms as well as a decarboxylase that was thermostabilized by directed protein evolution. We used the resulting 3D-printed parts for a continuous, two-step sequential biotransformation in a fluidic setup.

To further increase the volumetric activity of such reactors, we have recently developed self-assembling all-enzyme hydrogels with cofactor-regenerating capabilities, consisting 100% of either an (*R*)- or an (*S*)-enantiospecific ketoreductase combined with the NADPH-regenerating glucose 1-dehydrogenase.[6] Mounted in microfluidic reactors, the gels show excellent stereoselectivity (> 99% ee.) with near quantitative conversion (> 90%) in the reduction of different prochiral ketones along with high robustness under process and storage conditions. The gels constitute a compartment in which reaction intermediates are retained, thereby enabling extraordinary high total turnover numbers of the expensive cofactor NADP(H). Coupling of such reactor modules allows to facilitate multi step reaction cascades.

CONCLUSIONS

The field of biocatalysis demands practical and effective methods for the immobilization of the corresponding biocatalysts. We developed four different approaches including whole-cells, purified enzymes as well as enzymes bound or entrapped into carrier materials like magnetic microbeads or agarose, respectively.

Maximizing space–time yields (STY) of biocatalytic flow processes is essential for the establishment of a circular biobased economy. We present a comparative study in which different biocatalytic flow reactor concepts were tested with the same enzyme, the (*R*)-selective alcohol dehydrogenase from *Lactobacillus brevis* (LbADH).[7] To enable cross-platform comparison, STY values were determined for the various reactor modules. While mono- and multilayer coatings of the reactor surface led to STY < 10, higher productivity was achieved with packed-bed reactors (STY ≈ 100) and the densely packed hydrogels (STY > 450). The latter modules could be operated for prolonged times (>6 days). Given that our approach is not limited to specific enzymes, we anticipate that compartmentalized microfluidic reaction modules equipped with self-immobilizing biocatalysts would be of great utility for numerous biocatalytic and even chemo-enzymatic cascade reactions under continuous flow conditions.

ACKNOWLEDGMENT

This work was supported by the Helmholtz program BioInterfaces in Technology and Medicine and Deutsche Forschungsgemeinschaft. We thank Alessandro Angelin, Maximillian Grösche, Jens Bauer, Anke Dech, Ruben Garrecht, Marc Skoupi, Ann-Kathrin Schneider, Cornelia Ziegler for experimental help and Ishtiaq Ahmed for the synthesis of the nitrodiketone. SG & PB are grateful for a Kekulé fellowship by Fonds der Chemischen Industrie.

REFERENCES

[1] R. A. Sheldon, J. M. Woodley, Role of Biocatalysis in Sustainable Chemistry, Chem. Rev. 2017.

[2] K. S. Rabe, J. Muller, M. Skoupi, C. M. Niemeyer, Cascades in Compartments: En Route to Machine-Assisted Biotechnology, Angew. Chem. Int. Edit. 2017.

[3] T. Peschke, K. S. Rabe, C. M. Niemeyer, Orthogonal Surface Tags for Whole-Cell Biocatalysis, Angew. Chem. Int. Edit. 2017.

[4] T. Peschke, M. Skoupi, T. Burgahn, S. Gallus, I. Ahmed, K. S. Rabe, C. M. Niemeyer, Self-Immobilizing Fusion Enzymes for Compartmentalized Biocatalysis, ACS Catal. 2017.

[5] M. Maier, C. P. Radtke, J. Hubbuch, C. M. Niemeyer, K. S. Rabe, On-Demand Production of Flow-Reactor Cartridges by 3D Printing of Thermostable Enzymes, Angew. Chem. Int. Edit. 2018.

[6] T. Peschke, P. Bitterwolf, S. Gallus, Y. Hu, C. Oelschlaeger, N. Willenbacher, K. S. Rabe, C. M. Niemeyer, Self-Assembling All-Enzyme Hydrogels for Flow Biocatalysis, Angew. Chem. Int. Edit. 2018.

[7] T. Peschke, P. Bitterwolf, S. Hansen, J. Gasmi, K. S. Rabe, C. M. Niemeyer, Self-Immobilizing Biocatalysts Maximize Space-Time Yields in Flow Reactors, Catalysts 2019.

ELECTROSPINNING, PHOTOCROSSLINKING OF ARYLAZIDE CHITOSAN NANOFIBERS AND APPLICATION AS BIOCATALYST SUPPORT MATRIX

Henrik-Alexander Christ*, Henning Menzel*.

*Technische Universität Braunschweig, Institut für Technische Chemie, Hagenring 30, 38106 Braunschweig, Deutschland, h.christ@tu-braunschweig.de

ABSTRACT

A process yielding water stable chitosan nanofiber mats is described and their significance in the field of biocatalyst immobilization is proven. Electrospinning was adapted to produce nanofibers from chitosan derivatives bearing photoreactive arylazide groups. These photoreactive groups of chitosan were then crosslinked by irradiation with UV-light. This stabilizes the fiber morphology even upon incubation in water and provides an alternative to crosslinking with harmful chemicals. Applicability of the fiber mats as enzyme immobilization matrix was demonstrated, using β-*D*-galactosidase as model enzyme. Although an initial leaching of enzyme was observed, after 40 days of incubation a significant portion of active enzyme is still present on the fibers. Thus, the fiber mats are suitable matrices to support enzymes and can revolutionize future enzymatic production processes of e.g. active pharmaceutical ingredients.

Keywords: arylazide chitosan, electrospun nanofibers, photochemical crosslinking, enzyme immobilization.

INTRODUCTION

To this day, applications of enzymes in the production of active pharmaceutical ingredients (API) are limited by losses in enzyme activity or difficulties in reusability and handling. Enzyme immobilization onto a structural and porous support may help to overcome these obstacles (Sheldon, 2007). Chitosan nanofibers are promising candidates as immobilization matrices for biocatalysts because of their high surface-to-volume ratio in combination with an ease of handling. This may lead to the development of a new class of biocatalyst-supports (Misson et al., 2015). As chitosan is still one of the most promising polysaccharides derived from nature, its electrospinning process has been studied intensively for the last two decades (Ding et al., 2014). An important improvement came from (Zhang et al., 2008) by blending of chitosan with poly(ethylene oxide) (PEO) of a very high molecular weight. This enabled production of nanofibers. However, most of the previously spun nanofibers tend to lose structure completely upon contact with water. Chemical modification of chitosan with photo-reactive crosslinking groups before electrospinning can help to solve this problem (Hadler et al., 2017). In this way an UV-light induced crosslinking is possible and a very good alternative to common crosslinking agents such as Genipin or Glutaraldehyde. The crosslinked hydrophilic, but water stable nanofibers could be used for immobilization of enzymatic catalysts to improve production processes for various API's.

RESEARCH CONCEPT

All chemicals were obtained from Sigma Aldrich unless otherwise stated. Poly(ethylene oxide) (PEO, M_v = 5.000 kDa) was used as obtained. Chitosan (CsH, M_w = 190 – 310 kDa, 15 – 25 % degree of acetylation) was purified, using a method of (Gan and Wang, 2007). Arylazide chitosan (CsH-Az) was synthesized by 4-(4,6-dimethoxy-1,3,5-triazin-2-yl)-4-methylmorpholi nium chloride (DMT-MM) mediated aqueous amide coupling of sodium-4-azidobenzoate and amine functions of chitosan by a method of (Hadler et al., 2017). Spinning solutions were prepared using blends of CsH-Az and PEO in a solvent system consisting of 3 % acetic acid in deionized water and methanol (10:1 v/v) as a co-solvent. The blends had a PEO content of 5 % (w/w) and were prepared with an overall polymer concentration of 4 % (w/v). All fibers were spun on a custom-made electrospinning device (see Figure 1) by extruding spinning solution through a flat cannula (I, B/BRAUN, inner diameter = 0.2 mm) to a plastic syringe (II, B/BRAUN, 5 mL). A syringe pump (III, HLL LANDGRAF LABORSYSTEME, *LA 30*) was used to maintain a constant flow rate. A fiber-forming jet was achieved by applying a high electric potential (IV, HEINZIGER, *LNC-30000-2 pos* high voltage generator) between the spinneret and the collector. All fibers were collected on a rotating spherical alumina cylinder (V, IKA LABORTECHNIK, *RW20 DZM* stirrer, 1000 rpm) with a height of 5 cm and a radius of 3 cm. The collector was covered in a strip of plastic mesh

(WINDHAGER, *Fiberglas Anthrazit* (fly-screen) which improved the handling of the fibers. The distance between spinneret and collector, the electrical potential and the flow rate of spinning solution were varied in order to achieve a stable production process. Produced fibers were analyzed by IR-spectroscopy and SEM images.

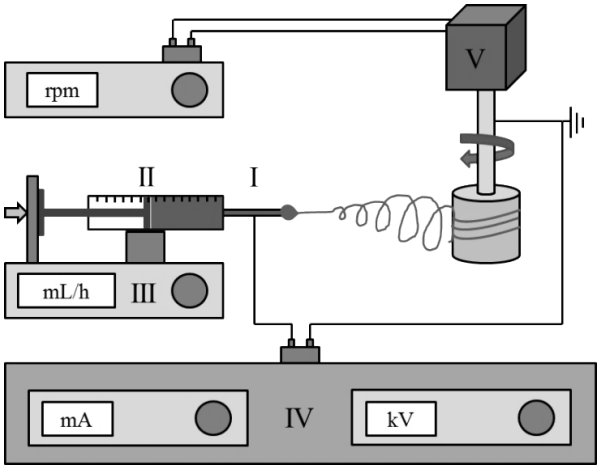

Figure 1: Schematic setup of custom-made electrospinning device (I = cannula, II = plastic syringe, III = syringe pump, IV = high voltage generator, V = collector).

Samples of the fiber meshes were photo-crosslinked by subjecting them to light of a mercury vapor UV-lamp (ORIEL, 100 mW/cm^2) for a given time. The lamp was equipped with a water IR-filter and a glass UV-filter (ν_{max} = 330 ± 70 nm). Completion of crosslinking was evaluated by recording IR-spectra of samples. Water stability tests were carried out by incubation of samples in deionized water for a given time and subsequent drying with a N_2-stream. Scanning electron microscopy (SEM) images were used to evaluate water stability of fibers. Samples with 100 mm^2 of photocrosslinked fiber mesh were used for immobilization of β-*D*-galactosidase (β-Gal) from *A. oryzae* as model enzyme via ionic interaction. Three samples per experiment were washed with citrate-phosphate-buffer (CP) at pH = 4.5 for 24 h, subsequently incubated with 0.506 units of β-*D*-galactosidase in CP at r.t. for 24 h and stored in Millipore water in fridge until further use. Remaining activity of immobilized enzymes was determined via O-Nitrophenyl-β-D-galactopyranoside (ONPG) at 0, 20 and 40 d. This was done by incubation of samples in ONPG (5 mM, 1 mL, 30 °C, 700 rpm inversion) and subsequent stopping of reaction after 10 min with borate buffer. UV-VIS-spectroscopy at 420 nm was used to determine the amount of cleaved ONPG and calculate the remaining activity of immobilized β-Gal relative to initial activity in immobilization solution before contact with samples.

RESULTS AND DISCUSSION

By reproducing electrospinning experiments from (Zhang et al., 2008) with our custom-made electrospining setup, we could obtain chitosan (CsH) nanofibers, that showed poor stability in water incubation tests. A complete loss of nanofiber morphology was observed after contact with water. This phenomenon has been described before and highlights the need of a crosslinking method to increase the water stability of the fibers. Previous approaches consist of a treatment of fibers with a crosslinking agent such as Genipin (Li et al., 2015), Glutaraldehyde (Schiffman and Schauer, 2007) or Tripolyphosphate (Sarkar et al., 2013). All of these methods have the drawback that fibers have to be treated with a chemical and can potentially be damaged during this process. A more elegant method is crosslinking of chitosan fibers by irradiation with UV-light. In order to enhance CsH with photocrosslinking functionalities, arylazide groups were introduced by a DMT-MM mediated aqueous amide coupling of sodium 4-azidobenzoate and amine functions of CsH. The resulting structure of chitosan-azide (CsH-Az) is shown in Figure 2. For this study we produced CsH-Az with a degree of modification (DM) in a range of 1 – 10 %. DM is defined as the fraction of modified repetition units over the sum of all repetition units in CsH (see Figure 2).

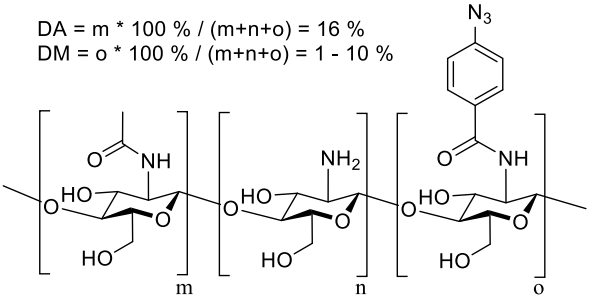

Figure 2: Schematic structure of CsH-Az: (m = acetylated glucosamine, n = glucosamine, o = arylazide modified repetition unit).

Modification of glucosamine repetition units with arylazide groups changes the properties of chitosan in a spinning solution drastically. Therefore, established parameters of the spinning process have to be adapted. Significant improvements of the spinning process and resulting fibers were achieved by substitution of DMSO

with Methanol (MeOH) as a co-solvent. This led to a decrease of viscosity of the spinning solution and by this, to a much more stable spinning process. We were able spin solutions of CsH-Az/PEO-blends (w/w = 95/5, DM = 0 % / 1.9 % / 3.8 % / 9.0 %) using the improved AcOH/MeOH-solvent system in a stable process (spinning time over 3 h, rotating drum collector at 1000 rpm, voltage of 14 kV, cannula-collector-distance of 25 cm, solution flow rate of 1 mL/h). Best results were achieved for the CsH-Az-6/PEO-blend (DM of 3.8 %). The resulting fibers, in contrast to other CsH-Az/PEO-blends, had nearly no bead-like defects and were well oriented in a mostly parallel and straight manner. The average diameter was 640 +/- 290 nm. A SEM image of this morphology is shown in Figure 4. Fibers of CsH-Az/PEO-blends with a DM of 1.9 % or 9.0 % respectively had bead-like defects and the complementary spinning process was less stable than for a DM of 3.8 % (CsH-Az-6). This clearly indicates that a change in DM of CsH-Az requires an adaption of the specific process conditions as it changes the behavior of the polymer chains in the spinning solution. After spinning, CsH-Az/PEO-fibers can be crosslinked via irradiation with UV-light. This was done with a Hg-vapor UV-lamp at a light intensity of 100 mW/cm^2. We were able to crosslink samples within a time spectrum of 30 – 180 s as established by ATR-IR-spectra, SEM-images and water stability tests.

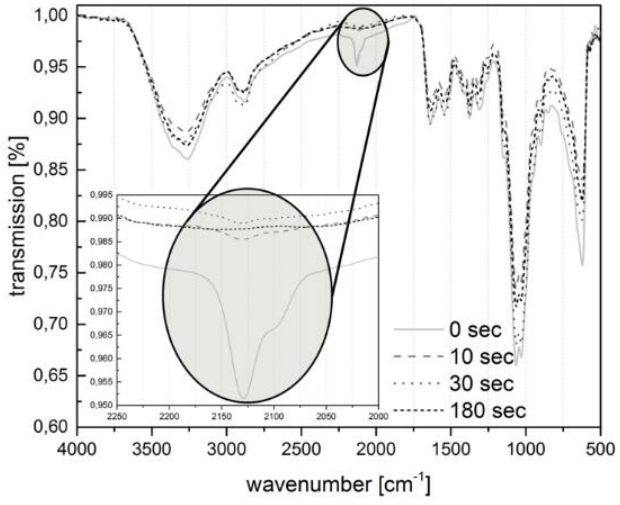

Figure 3: Decreasing intensity of azide signal (magnified section) in ATR-IR-spectra of CsH-Az/PEO fiber meshes at varying UV-light exposure times during photo-crosslinking process.

ATR-IR-spectra of fiber samples before and after irradiation show decrease of a signal at 2130 cm^{-1} (see Figure 3). This signal corresponds to azide groups of CsH-Az. Further evidence for a successful crosslinking process was provided by incubation experiments in water. CsH as well as CsH-Az is hydrophilic and can be dissolved in slightly acidic water conditions (pH 4-5). However, crosslinked chitosan forms a hydrogel in water. The crosslinked CsH-Az/PEO fibers behave similarly: Samples examined at macroscopic level during and after incubation showed complete water stability for over 24 h. The dry white fiber mesh becomes semi-transparent during incubation and reverses back during drying. Examination of the incubation process by light microscopy reveals a significant increase in fiber diameter during incubation. SEM-images of the fiber meshes after subsequent drying showed partial fusing of fibers but retention of general fiber mesh structure. A typical morphology of such partially fused fibers is shown in Figure 4.

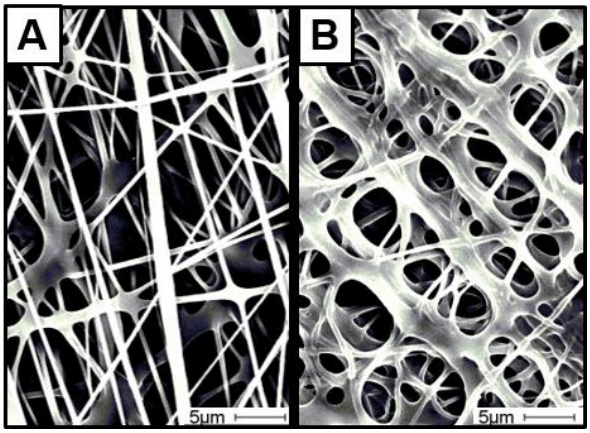

Figure 4: SEM image of fibers from CsH-Az-6/PEO-blend spun from AcOH/MeOH solvent system before (A) and after (B) crosslinking and incubation in deionized water.

Incubated fiber samples (Figure 4) appear, compared to non-incubated fibers, washed-out and fused together. A lot of pores have formed in between fusing fibers. Some fibers seem to stick together and form fiber bundles. This morphology did not change with irradiation time or incubation time. It seems that morphology changes happen during first contact with an incubation solution. To demonstrate a potential application of CsH-Az nanofibers, β-Gal was immobilized via ionic interaction and adsorption on fiber surfaces as proof of concept. As analysis of exact enzyme loading on fibers is not trivial, relative activity standardized with activity of free enzyme in CP buffer at pH = 4.5 was used. Initially directly after incubation, we found a high relative activity of 75 % in case of CsH-Az-6 and 80 % for CsH-Az-9 (Figure 5).

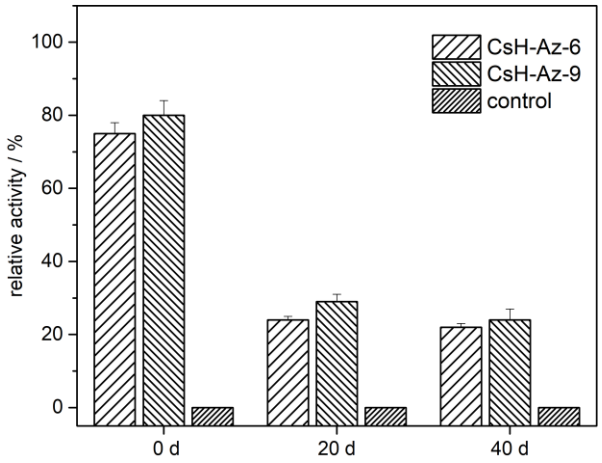

Figure 5: Remaining relative catalytic ability of β-Gal immobilized on photocrosslinked nanofiber samples after 0, 20 and 40 d of incubation in Millipore water.

Relative immobilized enzyme activity was reduced to under 30 % after storage of 20 to 40 days. These results suggest a good initial loading capacity of CsH-Az nanofibers but also a significant loss of activity over time. This could be attributed to leaching of enzymes or loss of active structure. Nevertheless, it can be concluded that at least 22 % of active enzymes were present on CsH-Az nanofibers after 40 days.

CONCLUSIONS

Adapting an electrospinning process for chitosan derivatives bearing photoreactive arylazide groups was accomplished using Methanol as co-solvent. Photoreactive arylazide groups from CsH-Az were used to induce crosslinking of polymer networks via irradiation with UV-light. Fully crosslinked fibers were shown to form a hydrogel-like structure when incubated in water or acidic buffer systems but retain fibrous morphology. Applicability as promising enzyme immobilization matrix was proven with β-*D*-galactosidase as model enzyme. After initial leaching during the first days, remaining catalytic abilities of immobilized enzymes could be retained over 40 days of incubation. These findings only hint the full potential of nanofibers from photoreactive chitosan, which is still subject of our ongoing research.

ACKNOWLEDGMENT

We gratefully thank working group of Prof. Jördening from TU Braunschweig for help and support with electrospinning and enzymatic assays.

REFERENCES

Ding, F., Deng, H., Du, Y., Shi, X., Wang, Q., 2014. Emerging chitin and chitosan nanofibrous materials for biomedical applications. *Nanoscale* 6 (16), 9477–9493.

Gan, Q., Wang, T., 2007. Chitosan nanoparticle as protein delivery carrier--systematic examination of fabrication conditions for efficient loading and release. *Colloids Surf., B* 59 (1), 24–34.

Hadler, C., Wissel, K., Brandes, G., Dempwolf, W., Reuter, G., Lenarz, T., Menzel, H., 2017. Photochemical coating of Kapton(R) with hydrophilic polymers for the improvement of neural implants. *Mater. Sci. Eng., C* 75, 286–296.

Li, Q., Wang, X., Lou, X., Yuan, H., Tu, H., Li, B., Zhang, Y., 2015. Genipin-crosslinked electrospun chitosan nanofibers: Determination of crosslinking conditions and evaluation of cytocompatibility. *Carbohydr. Polym.* 130, 166–174.

Misson, M., Zhang, H., Jin, B., 2015. Nanobiocatalyst advancements and bioprocessing applications. *J. R. Soc., Interface* 12 (102), 20140891.

Sarkar, S.D., Farrugia, B.L., Dargaville, T.R., Dhara, S., 2013. Physico-chemical/biological properties of tripolyphosphate cross-linked chitosan based nanofibers. *Mater. Sci. Eng.*, C 33 (3), 1446–1454.

Schiffman, J.D., Schauer, C.L., 2007. Cross-linking chitosan nanofibers. *Biomacromolecules* 8 (2), 594–601.

Sheldon, R.A., 2007. Enzyme Immobilization: The Quest for Optimum Performance. *Adv. Synth. Catal.* 349 (8-9), 1289–1307.

Zhang, Y.Z., Su, B., Ramakrishna, S., Lim, C.T., 2008. Chitosan nanofibers from an easily electrospinnable UHMWPEO-doped chitosan solution system. *Biomacromolecules* 9 (1), 136–141.

PARAMETERS INFLUENCING OSTWALD RIPENING OF NANOEMULSIONS PRODUCED BY PREMIX MEMBRANE EMULSIFICATION

Lara El-Hawari[1,2], Heike Bunjes[1,2]

[1]TU Braunschweig; Institut für Pharmazeutische Technologie; Mendelssohnstraße 1, 38106 Braunschweig;
[2]PVZ - Zentrum für Pharmaverfahrenstechnik; Franz-Liszt-Straße 35A, 38106 Braunschweig;
l.el-hawari@tu-braunschweig.de, heike.bunjes@tu-braunschweig.de

ABSTRACT

Premix membrane emulsification is a promising method to produce colloidal lipid carrier systems, e.g. triglyceride nanoemulsions, with small particle sizes and narrow particle size distributions for intravenous administration. The stability of these systems can be affected by Ostwald ripening. The process of Ostwald ripening in emulsions of medium chain triglycerides stabilized with sucrose laurate was monitored by particle size measurements with photon correlation spectroscopy. Two different preparation methods were used and the concentration of free emulsifier measured to learn more about the influencing parameters.
The concentration of free sucrose laurate turned out to be the main influencing parameter and should be about zero to minimize Ostwald ripening in the emulsions.

Keywords: Premix membrane emulsification, Ostwald ripening, triglyceride emulsion

INTRODUCTION

Premix membrane emulsification is a promising method to produce colloidal lipid carrier systems for intravenous administration with small particle sizes and narrow particle size distributions. In this procedure, a coarse pre-emulsion is repeatedly extruded through a nanoporous membrane leading to droplets in the nanometer range.

In a previous study triglyceride oil nanoemulsions with particle sizes below 100 nm could be prepared with aluminium oxide membranes (Anodisc™ 0.02 µm) and sucrose laurate (SL) as a nonionic emulsifier. The long-term stability of these nanoemulsions depended on the concentration of the emulsifier. The more sucrose laurate was used in the formulations the faster was the particle size growth induced by Ostwald ripening [El-Hawari, 2018]. Ariyaprakai and Dungan could also observe a negative effect of an excess of emulsifier [Ariyaprakai, 2010].

Ostwald ripening is the process where large droplets grow at the expense of smaller ones due to the higher solubility of the smaller particles. Simultaneously the particle size distribution gets narrower which is a major characteristic of Ostwald ripening.

The aim of this study was to investigate the relationship between the emulsifier concentration, the concentration of free emulsifier (emulsifier in continuous phase, not bound to any interfaces) and Ostwald ripening to be able to forecast the composition of nanoemulsions that have a good stability and to learn more about the parameters influencing Ostwald ripening in the emulsions.

RESEARCH CONCEPT

The nanoemulsions were produced by premix membrane emulsification with an instrumented small scale extruder [Gehrmann, 2016]. The extruder consists of a high pressure syringe pump connected to a membrane holder and a computer to control the flow rate. A coarse premix emulsion dispersed with an Ultra-Turrax (IKA T25 digital, S25N-10G, Ika-Werke) at 10.000 rpm for 2 min was processed 27 times through Anodisc™ membranes (0.02 µm pore size, d= 41 mm) with a constant flow rate of 0.4 ml/s. The

emulsions consisted of 10 % Miglyol® 812 (MCT) and various concentrations of sucrose laurate (1.5-10 %) in double distilled water. Sodium azide (0.05 %) was added as a preservative.

Two different production methods were used, termed "general method" and "addition method" in the following. In the general method the whole emulsifier was added to the aqueous phase at the beginning of the production. Using the addition method only 1.5 % emulsifier was added in the beginning and the difference to the defined concentration was added to the already prepared nanoemulsion under stirring for 2 hours. The emulsions were stored for 18 weeks under nitrogen at 20°C and the particle size and particle size distribution was measured at particular times.

The particle size (Z-Average diameter) and particle size distribution width (expressed as polydispersity index (PDI)) were determined using photon correlation spectroscopy (PCS) (Zetasizer Nano ZS, Malvern Instruments) at 25 °C and a backscattering angle of 173°. The emulsions were diluted to an attenuator of 6-8 and measured three times for 5 min with 5 min equilibration time. The mean number average diameter was determined applying the Mie theory (n_{lipid}= 1.45, n_{imag}= 0.01, n_{contin}= 1.33) and used for the calculation of the Ostwald ripening rates. The Ostwald ripening rate ω was calculated from the cube of the number average droplet radius as a function of time [Kabalnov, 1994].

The concentration of free emulsifier in the continuous phase of the nanoemulsions was measured after filtering 5 ml of the respective nanoemulsion through Vivaspin® 6 tubes (Sartorius, MWCO 300 kDa) with the aid of centrifugation for about 20 min (500xg, 22°C). Receiving a small volume of the continuous phase, without lipid droplets, the refraction index (Abbemat WR, Anton Paar) was measured and the SL concentration determined with the aid of a calibration curve.

The critical micelle concentration (CMC) was measured by the surface tension method with a Wilhelmy plate at 25°C (Tensiometer K100, KRÜSS GmbH). A solution of SL was stepwisely added to double distilled water and the values were plotted on a logarithmic scale against the surfactant concentration. The CMC was determined at the intersection of the linear fits.

RESULTS

With the general method all emulsions were successfully prepared but with different initial particle sizes, all smaller than 100 nm depending on the SL concentration. The initial particle size got smaller with higher SL concentrations using the same production parameters. The reason is that more emulsifier has a better stabilisation effect during the emulsification process and therefore smaller particles can be generated. Upon storage the droplet sizes increased up to a maximum of 135 nm (depending on SL concentration). The Ostwald ripening rates were linearly related to the SL concentration (Fig. 1) and in good agreement with results from earlier studies [El-Hawari, 2018]. When using the general method for emulsion preparation the Ostwald ripening rates are affected by the different initial particle size which is likely to have an influence on the results.

To tackle this problem an alternative processing method, the addition method, was tested. The particle size of the nanoemulsions was measured before and shortly after the second addition of SL. No significant alterations of the droplet sizes could be detected under these circumstances. After longer storage times a similar particle size growth as in emulsions prepared by the general method as well as decreasing PDI values could be measured. The Ostwald ripening rates were calculated and compared with that for emulsions prepared with the general method (Fig. 1). A linear relationship could also be determined for the addition method.

To obtain more detailed information about the parameters influencing Ostwald ripening the concentration of free SL was determined. The Ostwald ripening rate had a linear relationship to the concentration of free SL. The more free SL was available in the continuous phase the faster was the Ostwald ripening (Fig. 2). With regard to the overall as well as to the free SL concentration the slope of the linear fit for emulsions prepared with the two different methods are not completely equal.

The CMC (mean of three independent measurements) of SL was determined as 0.015%.

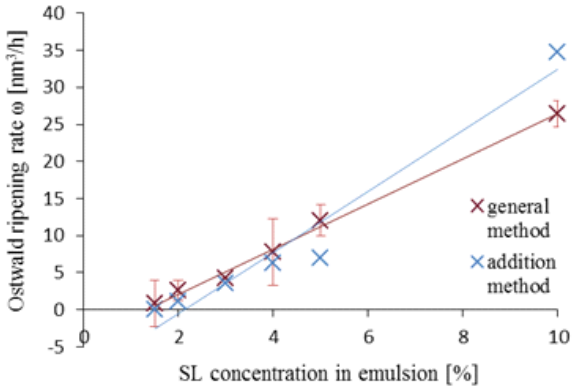

Fig. 1: Comparison of Ostwald ripening rates calculated for emulsions obtained by the general and the addition method at different SL concentrations.

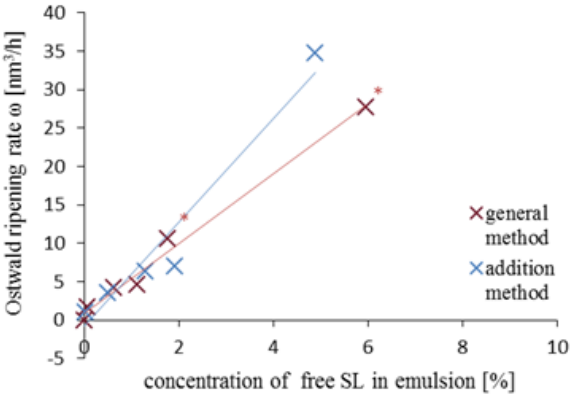

Fig. 2: Linear correlation between Ostwald ripening rates and the concentration of free SL for emulsions prepared with the general and the addition method. * values are affected by the presence of lipid droplets in the filtrate.

DISCUSSION

Ostwald ripening similarly occurred in the emulsions prepared by the two methods but somewhat unexpectedly the correlation between Ostwald ripening rate and SL concentration was not the same. The smaller slope observed for emulsions prepared by the general method may be a consequence of the different initial particle sizes of the emulsions prepared with different emulsifier contents.

Nevertheless, the higher the concentration of free SL the higher were the Ostwald ripening rates independent of the method. In these experiments the concentration of free SL seems to be the major factor determining the rate of Ostwald ripening. Different mechanisms have

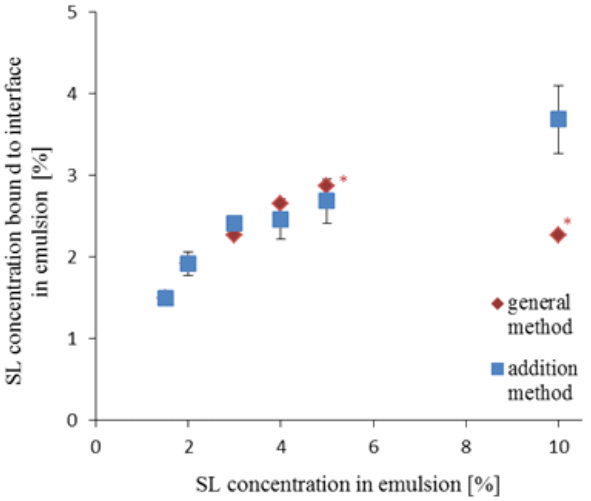

Fig. 3: Correlation between the amount of SL bound to the interfaces and the overall SL concentration for emulsions prepared by the general and the addition method. * values are affected by the presence of lipid droplets in the filtrate.

been discussed how the transport of lipid through the continuous phase may be going on. One possibility is the transport in micelles [Binks, 1999, Weiss, 2000]. The results obtained for the concentration of free SL were, except for emulsions containing 1.5 % SL, above the critical micelle concentration (CMC= 0.015 %). Transport in micelles thus seems to be a likely possibility but further investigation is necessary to prove the underlying mechanisms.

It is also an interesting point that the amount of SL bound to the interfaces (calculated from the difference of absolute concentration and free SL concentration) increased with higher SL concentration (Fig. 3). The curve progression leads to the assumption that at higher SL concentrations, a saturation of the interfaces will likely be reached. With regard to the storage stability nanoemulsions with less SL, e.g. 1.5 %, and therefore less SL bound to interfaces, were better stabilized against particle size growth as reflected by a low Ostwald ripening rate (Fig. 1). Higher surface coverage with emulsifier molecules does thus not have a protecting effect against Ostwald ripening of nanoemulsions.

CONCLUSIONS

For the emulsions under investigation here the free concentration of emulsifier is a main influencing parameter for the rate of Ostwald ripening probably by

its effect on micellar transport. In order to achieve long-term stable nanoemulsions the concentration of free SL should be about zero to minimize the Ostwald ripening rate. It seems to be of little importance for the speed of Ostwald ripening whether the emulsifier SL is completely added before processing (general method) or in two parts, before and after emulsification (addition method). The different initial particle sizes resulting from preparation with the general method probably affected the results obtained for the Ostwald ripening behaviour. The addition method can serve as an easy and time-saving method to produce nanoemulsions with the same particle size but different SL concentrations.

ACKNOWLEDGEMENT

The Ministry of Science and Culture (MWK) of Lower Saxony, Germany, is acknowledged for the financial support within the Smart BioTecs alliance.

REFERENCES

[Ariyaprakai, 2010] Ariyaprakai, S., Dungan, S.R., 2010, Influence of surfactant structure on the contribution of micelles to Ostwald ripening in oil-in-water emulsions, *J. Colloid Interface Sci.*, Vol. 343, pp. 102-108.

[Binks, 1999] Binks, B.P., Clint, J.H., Fletcher, P.D.I., Rippon, S., Lubetkin, S.D., Mulqueen, P.J., 1999, Kinetics of swelling of oil-in-water emulsions stabilized by different surfactants, *Langmuir*, Vol. 15, pp. 4495-4501.

[El-Hawari, 2018] El-Hawari, L., Jäschke, C., Bunjes, H., Premix membrane emulsification: Is it possible to obtain nanoemulsions with particle sizes below 100 nm?, October 2th to 5th 2018, *Annual Meeting of DPHG 2018*, Hamburg.

[Gehrmann, 2016] Gehrmann, S., Bunjes, H., 2016, Instrumented small scale extruder to investigate the influence of process parameters during premix membrane emulsification, *Chem. Eng. J*, Vol. 284, pp. 716-723.

[Kabalnov, 1994] Kabalnov, A.S., 1994, Can micelles mediate a mass transfer between oil droplets?, *Langmuir*, Vol. 10, pp. 680-684.

[Weiss, 2000] Weiss, J., Canceliere, C., McClements, D.J., 2000, Mass transport phenomena in oil-in-water emulsions containing surfactant micelles: Ostwald ripening, *Langmuir*, Vol. 16, pp. 6833-6838.

FORMULATION OF CANNABIDIOL IN LIPID CARRIERS

Nadine Francke[1], Linda Grüne[1], Heike Bunjes[1,2]

[1]TU Braunschweig; Institut für Pharmazeutische Technologie; Mendelssohnstraße 1, 38106 Braunschweig;
[2]PVZ - Zentrum für Pharmaverfahrenstechnik; Franz-Liszt-Straße 35A, 38106 Braunschweig;
nadine.francke@tu-braunschweig.de

ABSTRACT

Substances extracted from C*annabis* varieties are of increasing interest, especially cannabidiol as a non-psychoactive drug with various pharmacological effects. Formulation of cannabidiol is, however, challenging due to its low water solubility. In this study, different types of lipid carriers were investigated as formulation options for cannabidiol to enable parenteral or oral application.

The study included self-dispersing lipid formulations, nanoemulsions and liposomes. With regard to parenteral application, a higher load of cannabidiol was obtained in nanoemulsions than in liposomes. Lipid nanoemulsions are thus a very promising formulation option for parenteral formulations with a high drug load. Also in formulations intended for oral use a notably higher amount of cannabidiol could be incorporated in oil-containing self-dispersing formulations than in liposomes.

Keywords: Cannabidiol, lipid carriers, lipid-based formulations

INTRODUCTION

Cannabidiol (CBD) is a natural compound isolated from *Cannabis* varieties which has, unlike Δ^9-tetrahydrocannabinol, not shown psychoactive behaviour [Perez-Reyes, 1973]. Interest in CBD has increased since the beginning of the 2000s and several pharmacological effects are discussed, such as anti-inflammatory, anti-oxidative and neuroprotective action. It is further suggested that CBD might be beneficial in diseases such as Parkinson's disease, diabetes, nausea, cancer, inflammatory diseases and several others [Zuardi, 2008]. How to formulate cannabidiol is therefore an intriguing question in order to enable the use of this promising drug substance. Formulations in lipid carriers are especially promising options due to the lipophilicity of cannabidiol with regard to both parenteral and oral administration. Lipid carriers with sizes in the nanometer range can enable parenteral administration in the therapy with CBD which could be of interest due to the wide field of pharmacological effects. For oral therapy, self-dispersing lipid formulations can be generated using phospholipids as natural emulsifier and solubilizer. These formulations can be filled into hard capsules and disperse in the gastro-intestinal fluids due to mild agitation.

RESEARCH CONCEPT

The maximum amount of drug loaded into dispersed formulations was determined by passive loading, a formulation screening method [Göke, 2017; Rosenblatt 2017]. Using this method, the powdered drug is incubated with the respective carriers in aqueous media and loads into the dispersed carriers by diffusion. The excess of drug is removed from the dispersion by filtration and the amount of loaded drug is analyzed.

For loading experiments with oral formulations, 5 % self-dispersing formulation (38 % medium chain

triglycerides (MCT), 57 % Phospholipon 90 G, 5 % ethanol 96 %) was dispersed in phosphate buffer pH 7.0. 5 % Phospholipon 90 G was dispersed accordingly to generate liposomes for a comparison. The dispersions were then treated with an ultrasonic probe to reduce the particle sizes to around 200 nm. Centrifugation and subsequent filtration removed titanium particles of the probe and coarse materials from the dispersion. The phospholipid content was then determined by Stewart assay [Stewart, 1980] to check how much lipid was removed by these steps. Briefly, samples were dried under a flow of nitrogen at 40 °C and then dissolved in chloroform. Phospholipids were quantified by colorimetric reaction with ammonium ferrothiocyanate.

Liposomes for parenteral formulations were produced by membrane extrusion. 10 % Lipoid S 75 was dispersed in phosphate buffer pH 7.4 and, after stirring overnight, ten times extruded through a 0.1 µm polycarbonate membrane to achieve a particle size of around 90 nm (all particle sizes were determined by photon correlation spectroscopy).

Emulsions for parenteral application were produced by high-pressure homogenization. The production of the trimyristin emulsion was carried out at 75 °C, all other emulsions were produced at room temperature. Lipid (5 % trimyristin, 10 % MCT or 10 % soybean oil) and aqueous phase (poloxamer 188, sodium azide, water) were weighed in and dissolved separately. Afterwards the phases were united and processed by an ultra-turrax. These pre-emulsions were homogenized ten times in a Microfluidizer. The pressure applied depended on the formulation, resulting mean particle sizes were between 110 nm and 280 nm.

Lipofundin (5 % soybean oil, 5 % MCT, egg phospholipids) is a commercially available parenteral fat emulsion.

Cannabidiol was added to the respective dispersion which was placed on a shaker. In case of oral formulations, samples were drawn in several intervals and analyzed for drug content by UV spectroscopy at 215 nm (solute tetrahydrofuran/acetonitrile (8/2)) until saturation. Lipid carriers for parenteral application were incubated in independent vials and the drug content was analyzed by UV spectroscopy at 212 nm (solute tetrahydrofuran/water (9/1)).

RESULTS

Cannabidiol showed a remarkably high drug load in lipid formulations (up to approx. 47 % in relation to the lipid content (Fig. 1)).

In formulations for oral application, CBD was loaded to a significantly higher extent into the self-dispersing mixture than into liposomes. In parenteral formulations, the trimyristin emulsion showed a considerably higher CBD load compared to emulsions of other oils. Drug loading into the phospholipid- and thus charge-stabilized Lipofundin emulsion led to a comparable drug concentration as for a sterically(poloxamer)-stabilized MCT emulsion. In the same manner as for oral formulations, cannabidiol reached a much higher concentration in all emulsions as compared to liposomes.

DISCUSSION

The very high drug load in the trimyristin emulsion indicates a lipid dependence of achievable CBD load in emulsions. This is in agreement with literature reports, where lipid dependence is also shown for other drugs [Göke, 2017]. A comparable drug load in the differently stabilized Lipofundin and MCT emulsion implicates that there is no strict preference of CBD for sterically or charge-stabilized emulsions. Higher drug loading in emulsions and self-dispersing mixtures compared with liposomes emphasizes an advantage of oil-containing carrier systems for the formulation of CBD.

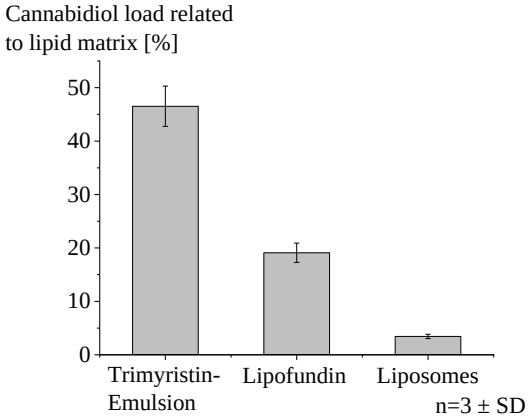

Fig. 1: Drug load of cannabidiol in parenteral formulations.

CONCLUSIONS

Lipid nanoemulsions achieve a high load of cannabidiol and therefore enable parenteral administration. Due to the lipid-dependent drug loading, the choice of the lipid has to be taken into account upon formulation of CBD in nanoemulsions. Self-dispersing mixtures are a promising option as well, as they facilitate oral administration and can be loaded with high CBD concentrations, too. Liposomes are a less interesting option for CBD formulation as notably less drug substance loaded into these carriers.

ACKNOWLEDGMENT

The Ministry of Science and Culture (MWK) of Lower Saxony, Germany, is acknowledged for financial support within the Smart BioTecs alliance. Support by the Phospholipid Research Center is acknowledged as well.

REFERENCES

[Göke, 2017] Göke, K., Bunjes, H., 2017, Drug solubility in lipid nanocarriers: Influence of lipid matrix and available interfacial area, *International Journal of Pharmaceutics*, Vol. 529, 1-2, pp. 617–628.

[Perez-Reyes, 1973] Perez-Reyes, M., Timmons, M. C., Davis, K.H. and Wall, E.M., 1973, A comparison of the pharmacological activity in man of intravenously administered Δ^9-tetrahydrocannabinol, cannabinol, and cannabidiol, *Experientia*, Vol. 29, pp. 1368-1369.

[Rosenblatt, 2017] Rosenblatt K. M., Bunjes, H., 2017, Evaluation of the drug loading capacity of different lipid nanoparticle dispersions by passive drug loading, *European Journal of Pharmaceutics and Biopharmaceutics*, Vol. 117, pp. 49–59.

[Stewart, 1980] Stewart, J. C. M., 1980, Colorimetric determination of phospholipids with ammonium ferrothiocyanate, *Analytical Biochemistry*, Vol. 104, 1, pp. 10–14.

[Zuardi, 2008] Zuardi, A. W., 2008, Cannabidiol: from an inactive cannabinoid to a drug with wide spectrum of action, *Revista Brasileira de Psiquiatria*, Vol. 30, pp. 271-280

MICROGRIPPERS TO HANDLE ORGANOIDS AND PANCREATIC ISLETS FOR PRECISION MEASUREMENTS OF BIOLOGICAL FUNCTION.

Früh E[1,3], Bütefisch C[1,3], Leester-Schädel M[2,3], Gursky B[2,3], Dietzel A[2,3], Bütefisch S[4] and Rustenbeck I[1,3]

[1]Institute of Pharmacology and Toxicology, [2]Institute of Microtechnology, University of Braunschweig,
[3]PVZ-Center of Pharmaceutical Engineering and
[4]PTB –Physikalisch-Technische Bundesanstalt/Federal Institute of Metrology, Braunschweig

Contact: i.rustenbeck@tu-braunschweig.de, +49531391-5670, Mendelssohnstraße 1, 38106 Braunschweig, Germany

ABSTRACT

The model of the cultured single cell is considered insufficient to explain the physiological regulation taking place at the organ level. The same is true for the prediction of drug action at the organ level or at the level of the intact organism. For these reasons 3D cell culture models are in increasing demand. It is thus necessary to develop the instruments to handle such cell aggregates and organoids in a controlled, precise and gentle manner. Here, a microgripper is presented which is able to work in aqueous solutions and which is compatible with electrophysiological recordings of the cells immobilized by it. It was successfully employed to position isolated pancreatic islets and a 3D cell culture model of insulin-secreting cells, the so-called MIN6-pseudoislet. As required it was possible to measure the membrane potential of cells within these aggregates without any interference from the microgripper.

Keywords: Diabetes mellitus, insulin secretion, Organ-on-chip, multiparametric measurements

INTRODUCTION

2D cell culture systems have been the workhorse for biomedical research for decades. However, it is increasingly becoming clear that this reductionist model of cellular physiology is insufficient to explain the regulation taking place at the organ level (**1**). In particular, it is insufficient to reliably predict the action of newly developed drugs in the intact organism (**2**). Consequently, 3D cell culture models are gaining in popularity and it is expected that more relevant information can be gathered from their use. However, the standard instrumentation in the cell biology laboratory is designed to deal with liquids and with cells suspensions but not with larger cell aggregates or organoids. In view of these tendencies it is imperative to develop the instruments to handle cell aggregates and organoids in a controlled, precise and gentle manner. Here we present the first version of a microgripper designed to deal with biological specimen.

The microgripper was used to position isolated pancreatic islets and a 3D cell culture model, the so-called MIN6-pseudoislet. Pancreatic islets contain multiple cell types, most notably the beta cells which synthesize and release insulin, the main glucoregulatory hormone of the human body (**3**). MIN6 cells are immortalized insulin-secreting cells, which share many similarities with the beta cells, but have a much higher tendency to proliferate (**4**).

RESEARCH CONCEPT

Microgripper The design of the microgripper is based on the microgripper toolbox developed at the IMT of the TU Braunschweig (**5**). To operate the microgipper in aqueous solutions and to be compatible with electrophysiological recordings of the cells immobilized by the gripper, the following design was chosen: The microgripper is fully made of SU-8, a UV sensitive, high contrast, epoxy based negative tone photoresist. Due to lithographic exposure with UV radiation and subsequent development and curing, the resin polymerizes. It is then fluid resistant and almost transparent. In order to prevent the electrophysiological investigations from being disturbed by the drive that opens and closes the gripper jaws, non-electrical actuator principles were selected and investigated. These are, on the one hand, a pneumatic and, on the other hand, a bowdencable based

actuator principle. The investigations described here are made with the latter principle. The total length of the gripper is 7.2 mm. The length of the gripper jaws is about 700 µm, and they can be opened to 400 µm. The actuator's linear positioning movement is transmitted via an integrated gripper gear to the gripper jaws, so that they move evenly and parallel to each other, thus having a centering effect. This ensures a reliable holding process safety and an even load on the object to be gripped (**Fig. 1**).

Cells and tissues Pancreatic islets of NMRI mice were isolated from the surrounding pancreatic exocrine tissue by a collagenase digestion technique. Isolated islets were collected under a stereomicroscope and were cultured overnight in cell culture medium RPMI1640 with 10% fetal bovine serum (FBS) and 5 mM glucose. Insulin-secreting MIN6 cells (kindly provided by Jun-Ichi Miyazaki) were cultured in DMEM medium (25 mM glucose, 6 mM glutamine), 10% FBS and penicillin/streptomycin in a humidified atmosphere of 95% air and 5% CO_2 at 37 °C.

Monitoring of islet function parameters: The plasma membrane potential and currents of single cells within islets or pseudo-islets were measured using the patch clamp technique (**Fig. 2**). Pipettes were pulled from borosilicate glass (2 mm o.d., 1.4 mm i.d., Hilgenberg, Germany) by a two-stage vertical puller (HEKA-Electronics, Lambrecht, Germany) and had resistances between 3 and 6 MΩ when filled with solution. The continuous measurements of the membrane potential and membrane currents were performed using an EPC 7 patch-clamp amplifier (HEKA-Electronics).

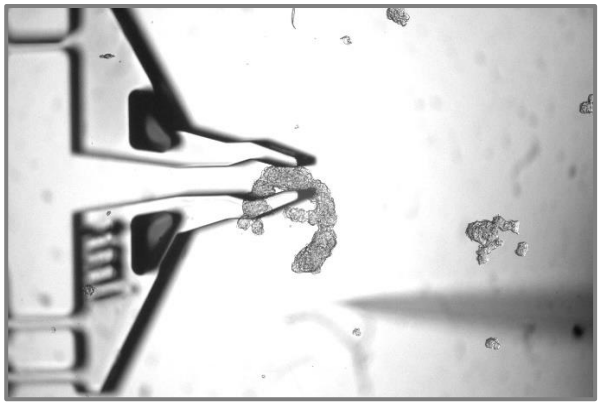

Fig. 1 Microgripper holding and moving a MIN6 pseudo-islet in the bath system of the patch clamp measuring stand

Fig. 2 Patch-Clamp measuring stand with the micro-gripper holder to the left of the organ bath (illuminated area) and the preamplifier to the right.

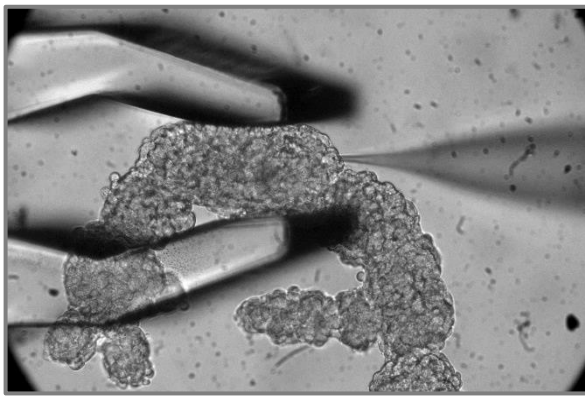

Fig. 3 Microgripper holding a MIN6 pseudo-islet while a Giga-Ohm seal is formed by the patch pipette, permitting electrophysiological measurements.

RESULTS

The jaws of the present version of the microgripper were actuated by a newly developed actuation system based on a stepper motor, a fine positioner and a bowdencable-like transmission system. With this actuation system the distance between the jaws could be adjusted extremely precise from 400 µm to a complete closed stage. This movement of the jaws generated a contact between the microgripper and the spheroid islet which was sufficiently stable to permit back and forth movements within the aqueous bath solution. The newest design of the microgripper is equipped with an integrated force

sensor to monitor the exerted gripping-forces. The determination of the exerted force by the jaws of the gripper is subject of current investigation (a calibration facility is currently under development). But it can be stated that the exerted gripping force only slightly deformed the islet shape. When MIN6 pseudo-islets were used it was difficult to establish a sufficiently stable contact, probably because they are more easily deformable.

Placing a patch pipette (tip diameter ca. 1 µm) on one of the outer pseudo-islet cells (**Fig. 3**) and applying gentle suction (8 cm water) led to the build-up of a Giga-Ohm seal, as could be seen from the diminishing currents elicited by the -10 mV test pulse. This close connection between the cell membrane and the glass surface of the pipette is indispensable to measure the very small currents flowing through the ion channels of the plasma membrane. It is easily disturbed by even small movements of the cell surface relative to the tip of the pipette. In the present experiments a seal of more than 1 Giga Ohm persisted reproducibly for more than 15 min.

DISCUSSION

The present design of a mechanically actuated microgripper for 3D cell culture models fulfills several of the pre-defined requirements. It can generate a sufficiently firm contact to permit the positioning of the multicellular aggregates within cell culture media or other bath solutions. It does not interfere with the sensitive measurements of membrane currents and potentials. It is sufficiently stable to permit extended periods of measurement. The more pronounced difficulties in handling the pseudo-islets suggest that changes in the jaw design may be necessary to deal with mechanically less stable cell aggregates.

CONCLUSIONS

The present microgripper demonstrates the feasibility of using this kind of instrumentation to handle multicellular aggregates. In particular, a good long-term stability is achieved. This now enables further development such automated pick and place using integrated object recognition.

ACKNOWLEDGMENT

This study was supported by the Bundesministerium für Wirtschaft, ZIM-Projekt 4433802SK7; 4433702SK7; 4104109SK7

REFERENCES

1. Langer G. Implementation and Use of State-of-the-Art, Cell-Based In Vitro Assays. Handb Exp Pharmacol. 2016;232:171-90.

2. Cavero I, Guillon JM, Holzgrefe HH. Human organotypic bioconstructs from organ-on-chip devices for human-predictive biological insights on drug candidates. Expert Opin Drug Saf. 2019 Jul 3:1-27.

3. Halban PA, Polonsky KS, Bowden DW, Hawkins MA, Ling C, Mather KJ, Powers AC, Rhodes CJ, Sussel L, Weir GC. β-cell failure in type 2 diabetes: postulated mechanisms and prospects for prevention and treatment. Diabetes Care. 2014;37:1751-8

4. Schulze T, Morsi M, Brüning D, Schumacher K, Rustenbeck I. Different responses of mouse islets and MIN6 pseudo-islets to metabolic stimulation: a note of caution. Endocrine. 2016 Mar;51(3):440-7.

5. Björn Hoxhold: Mikrogreifer und active Mikromontagehilfsmittel mit integrierten Antrieben. Dissertation, Shaker Verlag Aachen, Band 29, 2010, ISBN 978-3-8322-9678-0

CO_2 EXTRACTION – A PRODUCTION PROCESS FOR THE RECOVERY OF API

Dr. Dieter Gerard

FLAVEX Naturextrakte GmbH, Nordstrasse 7, D-66780 Rehlingen, Germany

dg@flavex.com

ABSTRACT

The desired valuable ingredients determine the required solvent. After some thermodynamic consideration about supercritical fluids and the advantages of liquid and supercritical carbon dioxide for extraction purposes some exceptional examples for the recovery of active pharmaceutical ingredients of medicinal plants are discussed.

Keywords: CO_2 extraction, active pharmaceutical ingredients, medicinal and aromatic plants

INTRODUCTION

Plant extracts are used in many fields of human life. The use as API in natural remedies, in functional foods or nutraceuticals or in natural cosmetics asks for 100% natural extracts. The versatile CO_2-extraction technology can help to satisfy the demands for tailor-made highly concentrated pure extracts. CO_2 extracts, with their unique spectrum of ingredients composed of non-polar secondary plant metabolites, offer new possibilities especially where quality and added value are important.

EXTRACTION SOLVENTS AND THEIR PROPERTIES

The production of plant extracts requires solvents. European legislation regulates the use of extraction solvents. Only a small number of solvents is allowed. For certified organic products only the solvents water, ethanol and carbon dioxide can be used. For the extraction of plant material the desired valuable ingredients determine the required solvent. For the recovery of pure lipophilic and less polar components CO_2 extraction is an established process. If the extraction of more polar components like steroids, phenolic compounds or phospholipids is desired then it is of advantage to mix some percent of ethanol into the carbon dioxide.

Fig 1: Thermodynamic state of an auxiliary material in separation procedures [Stahl 1986]

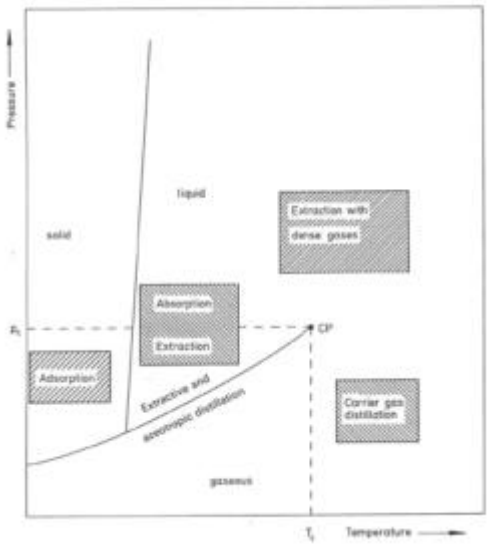

The CO_2 extraction method generates many positive properties. The selectivity of the solvent is adjustable by pressure and temperature in the extraction step. CO_2 works under gentle process conditions, sensitive ingredients can be recovered without thermal stress or oxidative degradation. Supercritical CO_2 has very good mass transfer properties, with a viscosity and a diffusion coefficient like a gas it has a density like a liquid. As a consequence high CO_2 flow rates allow short extraction times and this results in a favourable impact to the process costs. The frequently reported disadvantage of supercritical CO_2 extraction, the cost of the process,

needs to be put into context. The quality of the CO_2 extracts is unachievable with other extraction methods and the CO_2 extracts are usually part of new products.

Table 1: Solvent selection.

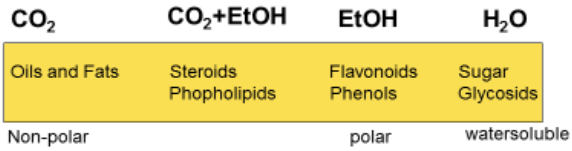

EXCEPTIONAL EXAMPLES

After a survey of the use of CO_2 extracts from botanicals in products of the daily life some exceptional examples are discussed. Flowers of the well known medicinal plants camomile, calendula or arnica are source material for the CO_2 extraction of products for natural remedies. CO_2 extracts of the roots of echinacea varieties are useful ingredients for medicinal skin care and boosting the immune system. A lot of medicinal and aromatic plants are extracted with supercritical CO_2 and these extracts are filled in capsules for convenient dietary supplements. Guggul CO_2 extract, from the gum of *Commiphora mukul* tree, is prepared with a supercritical CO_2 – cosolvent extraction with ethanol and recovers the active constituents that show tremendous promise for human well-being. The CO_2 extraction of some of these examples is described in more detail.

Table 2: examples of the use of medicinal plant extracts

MAP	Plant part	Active ingredients
Calendula	Flower	Faradiolesters
Arnica	Flower	Sesquiterpen-lactones
Oregano	Leaf	Carvacrol, thymol
Petasites	Herb, roots	Petasines
Echinacea	Roots	Alkylamides
Seabuckthorn	Berries	Omega fatty acids
Millet	Seeds	Phytosterol miliacin

CONCLUSIONS

Supercritical CO_2-extraction is a state of the art technology to recover highly concentrated pure extracts. CO_2 extracts can be used as API in pharmaceuticals but they have to be licensed. In Europe CO_2-extraction is meanwhile a standard method to produce extracts for food supplements or cosmetic ingredients, but only a few plants have the permission for pharmaceuticals because of the need for GMP processing.

REFERENCES

[Stahl 1986] Stahl, E., Quirin, K.-W., Gerard, D., 1986, Dense gases for extraction and refining, Springer Verlag

[Della Loggia 1990] Della Loggia R, Becker H, Isaac O, Tubaro A : Topical Anti- Inflammatory Activity of Calendula officinalis Extracts, Planta Médica 56, 658

[Della Loggia 1994] Della Loggia R, Tubaro A, Sosa S, Becker H, Saar S, Isaac O : The role of triterpenoids in the topical anti-inflammatory activity of Calendula officinalis flowers, Planta Medica 60(6), 516-520

[Klaas 2002] Klaas C., Wagner G, Laufer S, Sosa S, Della Loggia R, Bomme U, Pahl HL, Merfort I. : Studies on the anti-inflammatory activity of phytopharmaceuticals prepared from Arnica flowers, Planta Med. 68(5), 385-391

[May 2013] May, P., Arnica Flower CO2-Extract - Approved Efficacy in Topical Treatment : , Cosmetic Science Technology 2013

[Gensthaler 2003] Gensthaler, B.M., Extrakt aus Pestwurzblättern lindert allergische Rhinitis, Pharm Ztg. 3, 2003

[Quirin 1995] Quirin K. W., Gerard D.: Cosm. Toil. Manuf. Worldw. 1995, 57 ff.

PELLETS 4.0 – ADVANCED FLUIDIZED BED TECHNOLOGIES

Author(s); A. Grave

Glatt Pharmaceutical Services GmbH & Co, KG, 79589 Binzen, Germany.

Keywords: Fluid Bed Technology, multiparticulates, CPS™-Technology, continuous pelletizing, MicroPx™, PAT, DoE, QbD, pediatrics, geriatrics

INTRODUCTION

Fluid bed processes were first developed for the chemical industry to achieve better drying efficiencies than obtained with existing technologies *e. g* with tray drying. Implementation of spray nozzles in the fluid bed equipment enabled granulation processes, resulting in porous agglomerates and, processed to tablets, facilitating fast dissolution. With the development of the bottom spray technology highly efficient coating and layering processes became possible. While in the beginning this technology was mainly used for tablet coating, more and more processes were developed for coating of smaller particles, *i. e.* multiparticulates like pellets, minitablets and powders (*e. g.* API crystals).

Multiparticulate dosage forms consist of small discrete units with particle sizes of 100 – 2000 µm [1] showing a matrix structure (API implemented in the core) or being API layered. In case of pellets or minitablets, functional coatings can be applied, resulting in taste masking, gastroresistant coatings or other specific release profiles. Filling of multiparticulates into capsules or sachets and administration via sprinkling on liquids or food makes them attractive for patients who are not able to swallow monolithic dosage forms, as is the case for children or elderly. The possibility of administering different amounts of multiparticulates provides an opportunity for the development of individualized medicines. Also a compression into tablets is possible, orally disintegrating tablets (ODTs) release their discrete units in the stomach, ensuring a controlled drug release and less dependency on the gastric emptying.

Glatt offers several batch-wise or continuous technologies for the production of multiparticulates, matrix or layered pellets. Process development and optimization can be performed with quality by design approaches, process monitoring and control by state of the art PAT tools. The presentation will give an overview about the recent and most prevalent manufacturing methods.

BATCH FLUID BED TECHNOLOGIES

WURSTER TECHNOLOGY

The Wurster technology [Figure 1] is a classic fluid bed technology used for drug layering and (functional) coating of even very small multiparticulates and powders. The layering or coating liquid is sprayed concurrently with the fluidization air into the circulating fluid bed. The liquid is frequently and repeatedly applied as droplets on the substrate [Figure 1] in an environment of high heat transfer, finally resulting in a dense coating.

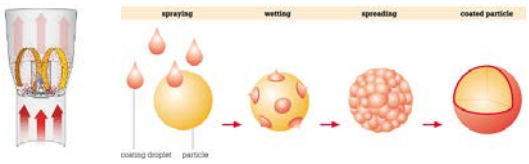

Figure 1: Wurster technology, coating process (Glatt Pharmaceutical Services GmbH & Co. KG)

CPS™ TECHNOLOGY

The CPS™ technology [Figure. 2] allows the preparation of both high drug loaded as well as low dosed matrix pellets, with sizes down to 150 µm. Based on advanced fluid bed rotor technology, the CPS™ technology works with a conical shaped rotating disc

and devices providing a directed product flow. No starting beads are required. The powder, containing API and typically microcrystalline cellulose is wetted by the pelletizing liquid until a pre-defined moisture level (and with this: particle size) is obtained. Due to centrifugal forces, spherical particles are formed and densified, characterized by smooth surfaces, narrow particle size distribution [Figure 3] and low porosity and attrition.

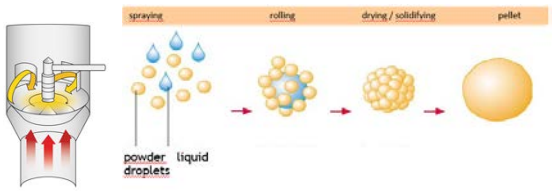

Figure 2: CPS™ technology, pelletizition process (Glatt Pharmaceutical Services GmbH & Co. KG)

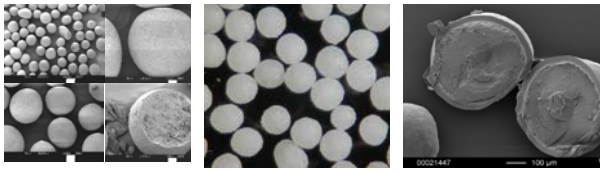

Figure 3: Matrix pellets produced with CPS™ technology (left), and MicroPx™ technology (middle, and right, Glatt Pharmaceutical Services GmbH & Co. KG)

CONTINUOUS FLUID BED TECHNOLOGIES

MICROPX™ / PROCELL TECHNOLOGY

The MicroPx™ technology is the preferred option for the production of high drug loaded pellets with API contents up to 95%. Spherical and smooth particles in the size of 150 µm or bigger can be obtained [Figure 3], exhibiting narrow particle size distributions. In this continuous process, the API containing liquid (solution, suspension, emulsion, melt [2]) is sprayed into the empty process chamber. Initially, fine powder is generated by spray drying, which is continuously agglomerated to seeds, and by further layering, to round pellets. Well-sized pellets are discharged by a sifter; the classifying air determines the resulting particle size. The process is characterized by a balanced ratio between spray drying, layering and discharging of well-sized pellets.

In contrast to the MicroPx™ technology the process gas enters the process chamber in the ProCell™ not through an inlet air distribution plate, but through slots in the lower part of the equipment, resulting in a spouted bed [Figure 4]. The contact of the product to hot surfaces is minimized, therefore this technology is applicable also for heat sensitive substances like enzymes.

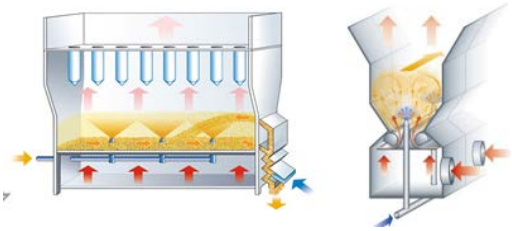

Figure 4: MicroPX™ (left) and Procell™ (right) technology, pelletization process (Glatt Pharmaceutical Services GmbH & Co. KG)

PROCESS CONTROL

For the implementation of robust and reproducible production processes, the critical quality attributes for a manufacturing process shall be known [3]. After a risk analysis, a design of experiments (DoE) with planned trials is applied, to define the design space and a control strategy for selected process parameters. PAT tools *e. g.* for online measurement of moisture, API content and particle size distribution can be applied for automated end point detection, to reduce the offline control and release testing.

SUBSCRIPT

API	Active pharmaceutical ingredient
DoE	Design of experiments
ODT	Oraly disintegrating tablet
PAT	Process analytical technology
QbD	Quality by Design

REFERENCES

[1] Poellinger, N., Innovative Glatt Fluid bed Pelletising Technologies, *International Pharmaceutical Industry*, Vol. 3, pp. 92 – 97

[2] Heinrich, S., Peglow, M., Henneberg, M., Drechsler, J., Mörl, l., Jacob, M., Pharmaceutical Process and Product Design by Fluidized Bed Spray Granulation: Modelling and Simulation Tools, Proc. International Meeting on Pharmaceutics, Biopharmaceutics and Pharmaceutical Technology, Nuremberg, 15 - 18 March 2004

[3] ICH Guideline, Pharmaceutical Development Q8 (R2) [2009]

STABILITY TESTS OF ALKYNYLGOLD(I)(NHC) COMPLEXES BY HPLC-DAD-MS

Henrik Hoffmeister and Ingo Ott

Institute of Medicinal and Pharmaceutical Chemistry; Technische Universität Braunschweig, Beethovenstraße 55, 38106 Braunschweig, Germany; henrik.hoffmeister@tu-bs.de

ABSTRACT

Gold organometallic compounds have been extensively investigated as potential anticancer metallodrugs and have shown a high potential regarding antiproliferative effects [Hickey, 2008; Andermark, 2016; Meyer, 2012; Schmidt, 2019]. Enhanced stability is a driving argument for the design of gold complexes with *N*-heterocyclic carbene (NHC) ligands. The more surprising is the lack of methods of pharmaceutical analytics for their stability and solution chemistry. Such analytical methods are important key elements for future metabolomic investigations and will help to ensure a better understanding of the biological behavior of the complexes [Kostiainen, 2003].

We selected complexes of the type of alkynylgold(I)(NHC) for detailed stability studies by HPLC-DAD-MS, in comparison to the well-known antirheumatic drug Auranofin. A RP-based chromatographic method was established to separate possible degradation products of alkynylgold(I)(NHC) complexes. The stability studies were performed at 37°C over 24h using dimethylformamide (DMF), dimethyl sulfoxide (DMSO), water and Dulbecco`s modified eagle medium (DMEM) solutions of each compound. Furthermore, interaction experiments of alkynylgold(I)(NHC) complexes with acetylcysteine are under way with the same set-up as the stability tests [Albert 2012].

ESI (+) and (-) ionisation with a quadrupole analyser was used for mass spectrometry. The first results indicate that alkynylgold(I)(NHC) complexes are stable in the analysed solvents with no significant changes in their AUCs [Fig 2].

INTRODUCTION

N-heterocyclic carbene (NHC) ligands with their strong σ-donating character can be coordinated well to several transition metals. Specifically, gold(I) complexes have been extensively investigated and have shown a high potential regarding antiproliferative effects [Hickey, 2008; Andermark, 2016; Meyer, 2012; Schmidt, 2019]. The enhanced stability has been a driving argument for the design of metal-NHC based drugs. However, extended studies on their solution chemistry and stability have not been frequently performed and aspects of pharmaceutical analytics have not been considered sufficiently. We selected complexes of the type alkynylgold(I)(NHC) (Fig. 1) for detailed stability studies by HPLC-DAD-MS, in comparison to the well-known antirheumatic agent Auranofin.

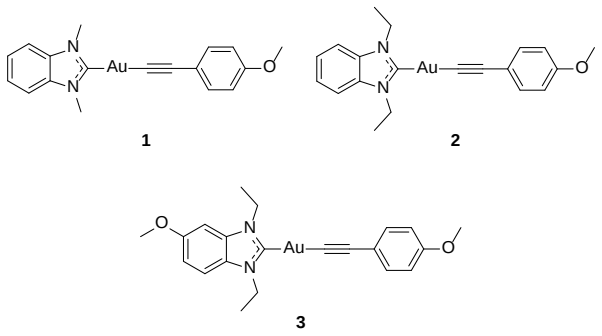

Figure 1: Structures of selected alkynylgold(I)(NHC) complexes

On top of that an interaction experiment of alkynylgold(I)(NHC) complexes with acetylcysteine is under way with the same set-up as the stability tests.

EXPERIMENTAL

The stability studies were performed in four different solvents (DMF, dimethyl sulfoxide (DMSO), water and

Dulbecco`s modified eagle medium (DMEM)) and were carried out with an established HPLC method. The first step was to prepare a DMF stock solution, which was diluted with the respective solvent. For the stability tests in water and DMEM the organic solvent (DMF) amount had to be increased to 50% of the total volume because of the poor water solubility properties of the compounds. After transferring the solutions into the HPLC vials the incubation at 37°C was done in the auto-sampler unit of the HPLC. The time-dependent injection could be automated. For this study the injection was done after 0h, 4h, 8h, 12h and 24h.

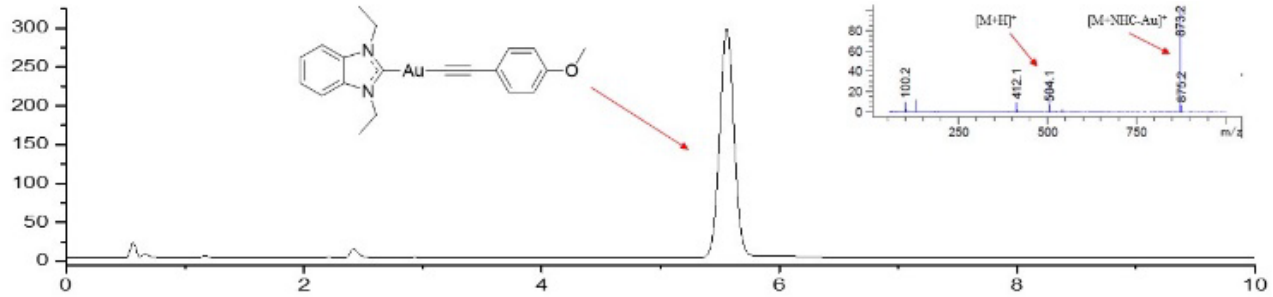

Figure 2: Chromatogram of a selected complex in DMEM after 24h. The insert shows the ESI (+) mass spectrum of the main peak.

The interaction experiment was performed in three different solvents: water, phosphate-buffered saline (PBS), 2-amino-2-(hydroxymethyl)propane-1,3-diol (Tris) buffer. Initially acetylcysteine and the alkynylgold(I)(NHC) complexes were characterized in the solvents mentioned above over a time period of 24 hours. After the characterization an equimolar solution of acetylcysteine and each alkynylgold(I)(NHC) complex were prepared and incubated together at 37°C over 24 hours in the autosampler unit. The injections were automated and measured under the same conditions as the stability tests.

DISCUSSION AND CONCLUSIONS

Over the exposure time no significant peak changes were observed. Moreover, the peak areas remained unaltered over 24 hours.

In the case of the interaction experiment a different behavior could be observed. In water the peak for the alkynylgold(I)(NHC) complex disappeared almost completely after 2h and a new peak with a much shorter retention time occurred in the chromatogram, which could be identified as $Au(NHC)_2^+$ by means of MS detection. A similar behavior can be observed in PBS and Tris buffer. In case of PBS the decrease of the main peak is much lower and even after 24h a significant amount of alkynylgold(I)(NHC) complex is still present in the sample. Almost the same behavior can be observed in Tris buffer, however, the effect is much less developed.

NOMENCLATURE

AUC	area und curve
DAD	diode array detector
DMEM	Dulbecco`s modified eagle medium
DMF	dimethylformamide
DMSO	dimethyl sulfoxide
ESI	electrospray ionisation
HPLC	high performance liquid chromatography
MS	mass spectrometry
NHC	*N*-heterocyclic carbene
PBS	phosphate-buffered saline
Tris	2-Amino-2-(hydroxymethyl)propane-1,3-diol

REFERENCES

[Hickey, 2008] Hickey, J. L., Ruhayel, R. A., Barnard, P. J., Baker, M. V. Berners-Price, S. J., Filipovska, A., 2008, Mitochondria-Targeted Chemotherapeutics: The Rational Design of Gold(I) N-Heterocyclic Carbene Complexes That Are Selectively Toxic to Cancer Cells and Target Protein Selenols in Preference to Thiols, *J. Am. Chem. Soc.*, Vol. 130 (38), pp. 12570–12571.

[Andermark, 2016] Andermark, V., Göke, K., Kokoschka, M., Abu el Maaty, M. A., Lum, C. T., Zou, T., Sun, R.W., Aguiló, E., Oehninger, L., Rodríguez, L., Bunjes, H., Wölfl, S., Che, C.M., Ott, I., 2016, Alkynyl gold(I) phosphane complexes: Evaluation of structure-activity-realationsships for the phosphane ligands, effects on key signaling proteins and preliminary in-vivo studies with a nanoformulated complex, *J. Inorg. Biochem*, Vol. 160, pp. 140–148.

[Meyer, 2012] Meyer, A., Bagowski, C.P., Kokoschka, M., Stefanopoulou, M., Alborzinia, H., Can, S., Vlecken, D., Sheldrick, W.S., Wölfl, S., Ott, I., 2012, On the Biological Properties of Alkynyl Phosphines Gold(I) Complexes, *Angew. Chem. Int. Ed.*, Vol. 51(35), pp. 8895–8899.

[Schmidt, 2019] Schmidt, C., Albrecht, L., Balasupramaniam, S., Misgeld, R., Karge, B., Brönstrup, M., Prokop, A., Baumann, K., Reichel, S., Ott, I., 2019, A gold(I) biscarbene complex with improved activity as a TrxR inhibitor and cytotoxic drug: comparative studies with different gold metallodrugs, *Metallomics*, Vol. 11(3) pp. 533–545.

[Kostiainen, 2003] Kostiainen, R., Kotiaho, T., Kuuranne, T., Auriola, S., 2003, Liquid chromatography/atmospheric pressure ionization-mass spectrometry in drug metabolism studies, *J. Mass Spectrom.*, Vol. 38(4), pp. 357–372.

[Albert 2012] Albert. A., Brauckmann, C., Blaske, F., Sperling, C.E., Karst, U., 2012, Speciation analysis of the antirheumatic agent Auranofin and its thiol adducts by LC/ESI-MS and LC/ICP-MS, *J. Anal. At. Spectrom.*, Vol. 27(6), pp. 975–981.

DEVELOPMENT OF SUITABLE WORKING PROTOCOL FOR IN VITRO TAPE STRIPPING: A CASE STUDY WITH BIOCOMPATIBLE ACECLOFENAC-LOADED TOPICAL NANOEMULSIONS

Tanja Ilić[1], Sanela Savić[2], Ivana Pantelić[1], Bojan Marković[3], Snežana Savić[1]

[1] Department of Pharmaceutical Technology and Cosmetology; University of Belgrade–Faculty of Pharmacy; 11221 Belgrade, Serbia; [2] DCP Hemigal, Leskovac, 16000 Leskovac, Serbia; [3]Department of Pharmaceutical Chemistry; University of Belgrade–Faculty of Pharmacy; tanjai@pharmacy.bg.ac.rs

ABSTRACT

Considering the numerous organizational and legislative issues associated with in vivo studies, the present study aimed to develop in vitro tape stripping protocol that could serve as a prospective technique for skin penetration studies. The research was mainly focused on the suitability of transepidermal water loss (TEWL) measurements, as a barrier integrity test for porcine ear skin subjected to freezing/thawing procedure, as well as on the selection of the most suitable device for pressing adhesive tapes onto the porcine ear surface during skin stripping procedure. Obtained results suggest that TEWL measurements were able to detect the damage of the stratum corneum (SC) caused by physical impairment (using adhesive tapes) and tissue degradation/dehydration (prolonged storage at –20ºC/ambient conditions). Penetration profiles of aceclofenac from nanoemulsions based on sucrose esters or polysorbate 80 as coemulsifiers, obtained in vitro (using a roller as pressure device), were in a good agreement with data obtained in vivo on humans, supporting the use of developed in vitro tape-stripping protocol in skin formulation development and optimization.

Keywords: tape stripping, porcine ear skin, nanoemulsions, in vitro-in vivo correlation, aceclofenac

INTRODUCTION

The rational approach for designing and optimizing novel skin formulations requires the use of well-defined method, which can enable the assessment of drug penetration into the skin. Among different techniques proposed, tape stripping stands out as a simple and minimally invasive technique for the assessment of drug dermal availability in vivo, in humans. However, considering that in vivo studies are frequently associated with numerous organizational and legislative issues (e.g. the need for complex documentation when applying for ethical committee approval, particularly for nanocarrier testing), the research efforts have been directed towards the validation of porcine ear skin as an alternative in vitro model for human studies [Klang, 2012; Leal, 2017]. Having in mind some unresolved issues, such as (i) the capability of applying TEWL measurements in assessing the integrity of the porcine ears subjected to freezing/thawing procedure and (ii) the selection of the most suitable device for pressing adhesive tapes onto the skin surface, the aim of present study was to develop the in vitro tape stripping working protocol that could be simply used in the averages laboratories, without the need for sophisticated equipment. Recently developed nanoemulsions intended for topical administration of aceclofenac (ACF) [Isailović, 2016] were utilized to assess the applicability of suggested protocol for the analysis of small variations in formulation composition on ACF delivery into the skin, by comparing with corresponding results obtained in vivo on humans.

RESEARCH CONCEPT

Development of in vitro tape stripping working protocol – evaluation of selected critical steps

Fresh porcine ears obtained from the local abattoir immediately after slaughter (before scalding), were washed under cold running water, blotted dry with the soft tissue, wrapped in the aluminum foil and stored at –20°C until use (within one to six months to evaluate the effect of storage duration on skin barrier integrity). On the day of experiment, after defrosting, hairs were shortened with scissors and when TEWL reached the values of approximately 15 $gm^{-2}h^{-1}$ (measured using a Tewameter® TM 210, Courage+Khazaka, Germany), ears were fixed on styrofoam plates [Klang, 2012]. In order to evaluate the capability of TEWL measurements to detect the changes in skin barrier

function of defrosted porcine ears, periodic measurements of TEWL were performed during the progressive removal of the SC by adhesive tapes. Additionally, the TEWL measurements were performed on intact porcine ears periodically during 6 h of storage at ambient conditions, in order to detect the potential changes in skin barrier (due to tissue dehydration). Additionally, since application pressure is one of the basic factors influencing the amount of SC removed during the tape stripping procedure, two different methods (roller *vs.* weight of 300 g) were examined regarding the impact on TEWL and total quantity of ACF and SC removed with each tape.

In vitro tape stripping – a case study

In order to assess the applicability of developed protocol to detect the potentially meaningful differences in ACF penetration in the SC from nanoemulsions differing in the both, type and proportions of surfactants employed for stabilization (table 1), tape stripping was performed in vitro under infinite dose conditions and correlated with the results previously obtained in vivo on human volunteers [Isailović, 2016]. Briefly, when TEWL reached the values of ~15 $gm^{-2}h$, investigated formulations were carefully distributed on assigned skin sites. After a 2 h incubation period, the residual formulations were gently removed with dry cotton swabs, and 12 adhesive D-squame® discs (CuDerm Corporation, USA) were utilized for sequential removal of SC layers, after being submitted to uniform pressure using a roller device.

Table 1: Composition of investigated nanoemulsions, prepared using high pressure homogenization method

Excipients	Composition (% w/w)	
	$L_2P_2A/L_1S_1P_2A/L_{1.5}S_{0.5}P_2A$	L_2P80_2A
MCT*	10	10
Castor oil	10	10
Egg lecithin	2/1/1.5	2
Sucrose stearate	-/1/0.5	/
Sucrose palmitate	2	
Polysorbate 80	/	2
BHT*	0.05	0.05
Aceclofenac	1	1
Ultrapure water to	100	100

* MCT – medium chain triglycerides, BHT – butylhydroxytoluene

After removal of SC layers, each tape was transferred into a centrifuge tube and ACF was extracted with 4 mL of ethanol (70%, v/v). The tubes were sonicated (Sonorex RK 120H, Bandelin, Germany) for 15 min and then centrifuged at 4000 rpm for 5 min (Centrifuge MPW-56; MPW Med. Instruments, Poland). Supernatants were analyzed for ACF content using UHPLC-MS/MS method [Isailović, 2016]. Validation of the extraction procedure was performed by spiking tape-stripped samples of untreated SC with the known quantity of ACF dissolved in ethanol (70%, v/v). After solvent evaporation, the extraction procedure was carried out as described above and drug recovery was determined. It was found that ACF recovery from the SC was 95.8 ± 2.9%.

RESULTS

During tape stripping procedure, TEWL progressively increased as barrier function was perturbed by sequential removal of SC layers (figure 1). However, TEWL increased only slightly during the removal of 40% of the barrier's thickness, but changed more noticeably when more than 50% of SC was removed (removal of ~80% of SC was accompanied with ~5-fold increase of TEWL).

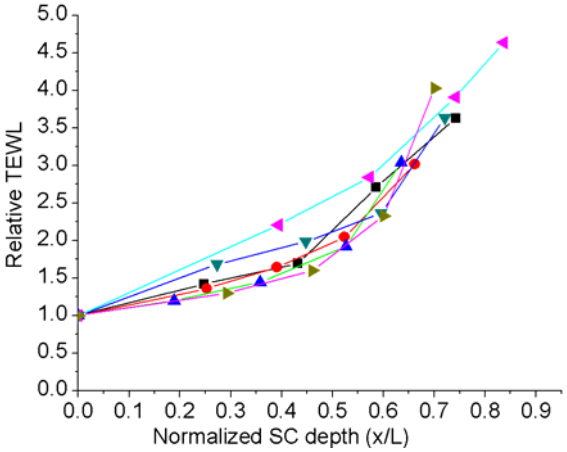

Figure 1: Relative TEWL (measured TEWL divided by pre-stripping value) as function of relative SC depth

Despite freezing/thawing procedure, the plots of 1/TEWL versus SC were highly linear for ears stored up to one month in the fridge (mean r^2 for six ears was 0.9723; representative plot is shown at figure 2), enabling the total thickness of SC (L) to be calculated as described previously using Fick's first law [Herkenne, 2006]. Interestingly, after three months (or more) storage of porcine ears at –20ºC, a linear correlation was deteriorated (r^2 = 0.8182, n=6), suggesting that prolonged storage impairs the barrier function of porcine ear skin.

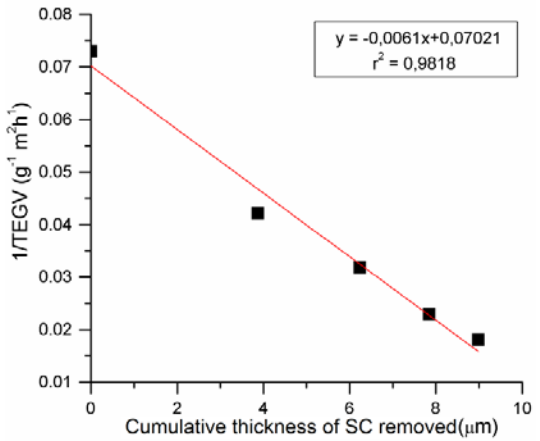

Figure 2: Representative linear plot of 1/TEWL as a function of the cumulative thickness of SC removed

Periodical TEWL measurements during 6 h-storage of porcine ears at ambient conditions revealed that TEWL values declined sharply 4 h after reaching the desired value of ~15 $gm^{-2}h^{-1}$, due to the tissue dehydration.

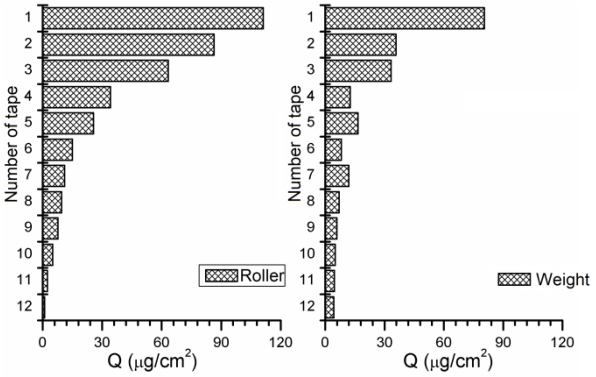

Figure 3: Quantity of ACF removed with each adhesive tape, reflecting the influence of different pressure device (roller *vs.* weight)

Further, TEWL values obtained during tape stripping performed using roller device were significantly higher compared to those obtained using weight (after 12th removed tape, TEWL was 54.1 and 37.2 $gm^{-2}h^{-1}$, respectively). Simultaneously, significantly higher thickness of SC was removed when roller was used to exert the pressure on the adhesive tape. Importantly, significantly higher amount of ACF was extracted from the SC when roller was used, clearly showing the gradual decrease of ACF quantity with increasing the number of removed tapes (figure 3).

Biocompatible aceclofenac-loaded nanoemulsions – a case study

ACF concentration versus relative SC depth profiles obtained after 2 h-application of investigated nanoemulsions on the porcine ear skin are shown in figure 4. Firstly, it could be seen that nanoemulsions based on sucrose esters as coemulsifiers enhanced cutaneous penetration of ACF, showing the higher drug levels at all depths into the SC in comparison with reference prepared with the polysorbate 80. However, due to high variability of obtained data, statistical significance was found only between $L_{1.5}S_{0.5}P_2A$ and L_2P80_2A formulations. Looking strictly at results obtained for sucrose esters-based nanoemulsions, investigated formulations could be ranked in the following order: $L_2P_2A < L_1S_1P_2A < L_{1.5}S_{0.5}P_2A$.

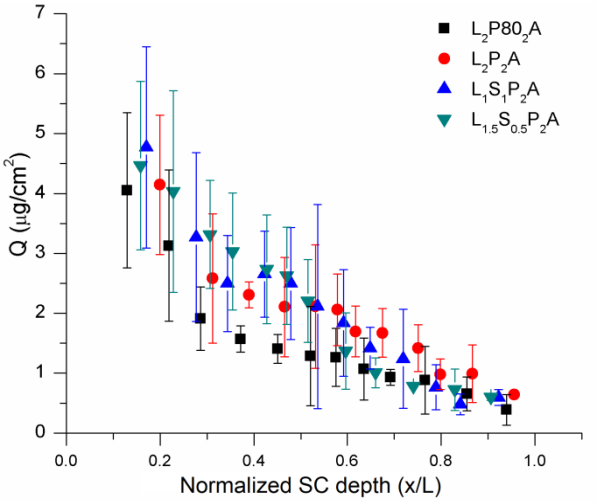

Figure 4: Comparative ACF penetration profiles across the SC path-length L (mean ± SD, n = 4)

Comparing the results obtained on porcine ears with results obtained in vivo, on human volunteers [Isailović, 2016], it could be noticed that results obtained in vitro are associated with significantly higher variability, probably due to difficulty in controlling the age, sex and way of pigs' nutrition.

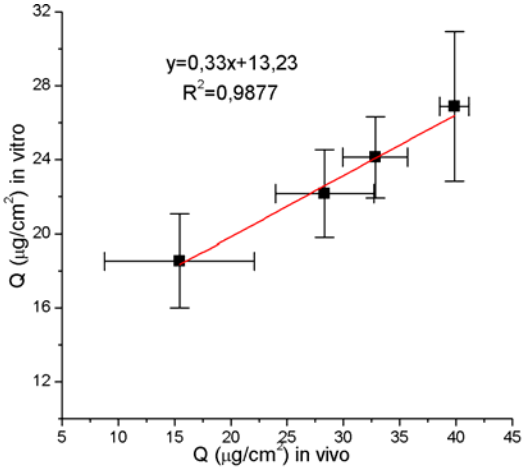

Figure 5: Correlation of the total amount of ACF recovered in the SC in vitro (porcine ear skin) and in vivo (human voluneteers)

When the total quantity of ACF recovered in the SC in vitro 2 h after nanoemulsions application were plotted against the total amount of ACF inside the SC in vivo, a high correlation was observed (figure 5). Formulations with comparatively high amounts of ACF in the SC in vivo were associated with the greater penetration of ACF into the SC in vitro.

DISCUSSION

Despite the increased number of publications dealing with in vitro tape stripping, the literature data regarding the use of TEWL for skin barrier integrity assessment are quite controversial. The average SC thickness of defrosted porcine ears determined using TEWL measurements was 10.9 ± 3.2 μm, which was in accordance with literature data for SC thickness of fresh porcine ears (11.8 ± 4.0 μm) [Sekkat, 2002; Herkenne, 2006], proving the usefulness of TEWL measurement for skin barrier monitoring during tape stripping procedure in spite of freezing/thawing procedure. Furthermore, TEWL measurements enabled to detect changes in skin barrier function due to tissue degradation (caused by prolonged storage at –20ºC) and dehydration (caused by prolonged skin storage at ambient conditions). These findings indicate that porcine ears should be stored up to one month at –20ºC, simultaneously proving that the isolated porcine ear could be a suitable model for the short-time application studies [Klang, 2012].

Analyzing the literature data dealing with in vitro tape stripping technique, it can be observed that different devices were utilized to press the tapes onto the skin surface. Obtained results suggest that the roller is better option than weight of constant mass. During the rolling movement, it appears that the skin surface flattens, enabling the optimal adhesive bond of the tape with the skin surface [Herkenne, 2006].

Penetration profiles of ACF from developed nanoemulsions obtained in vitro using developed protocol, in spite of relatively high variability, were in a good agreement with previously published in vivo results, obtained under infinite dose conditions. Since all tested nanoemulsions exhibited the similar physicochemical parameters that are considered as a crucial for drug delivery into the skin (droplet size ~ 180 nm, zeta potential ~40 mV, pH ~3.5, viscosity ~3.5 mPa s), these findings confirmed that perturbation of the SC barrier by surfactants employed for nanoemulsion stabilization was primary mechanism responsible for observed differences in ACF skin penetration profiles. In the other words, it seems that sucrose esters are more efficient as skin penetration enhancers than conventionally used polyethoxylated surfactants such as polysorbate 80.

CONCLUSIONS

In vitro tape-stripping of developed protocol permits good prediction of drug uptake into the SC in vivo and therefore it may be highly useful in skin intended drug formulation development and optimization.

ACKNOWLEDGMENT

This work was supported by the project TR34031, funded by Ministry of Education, Science and Technological Development, Republic of Serbia.

REFERENCES

[Herkenne, 2006] Herkenne, C., Naik, A., Kalia, Y.N., Hadgraft, J., Guy, R.H., 2006, Pig ear skin ex vivo as a model for in vivo dermatopharmacokinetic studies in man, *Pharm. Res.*Vol. 23, pp. 1850–1856.

[Isailović, 2016] Isailović, T., Đorđević, S., Marković, B., Ranđelović, D., Cekić, N., Lukić, M., Pantelić, I., Daniels, R., Savić, S., 2016, Biocompatible nanoemulsions for improved aceclofenac skin delivery: formulation approach using combined mixture-process experimental design, *J. Pharm. Sci*. Vol. 105, pp. 308–323.

[Klang, 2012] Klang, V., Schwarz, J.C., Lenobel, B., Nadj M., Auböck, J., Wolzt, M., Valenta, C., 2012, In vitro vs. in vivo tape stripping: validation of the porcine ear model and penetration assessment of novel sucrose stearate emulsions, *Eur. J. Pharm. Biopharm*. Vol. 80, pp. 604–614.

[Leal, 2017] Leal, L.B., Cordery, S.F., Delgado-Charro, M.B., Bunge, A.L., Guy, R.H., 2017,. Bioequivalence methodologies for topical drug products: in vitro and ex vivo studies with a corticosteroid and an anti-fungal drug, *Pharm. Res*. Vol. 34, pp. 730–737.

[Sekkat, 2002] Sekkat, N., Kalia, Y.N,, Guy, R.H., 2002, Biophysical study of porcine ear skin in vitro and its comparison to human skin in vivo, *J. Pharm. Sci*. Vol. 9, pp. 2376–2381.

APPLICATION OF LOWER PUNCH VIBRATION TO IMPROVE THE MECHANICAL STABILITY OF TABLETS

Alexander Kalies[1], Thomas Heinrich[2], Claudia S. Leopold[1]

[1]University of Hamburg, Division of Pharmaceutical Technology, Bundesstr. 45, 20146 Hamburg, Germany
Alexander.Kalies@uni-hamburg.de (corresponding author)
[2]Fette Compacting GmbH, Grabauer Str. 24, 21493 Schwarzenbek, Germany

ABSTRACT

A sufficient mechanical stability of tablets to be compacted prevents problems during tableting (e.g. sticking, capping, lamination) and is crucial with regard to further processing steps such as coating or packaging. Often, an improvement of the mechanical stability is only achievable by an adaption of the production settings (die disk speed) or an alteration of the powder blend composition. In the present study, a novel lower punch vibration device was developed and implemented on a rotary tablet press to improve the mechanical stability of the resulting tablets without changing the production conditions or the powder formulation. Various types of microcrystalline cellulose with different physical properties were selected. The powders were investigated concerning their powder flow, density, particle morphology and surface area and the tablets concerning their weight, tensile strength, and capping index. The results showed that externally applied lower punch vibration improved the mechanical stability of the investigated tablets beyond the adaption of the production settingss and the physical properties of the powder blend.

Keywords: Tableting, lower punch vibration, mechanical stability, lamination.

INTRODUCTION

The mechanical stability of a tablet is an important attribute and affects further handling steps of the tablet such as coating, packaging, and the end use by the patient. An insufficient mechanical stability of tablets is often caused by tablet failures such as capping or lamination. Capping describes the detachment of the top or bottom part of the tablet, whereas lamination is characterized by horizontal micro cracks [Mazel, 2015]. The reasons for the occurrence of these phenomena are complex and depend on the powder blend properties (deformation properties, relative density, compressibility) and/or the process settings (rotor speed, compaction force, tooling). In the past, only few solution approaches were introduced to reduce the capping or lamination tendency and to improve the mechanical stability of the tablet without changing the process conditions or altering the composition of the powder blend [Levina, 202]. A new promising approach to reduce or prevent tablet failures might be the application of externally lower punch vibration. Preliminary studies revealed that lower punch vibration during the die filling step enables the densification of the powder bed within the die leading to a different particle arrangement [Kalies, 2019]. Thus, the aim of the present study was to investigate in more detail the effect of external lower punch vibration under production conditions with regard to the mechanical stability of the resulting tablets.

RESEARCH CONCEPT

Materials

Microcrystalline cellulose (Parmcel 102, Parmentier, Germany; MC-12, Blanver, Brasilia; Vivapur® 200, JRS Pharma, Germany; Avicel® 301, FMC, USA), magnesium stearate (Lehmann & Voss, Germany).

Methods

Powder Characterization

According to the Ph. Eur., the bulk and tapped-density (jolting volumeter, Stav 2003, J. Engelsmann, Germany), the true density (helium pycnometer; AccuPyc 330; Micrometrics, Germany) and the relative density (bulk density / true density) were determined. The powder flow was characterized by the Hausner ratio, the compressibility index, and by ring shear cell measurements (RST-XS, Dr. Dietmar Schulze Schüttgutmesstechnik, Germany). Hence, the powder flow function (FFC) was examined at a mean consolidation stress of 5.0 kPa and calculated as follows:

$$\mathrm{FFC} = \frac{\text{Consolidation stress}}{\text{Unconfined yield strength}} \qquad (1)$$

In addition, the particle shapes were visualized with a scanning electron microscope (LEO 1525, Carl Zeiss, Germany) and the particle size distributions were determined with a laser diffractometer (Helios, Sympatec, Germany).

Tablet Characterization

The investigated tablets were analyzed with a multifunctional hardness tester (TBH 525; Erweka, Heusenstamm, Germany) with regard to their weight, thickness and crushing strength. Afterwards, the tensile strength (Eq. 2), and capping index (Eq. 3) were calculated.

$$\sigma = \frac{2 \cdot F}{\pi \cdot d \cdot t} \quad (2)$$

where F is the crushing force (N), d the tablet diameter (mm), and t the tablet thickness (mm).

$$\text{Capping Index} = \frac{(5 \cdot N_{op} + N_h)}{N_t} \quad (3)$$

where N_{op} is the number of capped/laminated tablets after tableting, N_h the number of capped/laminated tablets during hardness testing, and N_t the total number of investigated tablets.

Tableting

Tableting was performed in single punch mode on a Fette 102i rotary tablet press with 10 mm flat faced punches. An automatically rotating filling wheel was used as filling unit. Before tableting, 0.5 % (w/w) of magnesium stearate was added to the powder blends which were mixed for 3 min. The target tablet weight was approximately 300 mg for each powder blend. The vibration equipment, described by Kalies et al. [Kalies, 2018], was composed of a modified filling cam and an externally mounted pneumatic turbine vibrator (MTT 13; Mooser, Germany).

RESULTS

The determined physical powder properties are listed in Table 1.

Table 1: Physical properties of the investigated MCC types.

MCC Type	FFC	Hausner ratio	Relative density (g/cm³)	Particle size d_{50} (µm)
MCC 102	3.90	1.33	0.208	98.23
MCC 12	12.93	1.35	0.275	150.51
MCC 200	4.95	1.31	0.366	213.78
MCC 301	4.01	1.23	0.291	58.44

The resulting tensile strengths of the tablets manufactured conventionally and by application of lower punch vibration are displayed in Fig. 1A and B, respectively. Obviously, the tensile strength decreased distinctly at higher rotor speeds (Fig. 1A).

Application of externally lower punch vibration led to comparatively less pronounced decrease of the tensile strength (Fig. 1B) and it was possible to manufacture tablets with a sufficient tensile strength, even at high rotor speeds. The resulting tensile strengths of the tablets were obviously directly linked to the physical properties of the respective powder blends.

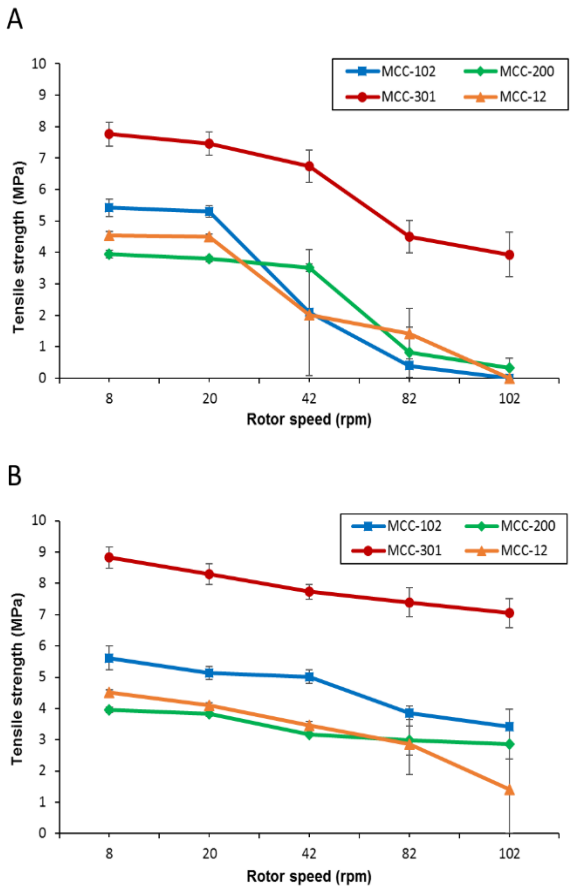

Fig. 1: Tensile strength of the investigated MCC tablet formulations depending on the applied rotor speed after conventional tableting (A) and by application of lower punch vibration (B) (means ± SD, n = 40).

The capping indices of the investigated MCC formulations are displayed in Fig 2. The results of the MCC-301 tablets are not shown, because no lamination occurred. In accordance with the results shown in Fig. 1A, the capping indices increased at higher rotor speeds during conventional tableting. In comparison, lower punch vibration was able to decrease the capping index and thus the lamination tendency to a significant extent even at high rotor speeds.

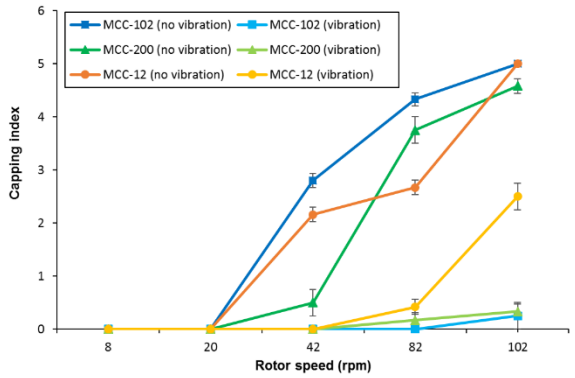

Fig. 2: Capping indices of the investigated MCC formulations depending on the applied rotor speed and the externally applied lower punch vibration (means ± SD, n = 20).

DISCUSSION

As shown in Fig. 1A, it was possible to manufacture tablets with sufficient tensile strength even at high rotor speeds by application of lower punch vibration. The applied lower punch vibration probably led to an enhanced die filling resulting in a more homogeneously and denser powder bed packing within the die. As a consequence of this "pre-densification" during the die filling process and prior to the main compaction step, the number of potential binding points and interparticle interactions between the particles increased, which ultimately led to an improved mechanical stability of the tablets. The lamination tendency was also distinctly decreased by the application of lower punch vibration (Fig. 2). This observation is attributed to the densification step of the powder bed within the die and the associated improved removal of entrapped air. The volume of entrapped air particularly depends on the physical powder properties and on the production settings (rotor speed). A low relative density in combination with a broad particle size distribution and needle shaped particles may increase the volume of entrapped air. Hence, a powder blend such as MCC-301 with a nearly spherical particle shape, a narrow particle distribution, a high relative density, and an adequate powder flow, showed a higher tensile strength and a less pronounced lamination tendency in comparison to MCC-102, MCC-12, and MCC-200. Furthermore, the removal of entrapped air is limited by the adjusted rotor speed.

CONCLUSIONS

In the present study, it was shown that the tensile strength as well as the lamination tendency of the tablets prepared from the investigated powder blends definitely depended on the physical properties of each powder blend. Moreover, the rotor speed and thus the resulting time for filling and compression strongly affected the mechanical stability of the prepared tablets. It is assumed that the application of external lower punch vibration during the die filling step and prior to the main compaction step leads to a pronounced increase of the tensile strength as well as a decrease of the capping index in comparison to conventional tableting. This is attributed to the removal of entrapped air and a rearrangement of the particles within the powder bed inside the die. Thus, external lower punch vibration might be a promising approach to improve the mechanical stability of tablets and to reduce or prevent capping or lamination during or after tablet manufacturing

ACKNOWLEDGMENT

The authors thank Gustav Parmentier, JRS and Blanver for the donation of the different MCC grades as well as Lehmann & Voss for providing magnesium stearate.

REFERENCES

[Mazel, 2015] Mazel, V., Busignies, V., Diarra, H., Tchoreloff., 2015, Lamination of pharmaceutical tablets due to air entrapment: direct visualization and influence of the compact thickness, *Int. J. Pharm*. Vol. 478, p.p. 702-704.

[Levina, 2002] Levina, M., Rubinstein, M.H., 2002, The effect of ultrasonic vibration on the compaction characteristics of ibuprofen, *Drug Dev. Ind. Pharm*. Vol. 28, p.p. 495–514.

[Kalies, 2019] Kalies, A., Özcoban, H., Leopold, C.S., 2019, Performance characteristics of a novel vibration technique for the densification of a powder bed within a die of a rotary tablet press - a proof of concept, *AAPS PharmSciTech*, Vol. 20, Article 148

[Kalies, 2018] Kalies, A., Özcoban, H., Leopold, C.S., 2018, Instrumentation of a lower punch vibration equipment on a rotary tablet press for enhanced die filling. *11th World PBP Meeting*, Granada, Spain

ENGINEERING YEAST FOR PRODUCTION OF BENZOPHENONES AND XANTHONES AS PRECURSORS OF POLYCYCLIC POLYPRENYLATED ACYLPHLOROGLUCINOLS

Benye Liu[1, 2], Lars Fabian Kalz[1], Yizhen Jia[1], Marco Grull[1, 2], Till Beuerle[1, 2], Ludger Beerhues[1, 2]

[1] Institute of Pharmaceutical Biology, Technische Universität Braunschweig, Mendelssohnstrasse 1, 38106 Braunschweig, Germany; [2]Center of Pharmaceutical Engineering (PVZ), Technische Universität Braunschweig, Franz-Liszt-Strasse 35a, 38106 Braunschweig, Germany; emial: b.liu@tu-bs.de

ABSTRACT

Polycyclic polyprenylated acylphloroglucinols (PPAPs) exhibit a broad range of biological activities, such as antidepressant, antibacterial, antiviral and antitumor properties. The content of PPAPs in the producing plants is often quite low, and their complex structures make total chemical synthesis difficult and economically impractical. Progresses in synthetic biology provide an alternative approach for the production of these valuable compounds. Here we present our results on reconstruction of the biosynthetic pathways of PPAP precursors in yeast. Based on our previous works on the biosynthesis of PPAPs, genes involved in the formation of benzophenones and xanthones from *Hypericum sp*. and other organisms were expressed in yeast either episomally or by integration into the genome. The production of the expected products reached around 0.5 mg/l, which is high enough to be the substrate for enzymes of subsequent biosynthetic steps. The yeast strains will be further engineered by introducing various prenyltransferase enzymes to reconstruct the full biosynthetic pathways of PPAPs.

Keywords: benzophenone, xanthone, yeast, prenyltransferase, synthetic biology

INTRODUCTION

Polycyclic polyprenylated acylphloroglucinols (PPAPs) are a group of structurally fascinating and synthetically challenging plant secondary products, which exhibit a broad range of biological activities, such as antidepressant, antibacterial, antiviral and antitumor properties [Yang, 2018]. The biosynthesis of PPAPs involves both the type III polyketide pathway and the terpenoid pathway. The acylphloroglucinol cores of PPAPs are produced via a characteristic type III polyketide biosynthesis process involving the condensation of one acyl-CoA and three malonyl-CoAs to form a tetraketide intermediate, which in turn cyclizes and aromatizes to yield acylphloroglucinols. Prenylation of this core structure and further cyclization of the prenyl side chains afford different PPAPs with diverse carbon skeletons. The type of acyl group, the number and position of isoprenyl residues, the degree of oxidation of isoprenyl side chains and the corresponding locations of ether rings as well as different types of secondary cyclizations (such as aldol, Diels−Alder, etc.) create PPAPs' structural diversity and complexity.

PPAPs have been exclusively isolated from plants of the families Hypericaceae and Clusiaceae, mainly from the genera *Hypericum* and *Garcinia* with only few exceptions [Fiesel, 2015]. The content of PPAPs in the producing plants is often quite low, and their complex structure makes total chemical synthesis very difficult and in general economically impractical because of the low yield. Recent progresses in synthetic biology provide an alternative approach for the production of these valuable compounds. For example, artemisinic acid, the precursor of the antimalarial drug artemisinin, was successfully produced in engineered yeast cells with a yield of 25 g/l. Here we present our results of reconstruction of the biosynthetic pathways of benzophenone and xanthone in yeast.

RESEARCH CONCEPT

Plasmid construction and yeast strains: *HpPKS006* is a type III polyketide synthase gene cloned from *Hypericum perforatum*, which has both benzophenone synthase (BPS) and isobutyrophenone synthase (IBS) activities [unpublished]. *RpBZL* is a benzoyl-CoA ligase gene from *Rhodopseudomonas palustris* [Egland, 1995]. *HcTXS* and *HcX6H* are xanthone synthase and xanthone 6-hydroxylase from *H. calycinum*, respectively [El-Awaad, 2016]. *HpPT8* is a xanthone prenyltransferase [Fiesel, 2015]. Yeast strains used are INV*Sc*1 (Invitrogen), CEN.PK102-5B

[Entian, 2007] and DD104, which contains down-regulation of endogenous farnesyl pyrophosphate synthase, ERG20, by site-directed mutation of K197G, proven to provide more free IPP/DMAPP and GPP [Fischer, 2011, Li, 2015]. Genome intergration was carried out using integrative EasyClone vectors with auxotrophic selection markers [Jensen, 2014].

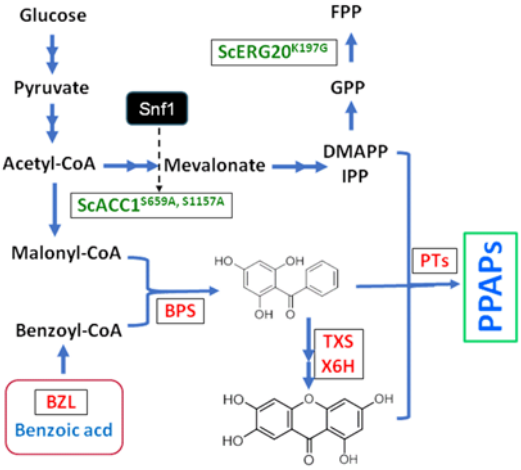

Fig. 1 Schematic illustration of the reconstruction of PPAP biosynthetic pathways in yeast. The endogenous yeast genes are in green, exogenous genes are in red.

Reconstruction of benzophenone and xanthone biosynthetic pathways in yeast: *HpPKS006* and *RpBZL* were subcloned into the vector pESC-URA (Agilent Technologies), *HcTXS* and *HcCPR* (cytochrome P450 reductase gene from *H. calycinum*) were subcloned into the vector pESC-LEU. *HcX6H* and *HpPT8* were subcloned into the vector pESC-HIS. The promoters of all the pESC vectors were changed to the constitutive promoter TEF1-PGK1.

Different combinations of the constructs were co-transformed into appropriate yeast strains using a high efficiency lithium acetate transformation protocol [Gietz, 2007]. The resulting positive yeast clones, after being verified by PCR, were cultured in 10 ml of synthetic dextrose dropout medium (-Leu, -His, -uracil) with D-glucose as the carbon source at 30°C and 200 rpm shaking for 36 hours. Then, the yeast cells were diluted into 20 ml of different media to OD_{600} 0.05 and cultured at the same conditions. Benzoic acid was added at different time points with a final concentration of 3.5 mM. One ml of yeast cultures were taken at different time points, extracted twice with the same volume of ethyl acetate. Extracts were combined and dried under a stream of nitrogen, the residues were dissolved in 50% (v/v) methanol for HPLC-DAD analysis. The product peaks were collected from HPLC and analyzed by LC-MS. The content of target compounds in the samples was quantified based on calibration curves of authentic references.

RESULTS

Selection of culture medium: Among the three common yeast culture media, YPD is the best for both growth and product formation (Table 1). There are no significant differences between episomal expression and genome integration of the pathway genes.

Table 1 Kinetics of growth and benzophenone production in YPD, YPGE and SGI media

Medium	Strain	μ_{max} (h^{-1})	OD_{30h} (rel. AU)	r (μg^{-1h-1})	Cmax ($\mu g\ l^{-1}$)
YPD	genome	0.389	16.60	12.5	180
	episomal	0.386	13.62	12.8	230
YPGE	genome	0.195	3.24	1.7	60
	episomal	0.190	3.50	1.1	40
SGI	genome	0.290	3.14	0	0
	episomal	0.250	2.80	0	0

Production of expected compounds: The engineered yeast strains produced the expected products at a level of 0.1 mg/l without feeding benzoic acid in yeast strain INVSc1. Feeding exogenous benzoic acid increased the 2,4,6-trihydroxybenzophenone yield by a factor of 4 (Fig. 2). In contrast, yeast strain DD104 produced product only without feeding benzoic acid. Adding benzoic acid to a final level of 0.15 mM abolished product formation completely (data not shown).

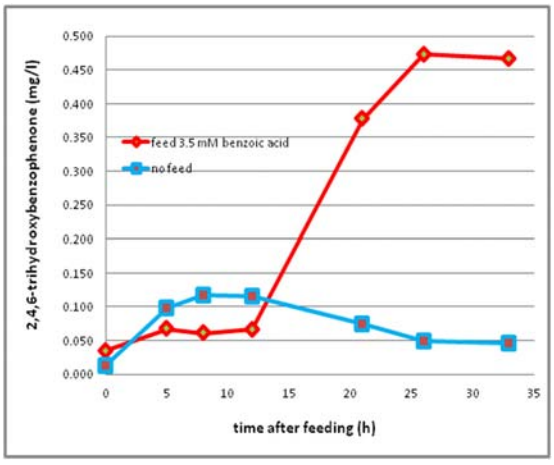

Fig. 2 Feeding benzoic acid increased the production of 2,4,6-trihydroxybenzophenone in yeast strain INVSc1 episomally over-expressing *HpPKS006* and *RpBZL* and grown in flask cultures.

DISCUSSION

Here we successfully reconstructed the benzophenone and xanthone biosynthetic pathway in yeast using constitutive promoters, which simplify the production procedure by eliminating the induction step. There was no significant difference between the episomal expression and the genome integration in terms of both growth and product formation, indicating that the pathways are independent of the copy number of the genes. A similar result has also been found in the production of resveratrol in engineered yeast [Li, 2016]. The formation of benzophenone and xanthone proceeded by a growth-dependent manner, which has also been reported for resveratrol engineering works [Vos, 2015].

Although there is no information about benzoic acid metabolism in yeast, the fact that the engineered yeasts produce benzophenone and xanthone without feeding benzoic acid indicates that endogenous benzoic acid exists in yeast. The engineered benzophenone and xanthone biosynthesis process in yeast is a *de novo* production system. Further modification of the benzoic pathway may be helpful for increasing the product yield.

Co-expressing *HpPT8* in the xanthone producing yeast strain failed to produce detectable amounts of prenylated xanthone, indicating that more optimization works are needed to enable the correct function of prenyltransferase activity in yeast, as shown previously by bitter acid biosynthesis in yeast [Li, 2015].

CONCLUSIONS

Engineered yeast strains produce the core structures of PPAPs at yields of around 0.5 mg/l. This amount is sufficient to serve as substrate for the downstream prenyltransferase enzymes, which have *K*m values at approx. 200 µM. Thus, the strains so far generated can serve as the host strains for further reconstructing the complete pathways of PPAPs, which then may be available in sufficient quantities for the detailed assaying of their biological activities.

ACKNOWLEDGMENT

The authors thank Dr. Irina Borodina from the Technical University of Denmark for providing the EasyClone vectors and helpful discussions. Thanks are also given to the Bachelor students David Quast and Henning Ummethum for their efforts to over-express PKS006 in yeast.

REFERENCES

Egland, P.G., Gibson, J. and Harwood, C.S., 1995, Benzoate coenzyme A ligase, encoded by BADA, is one of 3 ligases able to catalyze benzoyl-coenzyme A formation during anaerobic growth of *Rhodopseudomonas palustris* on benzoate. *J. Bacteriol.*, Vol. 177, pp. 6545–6551.

El-Awaad, I., Bocola, M., Beuerle, T., Liu, B. and Beerhues, L., 2016, Bifunctional CYP81AA proteins catalyse identical hydroxylations but alternative regioselective phenol couplings in plant xanthone biosynthesis. *Nat. Commun.*, Vol. 7, pp. 11472.

Entian, K.D. and Kötter, P., 2007, Yeast genetic strain and plasmid collections. *Method Microbiol.*, Vol. 36, pp. 629–666.

Fiesel, T., Gaid, M., Müller, A., Bartels, J., El-Awaad, I., Beuerle, T., Ernst, L., Behrends, S. and Beerhues, L., 2015, Molecular Cloning and Characterization of a Xanthone Prenyltransferase from *Hypericum calycinum* Cell Cultures. *Molecules*, Vol. 20, pp. 15616-15630.

Fischer, M.J., Meyer, S., Claudel, P., Bergdoll, M. and Karst, F., 2011, Metabolic engineering of monoterpene synthesis in yeast. *Biotechnol Bioeng*., Vol. 108, pp. 1883–1892.

Gietz. R.D. and Schiestl, R.H., 2007, High-efficiency yeast transformation using the LiAc/SS carrier DNA/PEG method. *Nat. Protoc.*, Vol. 2, pp. 31–34.

Jensen, N.B., Strucko, T., Kildegaard, K.R., David, F., Maury, J., Mortensen, U.H., Forster, J., Nielsen, J. and Borodina, I., 2014, EasyClone: method for iterative chromosomal integration of multiple genes in *Saccharomyces cerevisiae*. *FEMS Yeast Res.*, Vol. 14, pp. 238-248.

Li, H.,Ban, Z., Qin, H., Ma, L., King, A.J. and Wang, G., 2015, A heteromeric membrane-bound prenyltrans-ferase complex from hop catalyzes three sequential aromatic prenylations in the bitter acid pathway. *Plant Physiol.*, Vol. 167, pp. 650-659.

Li, M., Schneider, K., Kristensen, M., Borodina, I. and Nielsen, J., 2016, Engineering yeast for high-level production of stilbenoid antioxidants. *Sci Rep*., Vol. 11, pp. 36827.

Vos, T., de la Torre Cortes, P., van Gulik, W.M., Pronk, J.T. and Daran-Lapujade, P., 2015, Growth-rate dependency of *de novo* resveratrol production in chemostat cultures of an engineered *Saccharomyces cerevisiae* strain. *Microb Cell Fact.*, Vol. 14, pp. 133.

Yang, X.W., Grossman, R.B. and Xu, G., 2018, Research Progress of Polycyclic Polyprenylated Acylphloroglucinols. *Chem Rev*., Vol. 118, pp. 3508-3558.

THE EXTENDED ELUTION BY CHARACTERISTIC POINT METHOD TO DETERMINE ADSORPTION ISOTHERMS OF LABYRINTHOPEPTIN FOR PURIFICATION VIA ION-EXCHANGE CHROMATOGRAPHY

Jonas Lohr[1*], Dave Hartig[2*], Stephan Scholl[2], Antje Spieß[1]

[1] Technische Universität Braunschweig, Institute of Biochemical Engineering, Rebenring 56, 38106 Braunschweig

[2] Technische Universität Braunschweig, Institute for Chemical and Thermal Process Engineering, Langer Kamp 7, 38106 Braunschweig

[*]both authors contributed equally

ABSTRACT

Ion-exchange chromatography (IEC) is the most frequently used technique to purify proteins and therefore, plays an important role in process development for therapeutical proteins. To improve the purification using ion-exchange chromatography, adequate characterization of adsorption isotherms is obligatory. The Elution by Characteristic Point method (ECP) can be used to determine adsorption isotherms applying only minor amounts of sample material to the chromatography column. Here, the applicability of the extended ECP method to determine adsorption isotherms of the model protein bovine serum albumin (BSA) using bovine hemoglobin (bHb) as tracer substance to quantify all non-idealities of the system is shown. The resulting isotherm was validated using the static batch approach. In the next step, the gained knowledge is used to measure isotherms of Labyrinthopeptins A1 and A2, which show promising activity against retroviruses like *herpes simplex virus* or *human immunodeficiency virus*.

Keywords: Adsorption isotherm, Elution by Characteristic Point, Ion-Exchange Chromatography, Labyrinthopeptin

INTRODUCTION

The market for biopharmaceuticals is still growing, reaching the highest number of new approvals since 1996 in 2017 [Morrison, 2018]. In the same year sales of biopharmaceuticals reached 188 billion US$ with monoclonal antibodies alone combining for 65.6% of total sales [Morrison, 2018; Walsh, 2018].

General production schemes for biopharmaceuticals consist of the production of the target product using mammalian cells or microorganisms and subsequent downstream processing. Chromatography is the most frequently used technique for the purification of biopharmaceuticals. For industrial applications, 45% of all chromatographic purification steps are ion-exchange chromatography steps [Karlsson, 2011]. This implies the important role IEC plays in the production of biopharmaceuticals. However, chromatographic purification processes are still expensive making downstream processing with up to 80% of the overall process costs the most cost-intensive part in the production of biopharmaceuticals [Roque, 2004]. Hence, one should focus on finding efficient and therefore economic operation points for a specific chromatographic separation task.

Lanthipeptides, post-translationally modified peptides with a characteristic polycyclic structure, are such a promising group of biopharmaceuticals showing high potential against retroviruses *in vitro* [Meidl, 2010], but with large differences in their potential [Férir, 2013]. For example, Labyrinthopeptin A1 is 10-fold more potent against *herpes simplex virus* and *human immunodeficiency virus* than Labyrinthopeptin A2 making a separation of these peptides desireable. IEC is a very promising separation technique as shown for nisin, another prominent lanthipeptide [Abts, 2010].

A deep understanding of the interaction between peptides and stationary phase under various process conditions is needed to account for variations in the fermentation broth fed into the downstream processing. Hence, the characterization of adsorption isotherms is

essential for process development. While a variety of methods has been described in literature to determine adsorption isotherms experimentally, only the dynamic so-called Elution by Characteristic Point (ECP) method offers the possibility to gain complete isotherm data with just one experiment leading to smallest consumption of substance [Seidel-Morgenstern, 2004]. This low demand is a crucial advantage as the targeted peptides A1 and A2 are not commercially available but have to be produced and purified specifically for adsorption experiments. One of the most limiting factors for ECP, especially in early stage development, is the need for a high number of theoretical stages to provide accurate isotherm data. This limitation was recently overcome by an Extended Elution by Characteristic Point (EECP) method, where non-idealities of the system, *e.g.*, convection, dispersion or low number of theoretical plates are quantified by using a specific marker substance [Hartig 2015].

In this work, EECP is transferred to the system of labyrinthopeptins and ion-exchange resins. To this end, the cheap and easy available proteins BSA and bHb are used as model substances to characterize the required process conditions to generate adsorption isotherms and to understand occurring problems and limitations. Then, the knowledge is used to measure adsorption isotherms of labyrinthopeptins on ion-exchange resins.

THEORY

This section gives a brief summary of the derivation and use of EECP [Hartig, 2015]. The standard equilibrium model of chromatography neglects dispersion and assumes instantaneous adsorption equilibrium between the bulk fluid phase and the particle at every axial position. While the equilibrium assumption can be fulfilled by using low flow rates and small particle diameters, neglecting the axial dispersion leads to the need of a high number of theoretical plates in classical ECP. In contrast, EECP method assumes that all non-idealities, *e.g.*, non-rectangular injection profile and axial dispersion, are linearly independent from the effects of adsorption and can be determined by a tracer injection. Hence, all non-ideal influences are lumped into a concentration-dependent system dead volume V_S that is subtracted from the retention volume of the adsorptive V_R. Then, the loading is calculated using this corrected retention volume ($V_R - V_S$):

$$q(c_i) = \frac{c_{i,max}}{m_{Ad}} \int_0^{c_i^\circ} \left(V_R(\tilde{c}_i^\circ) - V_S(\tilde{c}_i^\circ) \right) d(\tilde{c}_i^\circ) \qquad (1)$$

$$c_i^\circ = \frac{c_i}{c_{i,max}} \quad c_j^\circ = \frac{c_j}{c_{j,max}} \qquad (2)$$

It is worth stressing that c_i° and c_j° represent the normalized concentrations of the adsorbing and the tracer substance, respectively. Both concentration profiles are normalized for comparability.

RESULTS AND DISCUSSION

As discussed in the last section, the application of EECP requires the flow rate to be small enough to allow for an establishment of equilibrium between bulk liquid and stationary phase. Hence, Fig. 1 shows the influence of the superficial velocity on the determined Henry coefficient for BSA vs bHb defined by:

$$H = \frac{V_{BSA} - V_{bHb}}{m_{Ad}} \qquad (3)$$

The superficial velocity was corrected for a decreased available cross section due to partial blocking of the bed as determined by total porosity measurements using glucose as tracer (see [Hartig, 2017] for further details on porosity measurement). It becomes obvious that the superficial velocity should not exceed 10 mm/min to allow neglecting kinetic effects.

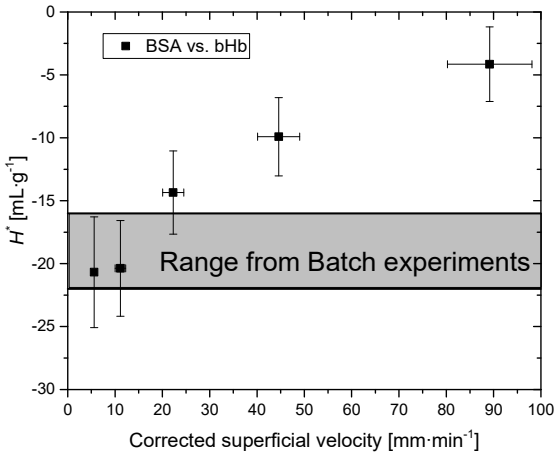

Figure 1: Henry coefficient between BSA and bHb on Q Sepharose FF at 25 °C in 20 mM sodium phosphate buffer (ph 7) determined by retention time of peak maximum at varying superficial velocity. Concentration of BSA and bHb was approximately 7 µM and 10 µM, respectively. Volumetric flow was varied between 25 µL/min and 400 µL/min. Data from [Hartig, 2017].

Besides the use of a feasible small flow rate, two additional factors had to be included to determine BSA isotherms. First, only 35% of the expected total porosity were measured leading to a correction of the mass of adsorbent to only 35% of the mass weighted into the column. Second, bHb showed a measureable

adsorption at the applied conditions. Hence, the slope of the bHb isotherm was determined in batch experiments (data not shown) and this slope was added to the BSA isotherm. With these corrections, the adsorption isotherms of BSA were determined. This is exemplary shown at 25 °C in Fig. 2.

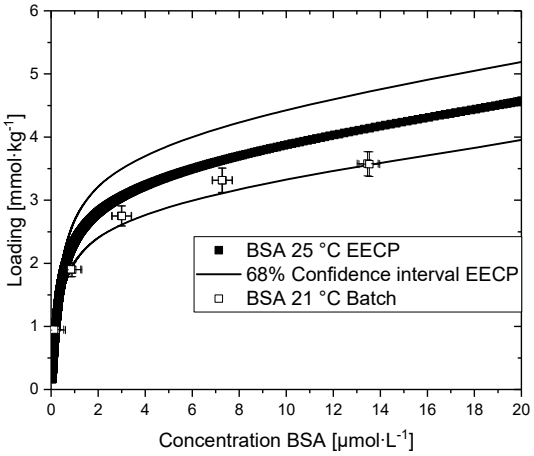

Figure 2: Adsorption isotherm of BSA at 25 °C in 20 mM sodium phosphate buffer (ph 7), bHb was used as tracer. Data from [Hartig, 2017].

A good agreement between the results of batch and EECP measurements can be seen. Size exclusion effects that could not be totally ruled out due to the different shape of BSA and bHb might cause the small deviation at higher concentrations. This stresses the importance to find feasible tracers for the particular adsorptive. With respect to used material, static adsorption experiments needed about 37 mg BSA whereas one EECP isotherm was measured with only 12 mg BSA. Although the calibration of the detector and the determination of a feasible flow rate lead to an additional consumption of about 25 mg BSA, recalibration is not necessary for the investigation of other conditions like different buffer concentrations or temperatures. Overall, EECP might reduce the material needed by nearly 70% for all further isotherms compared to batch.

The behavior of the small peptides Labyrinthopeptin A1 and A2, having molecular masses of 2.072 kDa and 1.922 kDa, respectively, might differ notably from the larger protein BSA (66.5 kDa) due to increased diffusion coefficient but also increased diffusion path inside the porous matrix. Hence, adjustment of the experimental conditions is mandatory to fulfill the equilibrium assumption before conducting EECP measurements. As indicated in Fig. 3, superficial velocities below 10 mm/min should be chosen for Labyrinthopeptin A1 to ensure establishment of equilibrium. It is worth noting that the similar value compared to BSA should rather be seen as coincidence since the impact of smaller molecule size on diffusion kinetic is complex. The retention coefficient can be calculated using the retention volume at the peak maximum:

$$k' = \frac{V_R - V_T}{V_T} \quad (4)$$

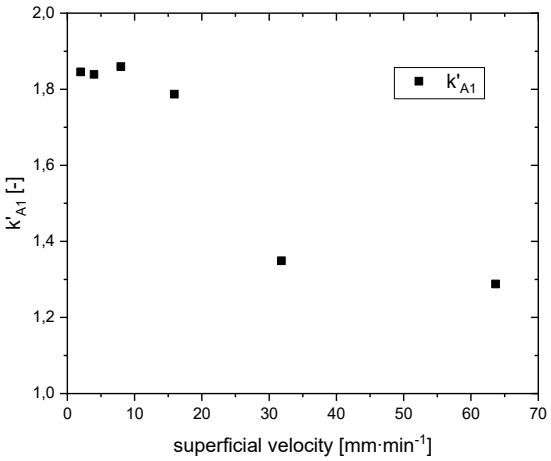

Figure 3: Retention coefficient of Labyrinthopeptin A1 on Q Sepharose FF at 25 °C in 20 mM Bis-Tris buffer (ph 7) with 200 mM sodium chloride at varying superficial velocities.

CONCLUSION AND OUTLOOK

The extended Elution by Characteristic Point method is a rapid approach to determine adsorption isotherms consuming only small amounts of sample material. This was successfully shown for model proteins BSA and bHb on Q Sepharose FF, where a good correlation to the well-established batch method can be seen.

Since the method has been established for the model proteins BSA and bHb and crucial process parameters for the determination of adsorption isotherms for labyrinthopeptins on Q Sepharose FF have been characterized, isotherm data for A1 and A2 will be generated in future experiments.

NOMENCLATURE

c	concentration, mg/L
k’	retention coefficient, 1
m	mass, mg

q	loading of adsorbent, mg/mg
V	volume, mL
BSA	bovine serum albumin
bHb	bovine hemoglobin
ECP	elution by characteristic point
IEC	ion-exchange chromatography

SUBSCRIPT

°	normalized
0	initial
A1	Labyrinthopeptin A1
Ad	adsorbent
i	solute
j	marker
max	maximum
R	retention
T	total

REFERENCES

[Abts, 2018] Abts, A., Mavaro, A., Stindt, J., Bakkes, P. J., Metzger, S., Driessen, A. J., Smith, S. H. M., & Schmitt, L. (2011). Easy and rapid purification of highly active nisin. *International Journal of Peptides,* 2011.

[Férir, 2013] Férir, G., Petrova, M. I., Andrei, G., Huskens, D., Hoorelbeke, B., Snoeck, R., Vanderleyden, J., Balzarini, J., Bartoschek, S., Brönstrup, M., Süssmuth, R. D., & Schols, D. (2013). The lantibiotic peptide labyrinthopeptin A1 demonstrates broad anti-HIV and anti-HSV activity with potential for microbicidal applications. *PloS One,* 8(5), e64010.

[Hartig 2015] Hartig, D., Waluga, T., & Scholl, S. (2015). Expanding the elution by characteristic point method to columns with a finite number of theoretical plates. *Journal of Chromatography A*, *1413*, 77-84.

[Hartig, 2017] Hartig, D., Waluga, T., Schmidt, C., Fieg, G., & Scholl, S. (2017). Extended elution by characteristic point method for characterization of protein ion-exchange adsorption. *Chemical Engineering & Technology*, *40*(10), 1940-1945.

[Karlsson, 2011] Karlsson, E., & Hirsh, I. (2011). Ion exchange chromatography. *Protein Purification: Principles, High Resolution Methods, and Applications (Vol. 151), John Wiley & Sons,* 93-134.

[Meindl, 2010] Meindl, K., Schmiederer, T., Schneider, K., Reicke, A., Butz, D., Keller, S. & Brönstrup, M. (2010). Labyrinthopeptins: a new class of carbacyclic lantibiotics. *Angewandte Chemie International Edition*, 49(6), 1151-1154.

[Morrison, 2018] Morrison, C. (2018). Fresh from the biotech pipeline--2017. *Nature Biotechnology, 36(2)*, 131-137.

[Roque, 2004] Roque, A. C. A., Lowe, C. R., & Taipa, M. Â. (2004). Antibodies and genetically engineered related molecules: production and purification. *Biotechnology Progress, 20(3),* 639-654.

[Seidel-Morgenstern, 2004] Seidel-Morgenstern, A. (2004). Experimental determination of single solute and competitive adsorption isotherms. *Journal of Chromatography A*, *1037*(1-2), 255-272.

[Walsh, 2018] Walsh, G. (2018). Biopharmaceutical benchmarks 2018. *Nature Biotechnology*, *36*, 1136-1145

SOLVATION FREE ENERGY PREDICTIONS FROM MOLECULAR DYNAMICS SIMULATIONS BY IMPROVED ALCHEMICAL PATHWAYS AND OPTIMIZED FORCE FIELD PARAMETERS

A. Mecklenfeld[1,2], G. Raabe[1*]

[1] Institut für Thermodynamik, TU Braunschweig, Hans-Sommer-Str. 5, 38106 Braunschweig
[2] Center of Pharmaceutical Engineering, TU Braunschweig, Franz-Liszt-Str. 35a, 38106 Braunschweig

g.raabe@tu-braunschweig.de

ABSTRACT

The rapid development of affordable medications relies on the knowledge of suitable solvents for potential active pharmaceutical ingredients. Molecular simulations can be interpreted as computational experiments and may complement laboratory experiments, as they not only enable the calculation of thermophysical properties but also allow for an insight into a systems behavior on the molecular level. Relative solubilities can be predicted by using molecular simulations to calculate the Gibbs free energy of solvation ΔG_{solv}. We developed algorithms to reduce the required computational effort and increase the statistical precision by improved alchemical pathways. However, the agreement between ΔG_{solv} predictions from simulations and experimental data depends on the molecular models (force fields) used. To consider polarization effects, we combined partial charges derived by the IPolQ-Mod method with the General Amber Force Field (GAFF) and found a comparable ΔG_{solv} accuracy to GAFF and its default RESP charges for a large set of compounds in various solvents. We initiated a parameter optimization to improve the accuracy of GAFF/IPolQ-Mod and present our current results of the refitting process.

Keywords: Molecular simulation, solvation free energy, force field optimization

INTRODUCTION

Molecular simulations, e.g. with the Gromacs (Abraham et al. 2015) software, can complement laboratory experiments, as they not only allow for the calculation of thermophysical properties but also for the qualitative assessment of a systems behavior on the molecular level. A property of special interest is the Gibbs free energy of solvation ΔG_{solv}, which is fundamental for the calculation of e.g. relative solubilities, partition coefficients or activity coefficients. ΔG_{solv} characterizes the isothermal isobaric change of states of a solute molecule that transitions from a vacuum into a condensed phase. The corresponding change in free energy describes the strength of the solute/solvent interactions as well as the impact of entropic effects. For accurate free energy results, the thermodynamic end states, i.e. solute in vacuum and solvent phase respectively, need to exhibit sufficient configurational space overlap. In practice, a linking chain of intermediate states with scaled solute/solvent interactions, the so called alchemical pathway, is constructed. It allows for overlap between neighboring states and partial free energy results are summed for the total outcome. However, while a large number of intermediates enables good overlap and high statistical precision, the required computational effort increases with the number of intermediates.

On the other hand, ΔG_{solv} results strongly depend on the molecular models (so called force fields) applied. Widely used force fields (Wang et al. 2004; Vanommeslaeghe et al. 2010; Jorgensen et al. 1996) for the description of drug-like molecules assign fixed partial charges to the atomic sites. Consequently, these force fields are not capable to consider important polarization effects. For an at least implicit representation of polarization effects, we combined the IPolQ-Mod (Muddana et al. 2014) partial charge calculation method with the General Amber Force Field (GAFF) (Wang et al. 2004) and compared the ΔG_{solv} results to those obtained with GAFF but with the default RESP (Bayly et al. 1993) charge calculation method. In a previous study (Mecklenfeld und Raabe 2017a), we found comparable agreement between results with GAFF/RESP and GAFF/IPolQ-Mod to experimental data and concluded that GAFF/IPolQ-Mod is a suitable basis for the application of the physically motivated IPolQ-Mod method. However, as the alteration of the charge calculation method perturbs the self-consistency of the GAFF model, we also proposed the optimization of relevant atom types in various chemical environments in order to improve the ΔG_{solv} predictions.

RESEARCH CONCEPT

OPTIMIZATION OF THE NUMBER AND DISTRIBUTION OF INTERMEDIATES STATES

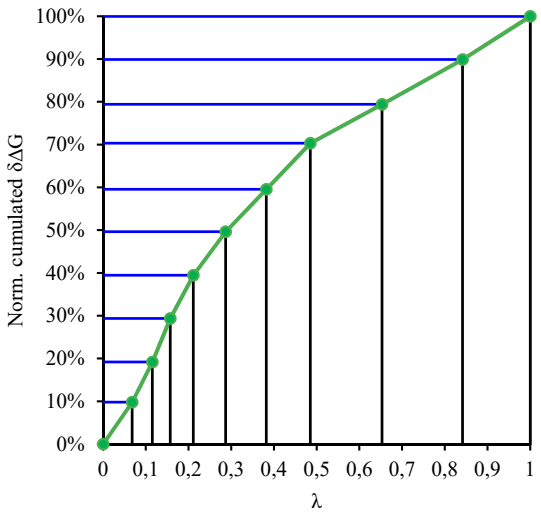

Fig. 1. Curve progression of normalized cumulated partial uncertainties with regard to λ. At the end of the λ state optimization, the objective of equal partial uncertainties, represented by equidistantly spaced cuts with the ordinate axis (blue lines), is well meet.

Intermediates states are characterized by λ-scaled solute/solvent interactions, whereas λ=0 equals no solute/solvent interactions (solute in vacuum) and λ=1 corresponds to full interactions in the condensed phase. By defining a vector of λ values between 0 and 1, configurational space overlap can be established. The solvation free energy difference is thereby split into partial results $\Delta G_{solv,i,i+1}$ between states λ_i and λ_{i+1}, which are summed for the total outcome. A priori, a suitable number or distribution of λ states is unknown and thus sufficient configurational space overlap is often accomplished by using a large number of intermediates.

As each partial result $\Delta G_{solv,i,i+1}$ contributes to ΔG_{solv}, our optimization goal is to ensure even partial uncertainties $\delta\Delta G_{solv,i,i+1}$ for improved statistical precision of the overall ΔG_{solv} result. We developed algorithms that allow for the adaptation of the number and distribution of the intermediates by a series of short trial simulations (Mecklenfeld und Raabe 2017b). As illustrated in Figure 1, cumulated partial uncertainties are interpreted as a function of λ. Using interpolation, new λ states can be defined to ensure the same level of statistical precision for all intermediate results. The configurational space overlap is analyzed after each of the short simulations and empirically derived algorithms adapt the number of intermediates if the overlap is considered to be insufficient or too excessive. After the number and distribution of intermediates converged, the actual production phase is initiated.

CALCULATION OF PARTIAL CHARGES

The IPolQ method is an abbreviation for “Implictly Polarized Charges” and was proposed by Cerutti et al. (Cerutti et al. 2013). The approach was later simplified by Muddana et al. and named IPolQ-Mod accordingly. Using ab initio calculations in Gaussian (Frisch et al. 2009), molecule geometries are optimized at the HF/6-31G* level of theory. Partial charges for the solute molecule are calculated both in the vacuum and condensed phase at the MP2/aug-cc-pVDZ level of theory and charges from both phases are then averaged. For the description of charges in the solvent, the PCM model by Mennucci et al. (Mennucci et al. 1998) is employed. For default GAFF charges, the HF/6-31G* level is applied. All partial charges are derived by a two-level RESP scheme.

OPTIMIZATION OF ATOM TYPES

For the optimization of Lennard-Jones parameters ε_{ii} and σ_{ii} for relevant atom types, we employed the robust Nelder-Mead (Nelder und Mead 1965) algorithm and use an objective function that considers weighted normalized root mean square deviations for solvation free energies and densities of the pure compounds. To reduce the computational effort, we utilize a thermodynamic cycle for the parameter optimization process. The training data set includes 358 solvation free energy results and 286 densities in a broad temperature range for a multitude of model compounds and chemical environments to account for prominent functional groups in potential drug candidates.

RESULTS AND DISCUSSION

In Figure 2, solvation free energies from GAFF/RESP and GAFF/IPolQ-Mod are plotted versus the corresponding experimental data. The figure demonstrates comparable accuracies for the different charge calculation methods, though specific outliers exists for both.

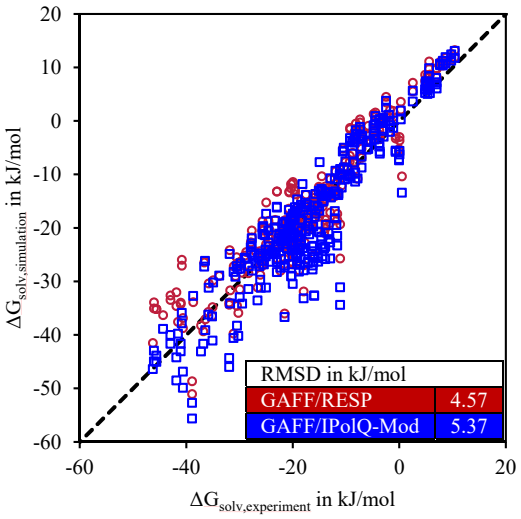

Fig. 2. Solvation free energy results from GAFF/RESP and GAFF/IPolQ-Mod over experimental data.

Simulation results for the ongoing optimization of atom types (ch2, ch3, ca, oh, ohP, os and cl already considered) are depicted in Figure 3. The figure highlights the improved agreement between ΔG_{solv} results using GAFF/IPolQ-Mod + LJ-refit and experimental data compared to the GAFF/RESP and GAFF/IPolQ-Mod models.

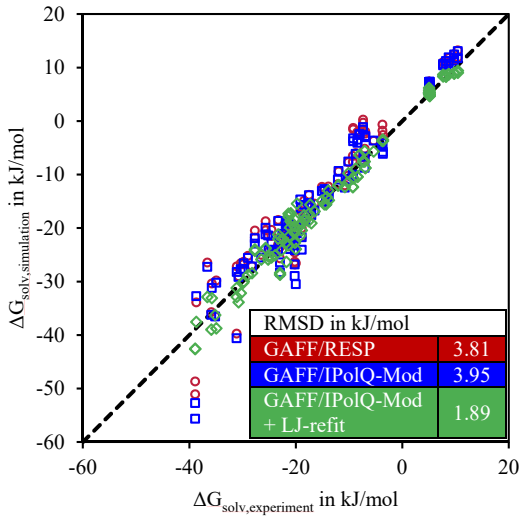

Fig. 3. Solvation free energy results from GAFF/RESP, GAFF/IPolQ-Mod and GAFF/IPolQ-Mod with refitted Lennard-Jones parameters over experimental data.

CONCLUSIONS

Molecular simulations are capable to complement laboratory experiments. The precise prediction of solvation free energies for the estimation of relative solubilities requires sufficient configurational space overlap for the ΔG_{solv} results to converge, and accurate molecular models for the description of the molecule interactions. We have developed methods to ensure statistical precise free energy results with reduced computational effort, and studied the impact of IPolQ-Mod partial charges for an implicit representation of polarization effects on the GAFF model compared to the default force field charges.

Though IPolQ-Mod adds physical details to the model, the charge scheme perturbs the self-consistency of the force field. We therefore optimize Lennard-Jones parameters of GAFF atom types for IPolQ-Mod partial charges, and our results demonstrate significantly improved agreement with experimental data.

Suitable molecular models for exact predictions of solvation free energies and linked thermophysical properties may improve the understanding of solubility processes in order to reduce the effort for the development of medications.

ACKNOWLEDGMENT

The study is funded by a Georg-Christoph-Lichtenberg grant. All simulations were performed on a cluster of the North-German Supercomputing Alliance (HLRN). We greatly appreciate the support.

REFERENCES

Abraham, Mark James; Murtola, Teemu; Schulz, Roland; Páll, Szilárd; Smith, Jeremy C.; Hess, Berk; Lindahl, Erik (2015): GROMACS. High performance molecular simulations through multi-level parallelism from laptops to supercomputers. In: *SoftwareX* 1-2, S. 19–25. DOI: 10.1016/j.softx.2015.06.001.

Bayly, Christopher I.; Cieplak, Piotr; Cornell, Wendy; Kollman, Peter A. (1993): A well-behaved electrostatic potential based method using charge restraints for deriving atomic charges. The RESP model. In: *J. Phys. Chem.* 97 (40), S. 10269–10280. DOI: 10.1021/j100142a004.

Cerutti, David S.; Rice, Julia E.; Swope, William C.; Case, David A. (2013): Derivation of fixed partial charges for amino acids accommodating a specific water model and implicit polarization. In: *J. Phys. Chem. B* 117 (8), S. 2328–2338. DOI: 10.1021/jp311851r.

Frisch, M. J.; Trucks, G. W.; Schlegel, H. B.; Scuseria, G. E.; Robb, M. A.; Cheeseman, J. R. et al. (2009): Gaussian 09, Revision A.02. Version. Wallingford CT: Gaussian, Inc.

Jorgensen, William L.; Maxwell, David S.; Tirado-Rives, Julian (1996): Development and Testing of the OPLS All-Atom Force Field on Conformational Energetics and Properties of Organic Liquids. In: *J. Am. Chem. Soc.* 118 (45), S. 11225–11236. DOI: 10.1021/ja9621760.

Mecklenfeld, Andreas; Raabe, Gabriele (2017a): Comparison of RESP and IPolQ-Mod Partial Charges for Solvation Free Energy Calculations of Various Solute/Solvent Pairs. In: *J. Chem. Theory Comput.* 13 (12), S. 6266–6274. DOI: 10.1021/acs.jctc.7b00692.

Mecklenfeld, Andreas; Raabe, Gabriele (2017b): Efficient solvation free energy simulations. Impact of soft-core potential and a new adaptive λ-spacing method. In: *Mol. Phys.* 115 (9-12), S. 1322–1334. DOI: 10.1080/00268976.2017.1292008.

Mennucci, Benedetta; Cammi, Roberto; Tomasi, Jacopo (1998): Excited states and solvatochromic shifts within a nonequilibrium solvation approach. A new formulation of the integral equation formalism method at the self-consistent field, configuration interaction, and multiconfiguration self-consistent field level. In: *J. Chem. Phys.* 109 (7), S. 2798–2807. DOI: 10.1063/1.476878.

Muddana, Hari S.; Sapra, Neil V.; Fenley, Andrew T.; Gilson, Michael K. (2014): The SAMPL4 hydration challenge: evaluation of partial charge sets with explicit-water molecular dynamics simulations. In: *J Comput Aided Mol Des* 28 (3), S. 277–287. DOI: 10.1007/s10822-014-9714-6.

Nelder, J. A.; Mead, R. (1965): A Simplex Method for Function Minimization. In: *Comput. J.* 7 (4), S. 308–313. DOI: 10.1093/comjnl/7.4.308.

Vanommeslaeghe, K.; Hatcher, E.; Acharya, C.; Kundu, S.; Zhong, S.; Shim, J. et al. (2010): CHARMM general force field: A force field for drug-like molecules compatible with the CHARMM all-atom additive biological force fields. In: *J. Comput. Chem.* 31 (4), S. 671–690. DOI: 10.1002/jcc.21367.

Wang, Junmei; Wolf, Romain M.; Caldwell, James W.; Kollman, Peter A.; Case, David A. (2004): Development and testing of a general amber force field. In: *J. Comput. Chem.* 25 (9), S. 1157–1174. DOI: 10.1002/jcc.20035.

HYDROGELS BASED ON POLYMERIZED IONIC LIQUIDS AS INNOVATIVE DRUG CARRIERS IN CONTROLLABLE AND INDIVIDUALIZED DOSAGE FORMS

A. Mildner, L. Henke, T. Gerdes, J. Großeheilmann

Technische Universität Braunschweig, Institute of Chemical and Thermal Process Engineering, Langer Kamp 7, 38106 Braunschweig, Germany; Center of Pharmaceutical Engineering, Franz-Liszt-Straße 35a, 38106 Braunschweig, Germany, a.mildner@tu-braunschweig.de

ABSTRACT

Novel Polymerized Ionic Liquids (PILs)-based Hydrogels as Innovative Drug Delivery Systems are presented. The embedding of drugs in hydrogels enables the "smart" delivery of bioactive molecules from drugs for an oral route of administration. Therefore, a high mechanical strength as well as a favorable pH-dependent swelling behavior is required which is shown in this study. A mechanical compression of PILs-based hydrogels up to 98.5% and a high swelling behavior of poly(VEImBr) hydrogels in a solution with a high pH value is achieved. A significant lower swelling is achieved in a solution with a lower pH value.

Keywords: Hydrogel, Polymerized Ionic Liquids, Drug Delivery

INTRODUCTION

Due to the growing demand for a controlled release of drugs in the pharmaceutical industry, there has been a considerable interest in the development of novel and reliable drug-delivery systems. Therefore, the literature considers various approaches, including the embedding of drugs in hydrogels. Such innovative systems enable the "smart" delivery of bioactive molecules from drugs. However, there are several disadvantages of already existing intelligent hydrogels, such as their low mechanical stability, limited and not completely reversible swelling capacity, and slow response to external stimuli. Due to the inadequate properties of these existing hydrogels our focus is on novel polymerized ionic liquids-based hydrogels as drug carriers for oral route of administration. The aim of this research is to achieve a selective drug release from hydrogels over a defined time period and at a specific location in order to control the duration of the action while minimizing undesired effects outside the site of action.

RESEARCH CONCEPT

In order to investigate the PILs-based hydrogels as innovative drug delivery systems, the dimensionally-stable PILs are being obtained by radical polymerization. An imidazolium-based ionic liquid bearing a vinyl group is polymerized with the cross-linker *N,N'*-methylenebisacrylamide. The embedding of a drug can be achieved by adding an active pharmaceutical ingredient (API) dissolved in water during the synthesis, as shown in Figure 2. As model substances simplified structures of protein kinase inhibitors are used. There are several variation possibilities during the synthesis, which have decisive effect on the synthesis of the hydrogel, e.g. content and type of cross-linker, water content and the ionic liquid. At the same time, however, the properties of the hydrogel is obviously also influenced by the variation.

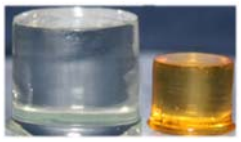

Figure 1. Synthesized Hydrogels in a fresh (left) and dried (right) state.

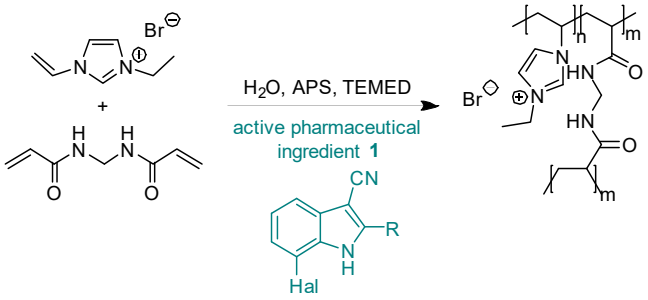

*Figure 2: Synthesis of PILs-based hydrogel poly(VEImBr); radical polymerization of [VEIm] [Br] – 1-Vinyl-3-ethylimidazolium bromide and cross-linker N,N'-methylenebisacrylamide. APS – Ammonium peroxydisulfate, TEMED – N,N,N',N'-tetramethylethane-1,2-diamine, **1** – 7-Halogenindol-3-carbonitrile.*

CHARACTERIZATION

Mechanical Properties

Due to their high water content hydrogels possess generally a weak mechanical strength. However, the advantage of PILs-based hydrogels over e.g. alginate-based hydrogels is their significantly higher mechanical stability [Bandomir, 2014]. The mechanical properties are affected by the IL monomer, composition, cross-linking density, degree of drying or swelling and drying method. A reversible compressibility (ε) of a fresh synthesized poly(VEImBr) hydrogel in physiological saline of up to 72% without crack formation is achieved. This compression behavior is increased by increasing the drying time in a climatic chamber.

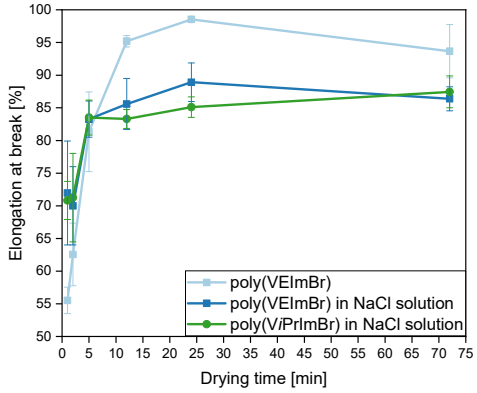

Figure 3: Elongation tests of poly(VEImBr) and poly(ViPrImBr) hydrogels with different degrees of drying at 25 °C and 60% RH partially in 0.9% NaCl solution with a loading speed of 0.1%/s.

With increased drying time, the reversible compression without crack formation increased already up to 98.5% in the air and up to 88.9% in physiological saline for poly(VEImBr), for poly(V*i*PrImBr) up to 87.4%, as shown in Figure 3.

Swelling behavior

The swelling property of hydrogels is a significant factor for controlled drug releases [Rizwan, 2017]. Drug release generally involves the simultaneous absorption of water and desorption of a drug via a swelling-controlled diffusion mechanism. The produced hydrogels show a pH-dependent swelling behavior, as shown in Figure 4**Fehler! Verweisquelle konnte nicht gefunden werden.**. Due to the large variations of pH-values at various body sites, the swelling and thus the release of the API will only take place at the desired site of action in the body. By further functionalization of the PILs, the swelling behavior of the hydrogels as well as the drug release can be affected crucial.

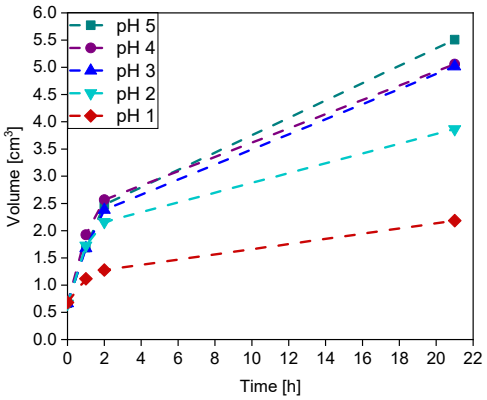

Figure 4: Swelling trend of fresh poly(VEImBr) hydrogels in 0.9% NaCl solution with different pH-values.

Drug release behavior

Initial findings on the drug release behavior can be adapted from catalyst-leaching experiments [Großeheilmann, 2015]. Leaching behavior with different drying methods, catalyst structures, water content, and solvents was investigated. Due to these experiments, drug release mechanisms can be influenced by various parameters, such as drying methods, crosslinker-to-IL ratio, IL monomer, solvent / pH of the aqueous medium, drug size, and drug polarity. The first studies on drug release behavior of model substances are currently under investigation. As model substances simplified structures of protein kinase inhibitors, which are used in the development of drugs for Down syndrome and Alzheimer's disease, are used.

Biocompatibility

Initial experiments show that most of the IL monomers are toxic before polymerization, except monomers with an isopropyl group. Fortunately, the PILs-based hydrogels show low to no toxicity after polymerization. Further biocompatibility tests are currently under investigation. In addition, the change from a batch process to a continuous process for washing out unreacted IL monomer from the PILs is currently being developed to obtain biocompatible PILs-based hydrogels.

CONCLUSIONS

Stable PILs-based hydrogels were successfully synthesized by a radical polymerization. The mechanical stability of these hydrogels is shown by a reversible compression up to 90% without crack formation. Initial findings show low to no toxicity after polymerization. Drug release can be controlled by pH-dependent swelling behavior. In future, an increased pH-responsive drug release should be obtained by functionalizing the PILs.

ACKNOWLEDGMENT

This work has been carried out within the framework of the SMART BIOTECS alliance between the Technische Universität Braunschweig and the Leibniz Universität Hannover. This initiative is supported by the Ministry of Science and Culture (MWK) of Lower Saxony, Germany.

NOMENCLATURE

API	Active Pharmaceutical Ingredient
APS	Ammonium peroxydisulfate
IL	Ionic Liquid
PILs	Polymerized Ionic Liquids
RH	Relative Humidity
TEMED	*N,N,N',N'*-Tetramethylethane-1,2-diamine
VEImBr	1-Vinyl-3-ethylimidazolium bromide
V*i*PrImBr	1-Vinyl-3-isopropylimidazolium bromide
ε	Compressibility

REFERENCES

[Bandomir, 2014] Bandomir, J., Schulz, A., Taguchi, S., Schmitt, L., Ohno, H., Sternberg, K., Schmitz, K. and Kragl, U., 2014, Synthesis and Characterization of Polymerized Ionic Liquids: Mechanical and Thermal Properties of a Novel Type of Hydrogels, *Macromol. Chem. Phys.*, Vol. 215, pp. 716-724.

[Rizwan, 2017] Rizwan, M., Yahya, R., Hassan, A., Yar, M., Azzahari, A., Selvanathan, V., Sonsudin, F. and Abouloula, C., 2017, pH Sensitive Hydrogels in Drug Delivery: Brief History, Properties, Swelling, and Release Mechanism, Material Selection and Applications, *Polymers*, Vol. 9, pp. 137.

[Großeheilmann, 2015] Großeheilmann, J., Bandomir, J. and Kragl, U., 2015, Preparation of Poly(ionic liquid)s-Supported Recyclable Organocatalysts for the Asymmetric Nitroaldol (Henry) Reaction, *Chem. Eur. J.*, Vol. 21, pp. 18957-18960.

CHARACTERISATION OF WATER UPTAKE AND SWELLING FORCE OF PHARMACEUTICAL TABLETS

Daniel Puckhaber[1,2], Jan Henrik Finke[1,2], Lennart Lange[1,2], Michael Juhnke[3], Edgar John[3], Arno Kwade[1,2]

[1]Institute for Particle Technology; TU Braunschweig; Braunschweig, Germany; d.puckhaber@tu-bs.de

[2]PVZ – Centre for Pharmaceutical Engineering, TU Braunschweig, Germany

[3]Novartis Pharma AG, Basel, Schweiz

ABSTRACT

Tablets are the most common dosage form in the pharmaceutical industry. Rapid drug release is ensured by quick tablet disintegration which is caused by the absorption of water into the tablet. Therefore, water uptake and subsequent volume expansion are necessary requirements for tablet disintegration. In this work, binary mixtures of excipients were compacted to tablets with varying structural and mechanical properties to determine the influence of formulation and process parameters on water uptake and resulting swelling force of tablets. Results showed strong influences of disintegrant concentration as well as tablet porosity on both absorbed amount of water and acting swelling force. Obtained results revealed that water uptake and swelling force measurements are useful tools for an improved understanding of tablet disintegration.

Keywords: Water uptake, swelling force, tablets, disintegrants

INTRODUCTION

The majority of commercial tablets are designed to release at least parts of their active pharmaceutical ingredient (API) immediately after administration. The API release is directly depending on the available surface area which can be greatly enhanced by rapid tablet disintegration. Therefore, disintegrants are added to tablet formulations ensuring the quick disintegration of tablets into smaller fragments. The intrusion of water into the tablet is a necessary requirement for disintegration to occur. The absorbed water mitigates interparticulate bonds and therefore, results in a deteriorated mechanical tablet strength. The disruption of the tablet matrix can be further accelerated by incorporated disintegrant particles which tend to swell up to a multiple of their initial volume.

For commercial products, the disintegration behavior of tablets is solely described by determining the disintegration time with a disintegration tester according to the applicable pharmacopeia. However, the derived disintegration time lacks any insight into processes involved during the tablet disintegration and gives no information about the course of the tablet disintegration. Therefore, custom-built apparatuses to describe acting subprocesses, namely water uptake rate and swelling force, were built by different authors to characterize the interaction of pharmaceutical tablets with water during disintegration [Caramella et al., 1988; Catellani et al., 1989]. The applied methods showed useful insight to gain an improved understanding of tablet disintegration. However, previously applied studies lack systematic investigations of the influence of formulation and process parameters as well as physical interpretation of derived data.

RESEARCH CONCEPT

Applied materials comprised microcrystalline cellulose (MCC; Vivapur 102, JRS Pharma) as filler/binder and both croscarmellose sodium (Primellose, DFE Pharma) and crospovidone (Polyplasdone XL, Ashland) as disintegrants.

Tableting

Binary mixtures of MCC and disintegrants with varying shares of disintegrants (0 – 20 wt.%) were compacted into tablets of 450 mg using the compaction simulator Styl'One evolution (Medel'Pharm, France). Tablets were compacted applying different levels of compaction pressures (25 – 400 MPa) using biplanar, round 11.28 mm Euro-D tooling.

Tablet analysis

Tablet porosities were calculated using the geometrical measures and mass of produced tablets. Diametrical compression strength was measured and tablet tensile

strength was subsequently calculated applying the equation of [Fell and Newton, 1970].

Water uptake and swelling force

Water uptake of tablets was measured using a tensiometer K20 (Krüss GmbH, Germany) with a customized setup until derived mass increase undercut 0.1 mN/s.

Swelling force of tablets was measured using material testing machine zwickiline Z2.5 (Zwick/Roell GmbH & Co. KG, Germany). Tablets were placed on metal petri dishes and fixed by applying 0.5 N with a steel punch acting as a force transmission element. 40 mL of distilled water were added and the axial swelling force was measured until a decrease of swelling force was detected.

RESULTS & DISCUSSION

Measured maximal water uptake revealed the ability of tablets to absorb a multiple of their own weight (Figure 1). Water uptake rises with increasing crospovidone concentration possibly due to the increased water absorption of disintegrant particles and increased disruption of tablet matrix allowing enhanced storage of water. Results revealed a considerable influence of the densification status of tablets as expressed by different water uptake masses for different compaction stresses.

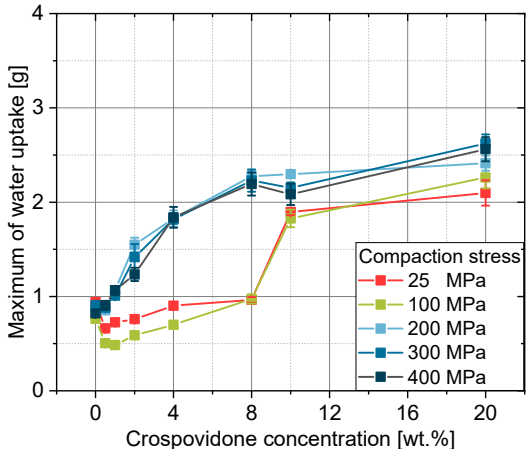

Figure 1: Water uptake of tablets of MCC + crospovidone for different levels of compaction stress and crospovidone

In contrast, swelling force decreases with increasing concentration of crospovidone (Figure 2) most likely caused by the rapid disruption and radial relaxation of the tablet matrix. Swelling force is found to depend on both formulation and process parameters and can exhibit considerably high values up to 600 N.

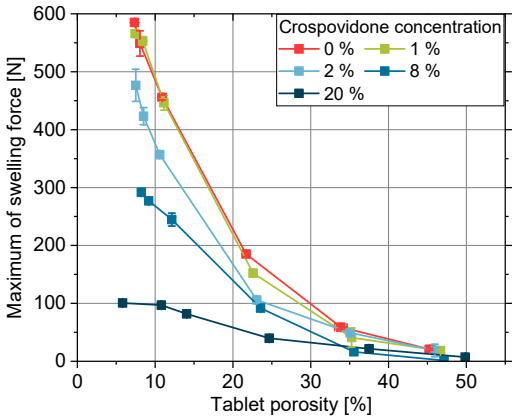

Figure 2: Swelling force of tablets of MCC + crospovidone for different disintegrant concentrations and tablet porosities

When correlated with the measured disintegration time, swelling force rate was found to be a better indicator for rapid tablet disintegration than the maximum values of the swelling force due to the rapid disintegration of the tablet matrix (data not shown).

CONCLUSIONS

Results showed a complex interplay of process parameters and formulation on both water uptake and swelling force. Applied methods revealed interesting insight into acting subprocesses during disintegration.

ACKNOWLEDGMENT

The authors like to thank DFE Pharma and Ashland for providing materials used in this study.

REFERENCES

Fell, J. T., Newton, M., 1970, Determination of Tablet Strength by the Diametral-Compression Test, *Journal of Pharmaceutical Sciences,* Vol. 59, pp. 688-691.

Caramella, C., Ferrari, F., Gazzaniga, A., Conte, U., La Manna, A., Geddo, M., 1988, A new Computer-Aided Apparatus for Simultaneous Measurements of Water Uptake and Swelling Force in Tablets, *Drug Development and Industrial Pharmacy*, Vol. 14, pp. 2167-2177

Catellani, P. L., Predella, P., Bellotti, A., Colombo, P., 1989, Tablet water-uptake and disintegration force, *International Journal of Pharmaceutics*, Vol. 51, pp. 63-66

CONTINUOUS KRAPCHO DEALKOXYCARBONYLATION IN API SYNTHESIS

M. C. Rehbein[1,2], S. Husmann[1], J. Wolters[1], L. Priess[1], C. Lechner[3], C. Kunick[2,3], S. Scholl[1,2*]
[1]TU Braunschweig, Institute for Chemical and Thermal Process Engineering, Langer Kamp 7, 38106 Braunschweig, Germany
(*Corresponding author: s.scholl@tu-braunschweig.de)
[2]TU Braunschweig, Center for Pharmaceutical Engineering, Franz-Liszt-Str. 35a, 38106 Braunschweig, Germany
[3]TU Braunschweig, Institute for Medicinal and Pharmaceutical Chemistry, Beethovenstr. 55, 38106 Braunschweig, Germany

ABSTRACT

A high pressure and high temperature continuous flow reactor has been used to intensify a Krapcho dealkoxycarbonylation reaction in the context of API synthesis. The reactor enables operation of the reaction above temperatures possible in batch and thus significantly increased conversion rates are achieved. Also a broader choice of solvents is possible by the use of the continuous process. Batch and continuous reaction are compared in terms of operation range and space-time-yield. Despite lower concentrations of the reactants in the continuous process, space-time-yield exceeds that of the batch process by more than an order of magnitude due to the higher reaction rates.

Keywords: Flow synthesis, process intensification, Krapcho dealkoxycarbonylation

INTRODUCTION

The method of Krapcho is a simple procedure for the selective dealkoxycarbonylation of molecules under neutral conditions [1,2]. It involves heating of the respective reactant molecule in an aprotic polar solvent with added water and sometimes salts. At ambient pressure, the choice of solvent is limited to high boiling polar aprotic solvents such as DMF and DMSO due to the demanding temperatures. Figure 1 displays reaction temperature and time for several Krapcho reactions reported in literature [3,4].

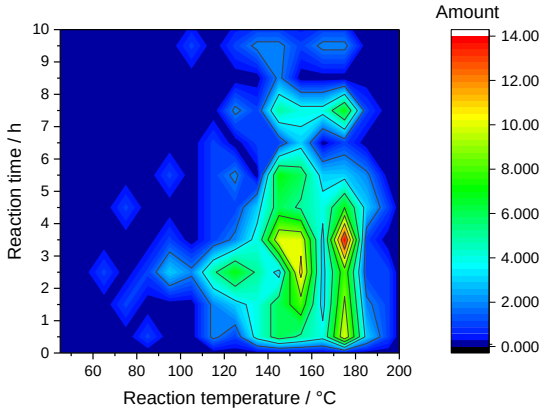

Figure 1: Overview over reaction conditions for different Krapcho reactions reported in literature, n_{total} = 364 [3,4]

Obviously, the majority of these reactions only progresses at temperatures well above 140 °C, still requiring reaction times of several hours. In order to intensify the reaction beyond the original batch protocol, a continuous high pressure and high temperature flow reactor is utilized to access reaction temperature windows not possible in batch. By pressurizing the reactor, also alternative low boiling solvents could be employed, benefiting from their high volatility for easier workup. The continuous reactor is tested for a typical Krapcho reaction with pharmaceutical relevance, namely the synthesis of 3,4-dihydro-1*H*-1-benzazepine-2,5-dione (**DHBD** [5], Figure 2. **DHBD** and its derivatives are important precursor molecules for the synthesis of substituted paullones and paullone derivatives, a class of protein kinase inhibitors and anti-cancer agents [6–8].

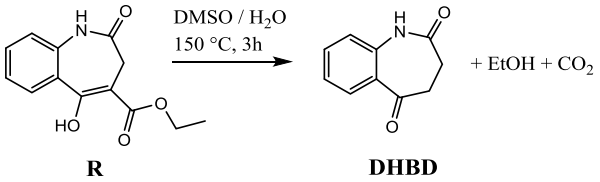

Figure 2: Krapcho dealkoxycarbonylation for the synthesis of DHBD in batch mode

RESEARCH CONCEPT

In order to examine the reaction in detail, a continuous high pressure and high temperature flow reactor has been designed and characterized [9].
As shown in Figure 3, the center piece of the setup is a stainless steel coil reactor with dimensions d_i x L = 1.016 x 2,500 mm, V_R = 2.027 mL, which is submerged in and heated by an oil bath. The reactor is fed by a HPLC pump and kept at a constant pressure of 37.5 bar to prevent boiling of the solvent. At a given flow rate, 500 µL of the reactant solution are loaded in the sample loop and injected into the inlet stream.

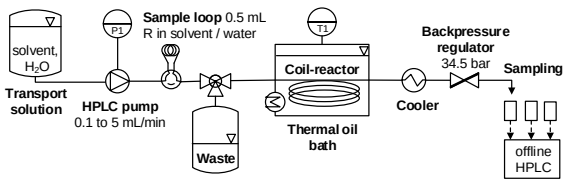

Figure 3: Setup of the continuous flow reactor used to study the Krapcho reaction

The reactor outlet stream is collected and analyzed via HPLC. In order to generate conversion-time-profiles

this procedure is repeated for various combinations of temperature (160 – 200 °C) and flow rate (0.1 – 2 mL min^{-1}). For comparison batch reactions are performed in a Mettler Toledo EasyMax 102 synthesis workstation.

Kinetic analysis

The conversion-time-profile of the reactant X_R can be described by a pseudo 1st order kinetic equation, where t_R is the residence time of sample fluid element in the heated zone of the continuous reactor [10]:

$$X_R = 1 - exp(-k \cdot t_R) \quad (1)$$

Since residence time distribution in the coil reactor is found to closely follow plug flow behavior [9], residence time t_R is calculated via reactor volume V_R and volumetric flow rate $\dot{V}$, corrected by the expansion of the fluid upon heating:

$$t_R = \frac{V_R}{\dot{V}} \frac{\rho_{S,T}}{\rho_{S,25°C}} \quad (2)$$

By fitting equation (1) to experimentally determined conversion-over-time data, rate constants k can be determined. By employing Arrhenius´ law, activation energy E_A and frequency factor k_0 may be calculated:

$$k(T) = k_0 \cdot exp(-E_A/(R \cdot T)) \quad (3)$$

Combination of equations (1) – (3) results in an expression for the conversion in the continuous reactor as function of temperature and flow rate [9]:

$$X_R(T, \dot{V}) = 1 - exp\left[-k_0 \cdot e^{-\frac{E_A}{RT}} \cdot \frac{V_R}{\dot{V}} \frac{\rho_{S,T}}{\rho_{S,25°C}}\right] \quad (4)$$

RESULTS AND DISCUSSION

Reaction characterization

Since water is added as reactant, the influence of its concentration on reaction rate was examined.

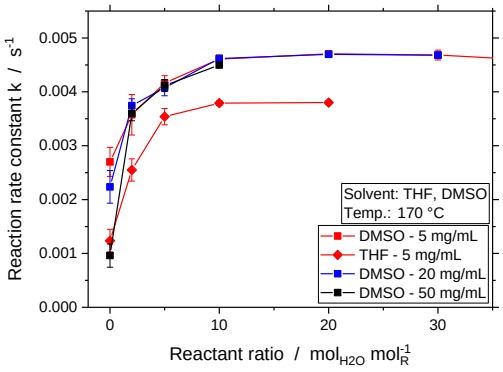

Figure 4: Influence of the ratio of water and reactant on the rate of the dealkoxycarbonylation

Figure 4 displays reaction rate constants for different ratios of added water to reactant concentration at varied reactant concentrations in solvents DMSO and THF. In general, rate constants increase with the amount of water added per reactant, until a maximum k-value is reached at a ratio of about 10. This behavior can be observed for different reactant concentrations ranging from 5 to 50 mg mL^{-1} in DMSO.

For no added water, the reaction still takes place. This might be due to the hygroscopic nature of DMSO, which always contains small amounts of water. For low ratios of added water to reactant concentration, error bars are significantly larger, indicating a lower accuracy of the used 1st order fit. In this regime, the reaction behaves more like a 2nd order reaction where water concentration becomes limiting. For THF as solvent, a similar behavior is observed, however, the maximum value of k is significantly lower than that observed in DMSO.

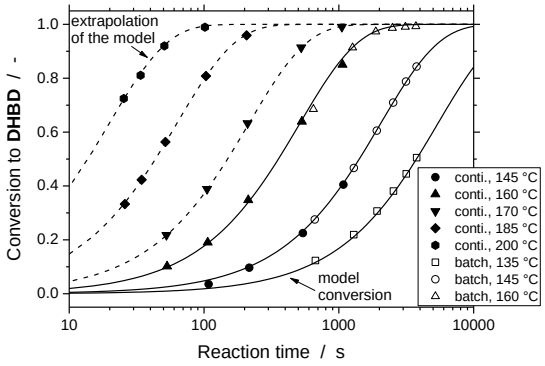

Figure 5: Conversion profiles at different temperatures in DMSO in batch and continuous mode [9]

Figure 5 displays typical conversion-time profiles of **R** to **DHBD** in DMSO for different temperatures in the batch and continuous reactor. Conversion profiles were also modeled using equation (4) and batch data to fit the parameters. Dotted curves represent extrapolations of that model to higher temperatures, with parameters extracted from reactions ≤ 160 °C.

Batch and continuous conversions are in very good agreement, however, the reaction temperature in batch is limited. Employing the continuous reactor, temperatures of up to 200 °C can be realized resulting in a significantly intensified reaction. Consequently, shorter reaction times are sufficient to reach complete conversion (~ 3 min vs. ~ 3 h respectively).

Solvent selection

To identify an optimal solvent for the Krapcho reaction, different solvents have been examined as reaction medium. Figure 6 summarizes the derived rate constants at different temperatures. Whilst aprotic-polar solvents show significant reaction rates, ethanol and i-propanol are not suited as reaction medium. Here, the equilibrium between the reactant and a carboxylate intermediate might be affected negatively. Considering aprotic-polar solvents, rate constants do not differ dramatically. However, DMSO and acetone show the highest rate

constants while values of propylene carbonate (PC) and ethyl acetate (EA) are about 25 % lower.

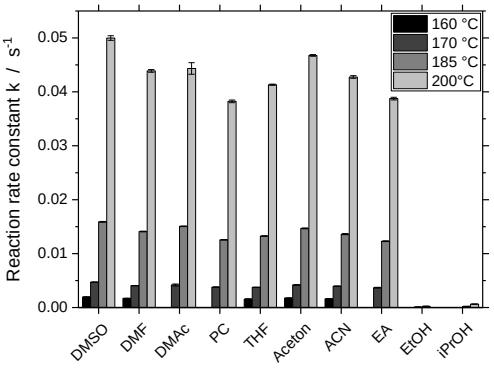

Figure 6: Reaction rate constants k in different solvents

Besides reaction rate, reactant solubility in the respective solvent is an important property. Solubility curves of **R** in different solvents, measured via HPLC from a saturated solution, for n ≥ 3 samples each, are given in Figure 7. Only DMSO, DMF and DMAc exhibit high solubility for the reactant **R** while acetone, PC, EA and ACN show unsatisfactory solubility especially at room temperature. Taking a combined look at reaction rate and solubility, it becomes apparent that DMSO, DMAc and DMF are the most promising solvent candidates, since they show both, relatively high rate constants and good solubility. THF is the best of the low boiling solvents. While the solubility for the reactant is not as high as in DMSO for example, it still exceeds the other low boiling solvents by a factor ~ 3.

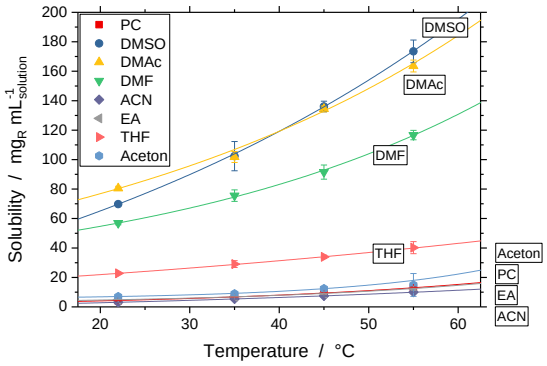

Figure 7: Solubility curves of the reactant R in different aprotic-polar solvents, n ≥ 3

Comparison of batch and continuous process

To assess the process modes, it is interesting to consider the operation range of the respective process and compare the space-time-yield (STY) as a measure of process performance.

Operation ranges, given in Figure 8, can be interpreted as follows: In the batch process, solubility is not an issue since dissolution of the reactant can take place during heating of the mixture and at reaction temperature, solubility is high anyway. In contrast, in continuous mode, the reactant has to be dissolved prior to pumping to prevent reactor clogging and pump damage by un-dissolved solids, so reactant concentration is limited. In the batch process reaction temperature is limited by the boiling temperature of the reaction mixture. Since water is added proportional to the reactant concentration, maximum possible reaction temperature is decreasing with increasing reactant concentration (see Figure 8). In the pressurized continuous reactor, this is not an issue and higher reaction temperatures can be reached.

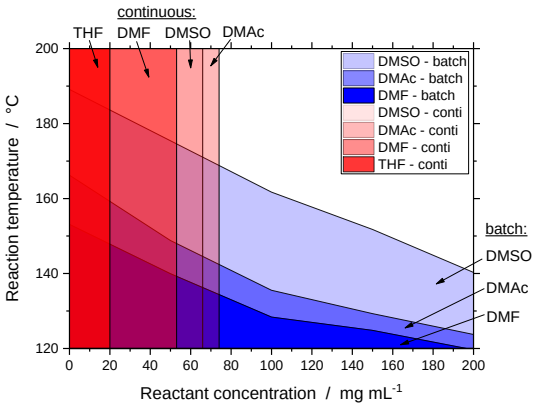

Figure 8: Operation range of the batch and the continuous process

To quantitatively the influence of reaction temperature and concentration on the performance of both processes, *STY* is theoretically assessed as follows: For the batch, *STY* depends on the chosen reactant concentration c_R and the resulting processing time t_{proc} which is a function of the reaction temperature und ultimately of the reactant concentration due to added water as stated above:

$$STY_b = \frac{c_R}{t_{proc.}(c_R)} \cdot M_{DHBD}/M_R \qquad (5)$$

For the continuous process, *STY* follows from the maximum solubility of the reactant S_R and the volumetric flow rate necessary to provide a sufficient reaction time for a conversion of 99.9 %:

$$STY_c = S_R(T_S) \cdot \frac{\dot{V}_{X=99.9\%}(T_R)}{V_R} \cdot M_{DHBD}/M_R \qquad (6)$$

The calculated *STY* are displayed in Figure 9, where values for batch represent the highest *STY* possible at the optimum reactant concentration and temperature while the values for the continuous process are calculated for dissolution temperature T_S = 25 °C and reaction temperature T_R = 200 °C.

It can be concluded that the *STY* possible in the batch process is about an order of magnitude smaller than in the continuous process for the high boiling solvents. This can be contributed to the low temperatures and therefore slow reaction in batch. This effect can be seen especially for THF where the low boiling point would lead to reaction times of several years. Although reactant

concentration is higher in the batch process, this advantage does not balance out the slow rates. In continuous mode, due to the fast reaction, DMF, DMSO and DMAc show the highest *STY* of around 10 – 20 mg $mL^{-1}_{reactor}$ min^{-1}.

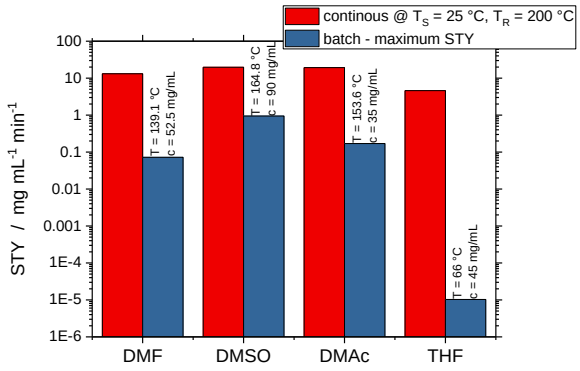

Figure 9: Calculated STY for the batch and continuous process in logarithmic scaling

In conclusion, the superior performance of the continuous process can mainly be attributed to the possibility to operate at high temperatures. Although similar temperatures could also be reached in a sealed or pressurized batch reactor, the distinct advantage of a high surface to volume ratio and therefore excellent heat transfer properties of the continuous reactor would still lead to an advantage over a pressurized batch reactor. The batch reactor would need longer heating and cooling times and therefore an overall longer processing time rendering the fast reaction times useless. In addition, higher safety properties usually attributed to continuous systems and low cost for the commonly available materials are distinct advantages of the continuous process.

CONCLUSIONS

In this contribution, a continuous process for the intensification of the Krapcho dealkoxycarbonylation reaction is established and the synthesis of the pharmaceutically relevant molecule DHBD is studied as model process in detail. To assess the performance of the continuous reactor it is compared to the original batch process.

It was found that the dealkoxycarbonylation can be significantly intensified in the continuous reactor due to the high reaction temperatures possible, resulting in a reaction time reduction from 3 h in batch to < 3 min in the continuous reactor. Exploiting the pressurized reaction conditions in the continuous reactor, the choice of solvent can be broadened significantly. It was found, that all aprotic-polar solvents under investigation are principally suited as reaction medium since similar rates were measured. However, due to the higher solubility DMSO, DMF and DMAc are preferred.

Compared to the batch process, *STY* in the continuous reactor is one to two orders of magnitude higher when operated under higher temperatures that cannot be realized in the batch reactor due to boiling of the reactant mixture.

ACKNOWLEDGEMENT

This study was partially funded by the Lower Saxony Ministry for Science and Culture (MWK) in the joint research project µ-Props of the Center of Pharmaceutical Engineering (PVZ).

NOMENCLATURE

c_R	[mmol mL^{-1}]	reactant concentration
d_i	[mm]	inner diameter
E_A	[J mol^{-1}]	activation energy
k	[s^{-1}]	reaction rate constant
k_0	[s^{-1}]	frequency factor
L	[m]	length of the coil-reactor
M	[g mol^{-1}]	molar mass
R	[J K^{-1} mol^{-1}]	universal gas constant
ρ_S	[g mL^{-1}]	solvent density
S	[mg mL^{-1}]	solubility
STY	[mg mL^{-1} min^{-1}]	space time yield
T	[°C], [K]	temperature
V_R	[mL]	reactor volume
$\dot{V}$	[mL min^{-1}]	volumetric flow rate
X_R	[-]	reactant conversion

REFERENCES

[1] A. P. Krapcho, et al., Tetrahedron Letters 8 (1967) 215–217.
[2] A. P. Krapcho, et al., Tetrahedron Letters 15 (1974) 1091–1094.
[3] A. P. Krapcho, Arkivoc 2007 (2007) 1–54.
[4] A. P. Krapcho, Arkivoc 2007 (2007) 54–121.
[5] C. Kunick, Arch. Pharm. Pharm. Med. Chem. 324 (1991) 579–581.
[6] N. Tolle, C. Kunick, Curr. Top. Med. Chem. 11 (2011) 1320–1332.
[7] C. Schultz, et al., J. Med. Chem. 42 (1999) 2909–2919.
[8] H. Falke, et al., J. Med. Chem. 58 (2015) 3131–3143.
[9] M. C. Rehbein, et al., J. Flow Chem. 9 (2019) 123–131.
[10] M. C. Rehbein, et al., Eur. J. Pharm. Biopharm. 126 (2018) 95–100.

INFLUENCE OF AMORPHOUS SOLID DISPERSIONS OF PARACETAMOL AND PVP VA 64 ON THE THERMORESPONSIVE BEVAHAVIOUR OF THE POLYMER

Lena Ritters; Stephan Reichl

Institut für Pharmazeutische Technologie, Technische Universität Carolo-Wilhelmina zu Braunschweig, Mendelssohnstraße 1, 38106 Braunschweig, Germany
Zentrum für Pharmaverfahrenstechnik, Technische Universität Carolo-Wilhelmina zu Braunschweig, Franz-Liszt-Straße 35 A, 38106 Braunschweig, Germany
l.ritters@tu-braunschweig.de

ABSTRACT

The dissolution of spray-dried amorphous solid dispersions consisting of paracetamol and PVP VA 64 at room temperature leads to the formation of different systems, depending on the drug/polymer ratio. Aqueous systems at room temperature with poor paracetamol/PVP VA 64 ratio are transparent solutions, while higher drug loads lead to phase separation of the solution. PVP VA 64 is known as thermoresponsive polymer. The aim of the study was to investigate the dissolution behaviour of these amorphous solid dispersions in water and their influence on the thermoresponsive behaviour of this polymer. Therefore, the demixing temperature was determined using DSC, since a change in the system constitutes an endothermic process. It could be shown that PVP VA 64 has lower critical solution temperature (LCST) behaviour around 70 °C, which decreases with increasing content of paracetamol due to the complex formation between the polymer and paracetamol.

Keywords: amorphous solid dispersion, thermoresponsive polymer, dissolution, lower critical solution temperature

INTRODUCTION

A large number of new active pharmaceutical ingredients shows poor water solubility. Amorphous solid dispersions (ASD) are a common approach to improve solubility and bioavailability. [Grohganz 2014]

The dissolution of ASD in water or physiological media can lead to super-saturation and two-phase separation, known as liquid liquid phase separation (LLPS) [Saboo, 2019].

Many polymers, which might be used for ASD, are known to separate into two phases when heating or cooling their aqueous solution. Two different behaviours of the so-called thermoresponsive polymers have to be distinguished: If the phase separation occurs during heating, the upper critical solution temperature (UCST) can be determined. If this happens during cooling, the lower critical solution temperature (LCST) can be measured. At this temperature, the system changes between one and two phases. A polymer-rich and polymer-poor phase are formed in the separated system. [Aseyev, 2011] Additives can increase or decrease the LCST [Van Durme, 2005].

The aim of the study was to investigate the dissolution behaviour of ASD, consisting of paracetamol and PVP VA 64, in water and their influence on the thermoresponsive behaviour of this polymer.

EXPERIMENTAL METHODS

Materials

Paracetamol was a generous gift from STADA, Germany. PVP VA 64 was kindly donated by BASF, Germany. Demineralized water was used for solutions.

Amorphous solid dispersions (ASD)

Preparation of ASD was done by spray drying using a Büchi Mini-Spray Dryer B-191. Paracetamol and PVP VA 64 were dissolved in demineralized water in ratios of 1 : 9 (total concentration of mixture in aqueous solution 12.0 % (m/v)), 2 : 8 (6.0 %) and 3 : 7 (4.0 %). The following conditions were used for spray drying: inlet temperature 80 °C, outlet temperature 45 °C to 50 °C, pump rate 7 %, aspirator flow rate 100 %.

Physical mixture (PM)

The PM of drug and polymer (same ratios as for ASD) were mixed in a TURBULA® mixer for ten minutes.

Differential Scanning Calorimetry (DSC)

The solutions were analysed in aluminum pans on a Mettler Toledo DSC 1 with HSS7 sensor. The measurement was performed in duplicate at a heating rate of 5 K/min between -10 °C to 85 °C, depending on the estimated demixing temperature. The onset temperature of the endothermic process was determined [Van Durme, 2004]. All measurements were analysed under nitrogen purge.

RESULTS

Dissolution of ASD in water

Various systems made of paracetamol, PVP VA 64 and water (see Figure 1) were manufactured and optically evaluated at room temperature.

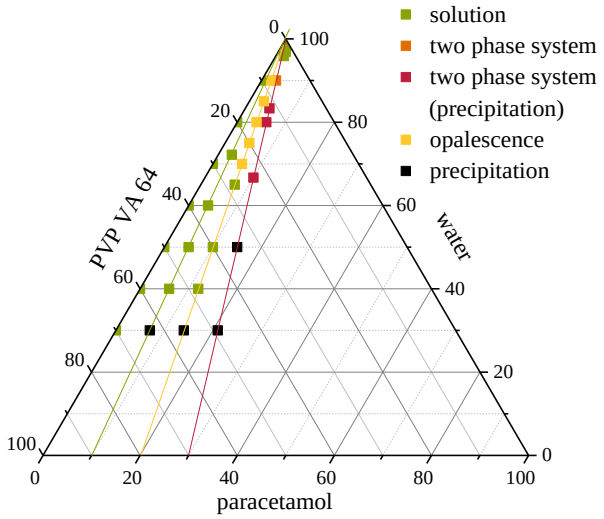

Figure 1: Ternary phase diagram of paracetamol, PVP VA 64 and water at room temperature.

Samples of the pure polymer and mixtures of paracetamol and the polymer in the ratio 1 : 9 (green line) show transparent solutions in water at room temperature, while mixtures in the ratio 2 : 8 (yellow line) are opalescent up to a concentration of 25 % PVP VA 64. Mixtures in the ratio 3 : 7 (red line) are in the form of an emulsion during stirring, while two-phase separation can be observed without moving the system.

LCST of ASD and PM

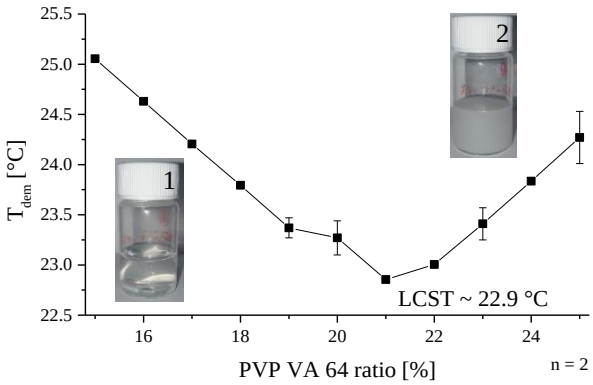

Figure 2: Demixing temperature (T_{dem}) of ASD 2 : 8 as a function of PVP VA 64 content; mean ± SD.

The demixing temperatures were determined for different concentrations of PVP VA 64. Below this temperatures the system is a transparent solution. In the near of the curve, the system becomes opalescent (see picture 1, Figure 2). Turbidity can be detected above the curve (see picture 2, Figure 2). Below the LCST there is a clear solution for each polymer concentration. The phase transition is reversible.

Table 1: LCST of ASD and PM for different systems.

Sample (PCM : PVP VA 64)	LCST ASD [°C]	LCST PM [°C]
pure PVP VA 64	-	69.7
1 : 9	52.6	53.4
2 : 8	22.4	22.9
3 : 7	14.2	14.7

The LCST decreases with increasing amount of paracetamol (absolute data not shown). The results for ASD and PM are similar for each ratio.

DISCUSSION

A large number of polymers exhibits thermoresponsive behaviour in aqueous solution [Aseyev, 2011]. Below the LCST the polymer chains are hydrated and thus water-soluble, resulting in a transparent solution. Temperatures above LCST lead to aggregation of the polymer chains by hydrophobic interactions, which results in turbidity of the solution and later in phase separation. [Van Durme, 2005]

By forming a complex of paracetamol and PVP VA 64, the LCST decreases with increasing part of paracetamol. The formation of hydrogen bonds [Afrasiabi Garekani, 2003] or Van-der Waals forces [Wen, 2005] between the molecules are discussed as reasons.

The aqueous solutions of pure PVP VA 64 as well as ASD and PM in the ratio 1 : 9 are transparent at room temperature because their LCST is between 50 °C and 70 °C. Close to the critical point, solutions become opalescent [Monval, 1939]. The LCST of aqueous solutions of ASD and PM in the ratio 2 : 8 is around room temperature, resulting in opalescence.

Aqueous systems with drug/polymer ratio of 3 : 7 have a LCST that is lower than room temperature. Such mixtures result in an emulsion that separates rapidly into two phases when it is no longer shaken. The so-called liquid liquid phase separation is well known for ASD [Saboo, 2019]. Previous experiments have shown that on the one hand an aqueous, drug-poor phase with a drug concentration similar to the amorphous solubility results. On the other hand, a drug-rich phase is formed and it is discussed that it serves as a drug reservoir [Saboo, 2019].

CONCLUSIONS

It could be shown that PVP VA 64 is a thermoresponsive polymer with LCST behaviour. With increasing part of paracetamol the LCST decreases due to complex formation between the polymer and drug. The results for the different ratios are similar for ASD and PM.

As already mentioned, phase separated systems may act as drug reservoirs and therefore be of interest for modified drug release. The aim of the next investigation is to study the drug permeation from phase separated systems through Caco-2 cells.

REFERENCES

[Grohganz, 2014] Grohganz, H. et al., 2014, Refining stability and dissolution rate of amorphous drug formulations, *Expert Opin. Drug Deliv.*, Vol. 11, pp. 977-989.

[Saboo, 2019] Saboo, S. et al., 2019, Congruent release of drug and polymer: A “sweet spot” in the dissolution of amorphous solid dispersions, *J. Control. Release*, Vol. 298, pp. 68-82.

[Aseyev, 2011] Aseyev, V., Tenhu, H. and Winnik F. M., 2011, Non-ionic Thermoresponsive Polymers in Water, *Adv Polym Sci*, Vol. 242, pp. 29-89.

[Van Durme, 2005] Van Durme, K., Rahier, H. and Van Mele, B., 2005, Influence of Additives on the Thermoresponsive Behavior of Polymers in Aqueous Solution, *Macromolecules*, Vol. 38, pp. 10155-10163.

[Van Durme, 2004] Van Durme, K., Verbrugghe, S., Du Prez, F. E. and Van Mele, B., 2004, Influence of Poly(ethylene oxide) Grafts on Kinetics of LCST Behavior in Aqueous Poly(N-vinylcaprolactam) Solutions and Networks Studied by Modulated Temperature DSC, *Macromolecules*, Vol. 37, pp. 1054-1061.

[Afrasiabi Garekani, 2003] Afrasiabi Garekani, H., Sadeghi, F. and Ghazi A., 2003, Increasing the Aqueous Solubilty of Acetaminophen in the Presence of Polyvinylpyrrolidone and Investigation of the Mechanisms Involved, *Drug Dev. Ind. Pharm.*, Vol. 29, pp. 173-179.

[Wen, 2005] Wen, H., Morris, K. R. and Park, K., 2005, Study on the Interactions between Polyvinylpyrrolidone (PVP) and Acetaminophen Crystals: Partial Dissolution Pattern Change, *J. Pharm. Sci.*, Vol. 94, pp. 2166-2174.

[Monval, 1939] Monval, P. and Quiquerez J., 1939, In zwei Schichten getrennte Flüssigkeitsgemische und kritische Opaleszenz, *Kolloidchemie*, Vol. 88, pp. 140-144.

LIGANDS FOR M-NHC SYNTHESIS: CONTINUOUS FLOW DI-*N*-ALKYLATION OF 1*H*-BENZIMIDAZOLE IN A FIXED BED REACTOR

T. Sauk[1,2], C. Heiduk[1,2], L. Henke[1,2], C. Xiao[1,2], S. Scholl[1,2*]

[1]Institute for Chemical and Thermal Process Engineering, TU Braunschweig
[2]Center for Pharmaceutical Engineering, TU Braunschweig
[*]Institute for Chemical and Thermal Process Engineering, TU Braunschweig,
Langer Kamp 7, DE-38106 Braunschweig, s.scholl@tu-bs.de (*Corresponding author)

ABSTRACT

The successful transfer from batch to a continuous flow process in a fixed bed reactor of a ligand in metalorganic API synthesis, the diazolium salt 1,3-methyl-benzoimidazol-3-ium iodide, is presented. Results show similar yields and conversion rates at corresponding process parameters in batch and continuous mode. By exceeding temperature limitation of a non-pressurized batch process, the pressurized continuous reactor system shows the potential for outperforming the batch synthesis regarding space time yield. Hence, process intensification by continuous flow presents itself as a viable approach for the heterogeneous di-*N*-alkylation of diazoles. Alternative basic reagents and solvents further enhance the viability of a continuous approach by addressing limitations such as side reactions and solubility of the reagent.

Keywords: Continuous flow synthesis, fixed bed reactor, heterogeneous synthesis, 1H-benzimidazole

INTRODUCTION

Over the last decades imidazole and benzimidazole derivatives gained interest due to their capability of forming stable *N*-heterocyclic carbenes (NHC) [Dröge 2010]. Since then NHC have been widely used as ligands in organometallic complex synthesis (M-NHC) [Jacobsen 2009]. The initial derivatives of e.g. benzimidazole can be prepared in various forms adjusting their properties and possible applications. Hence diazoles can be considered as scaffold chemicals for e.g. M-NHC synthesis with applications in catalysis and especially as active pharmaceutical ingredients (API) [Rubbiani 2011; Oehninger 2013; Aher 2014]. Carbenes are often synthesized by deprotonation of a corresponding diazolium salt. Diazolium salts can be synthesized e.g. by reductive cyclization which requires and metal catalysts (e.g. Pd) or by *N*-alkylation of diazoles [Boiani 2005; Jacobsen 2009; Guillena 2010; Grieco 2015]. Both routes are often also time-consuming. A transfer to continuous processing offers advantages due to process intensification and low holdup e.g. reducing overall time required for total conversion and precise as well as fast process controllability.

By establishing the *N*-alkylation in presence of a solid basic reagent and a halogenated alkylating agent for continuous operation another downside of both batch and continuous approaches can be addressed. Syntheses of diazolium salts can be performed with an abundant and non-expensive basic reagent such as K_2CO_3 instead of costly catalysts [Sauk 2019]. Catalysts which are often discarded or offer limited regeneration cycles.

In this work the successful transfer of the synthesis of 1,3-dimethyl-1H-benzoimidazol-3-ium iodide (DBI) from batch to continuous processing is presented. Synthesis is performed in a continuous flow fixed bed reactor via a di-*N*-alkylation of 1*H*-benzimidazole (see Fig. 1) in presence of methylene iodide and K_2CO_3.

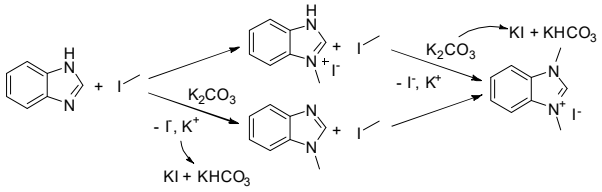

Figure 1: Assumed reaction scheme of the 2-step synthesis of 1,3-methyl-benzoimidazol-3-ium iodide (DBI) in the presence of a solid base (K_2CO_3) and methylene iodide (MI). Intermediate: 1-methyl-1H-benzoimidazol-3-ium iodide (MBI)

In addition, the viability but also limitations of this process are addressed such as negative effects of elevated reactor temperature on conversion rates and occurrence of side reactions. Chances to overcome these limitations and further enhance the process by screening for alternative solvents and basic reagents are addressed as well.

CONTINUOUS FLOW SYSTEM

Figure 2 presents the experimental set-up. The continuous flow synthesis is performed in an electrically heated HPLC column (L = 250 mm, ID = 8 mm). Peripheral components are two HPLC pumps as well as a mixer combining the reagents before entering the column. Subsequent to the column the back-pressure regulator (7 bar) protected by a filter secures constant system pressure. Valves (magnetic and manual) enable

sampling at certain stages of the process as well as switching between conditioning, cleaning and synthesis. In addition, a conductivity sensor is integrated enabling qualitative tracking of the synthesis progress.

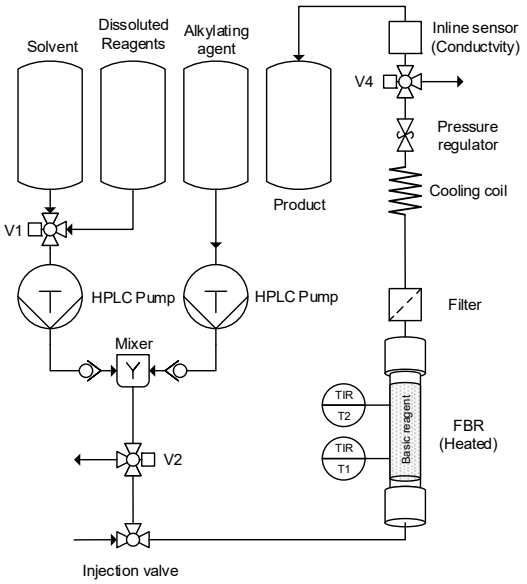

Figure 2: Process flow chart of the continuous flow synthesis of diazolium salts in a fixed bed reactor

CONTINUOUS FLOW PROCESSING

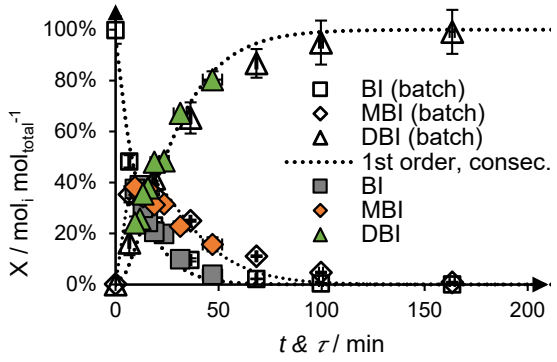

Figure 3: Comparison of conversion to DBI in batch and continuous processing with K_2CO_3 as basic reagent (r = 5 mol_{MI} mol_{BI}^{-1})

By performing the continuous synthesis at similar process parameters as the batch synthesis both show a good agreement (see Figure 3). In addition, the synthesis progress can be approximated by a kinetic model for consecutive reactions of first order as expected from the reaction scheme (see Figure 1). The pressurized continuous system enables higher reaction temperature (T > 82°C for acetonitrile) hence outperforming the batch system regarding accessibility (e.g. sampling), safety and potentially space time yield STY. Figure 4 shows the beneficial influence of the elevated fixed bed temperature on the synthesis. Nonetheless higher temperatures result in yet unknown side reactions reducing overall yield and purity of the product.

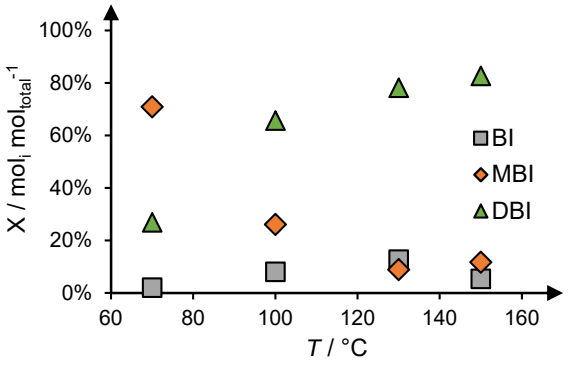

Figure 4: Influence of temperature on the reactor outlet composition in a continuous flow fixed bed reactor (K_2CO_3; n = 1 per temperature; $\dot{V}$ = 200 µL min^{-1}; r = 2.5 mol_{AX} mol_{BI}^{-1})

Thus, alternate synthesis approaches by changing the basic reagent and also solvent are addressed as well.

SCREENING OF BASE AND SOLVENT

Besides unfavorable side reactions, the formation of $KHCO_3$ (see Figure 1) and possible decomposition to CO_2, H_2O and K_2CO_3 thus degradation of the fixed bed is ubiquitous. Hence screening for alternative abundant and non-expensive basic reagents is performed.

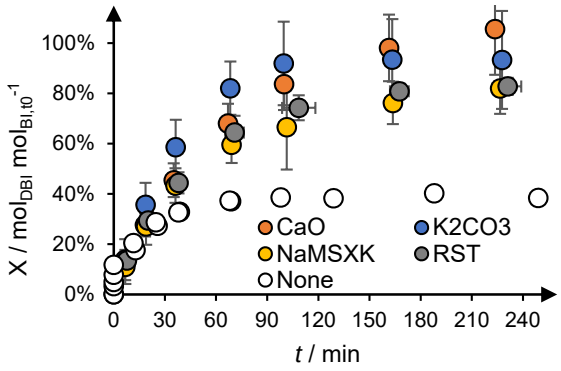

Figure 5: Conversion to DBI with none and a selection of basic reagents from the groups of metal oxides, activated carbon, zeolites and alkali (r = 2.5 mol_{MI} mol_{BI}^{-1}, batch, n = 3)

Figure 5 shows the conversion to the product when different basic reagents are applied in a batch synthesis. CaO offers the best similarity to K_2CO_3, whereas basic zeolites (NaMSXK) or basic activated carbon (RST) exhibit good conversion but also adsorption of the product, intermediate as well as initial reagent. Adsorption has been observed for several types of activated carbon as well as zeolites, hence both substances are not applicable for synthesis or as subsequent adsorbents for purification of the synthesis solution. Also, the necessity of a basic reagent is shown as the synthesis course without a basic reagent (None)

indicates the lowest and stagnating conversion to the product.

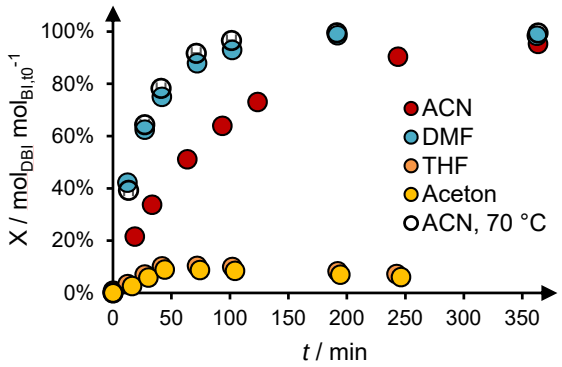

Figure 6: Conversion to DBI for different synthesis solvents (K_2CO_3, T = 50 °C, r = 5 mol_{MI} mol_{BI}^{-1}, batch, n = 3)

Batch syntheses for a selection of aprotic polar solvents have been conducted as shown in Figure 6. Regarding the low boiling point of acetone, batch syntheses have been performed at 50 °C. Both THF and acetone show low conversion rates as well as a decreasing ratio of product. This decrease is related to a low solubility of the product and precipitation rendering both solvents unsuitable for continuous operation. DMF exhibits conversion rates exceeding acetonitrile by a factor of 4 similar to a reaction in acetonitrile at 70 °C.

Results of both base and solvent screening indicate a high potential of e.g. calcium oxide (CaO) and DMF. Hence increase of space-time-yield (STY) by a factor of approximately up to 49 is possible due to high solubility and conversion rates of the reagents as well as low occurrence of side reactions.

CONCLUSIONS AND OUTLOOK

Continuous flow synthesis in a fixed bed of an exemplary diazolium salt has been successfully performed. In addition, first results of a selection of alternative basic reagents and solvents have been presented. Results show the potential and viability of a fixed bed reactor with basic reagents for di-*N*-alkylation of diazoles though further investigations on column degradation as well as side reaction must be conducted. Current investigation focuses on long term stability of the fixed bed as well as identification and reduction of side reactions.

ACKNOWLEDGMENT

This study was partially funded by the Lower Saxony Ministry for Science and Culture (MWK) in the joint research project *"Processing of poorly soluble drugs at small scale - µ-Props"* of the Center of Pharmaceutical Engineering (PVZ) of the Technische Universität Braunschweig.

NOMENCLATURE

BI		1*H*-benzimidazole
DBI		1,3-methyl-benzoimidazol-3-ium iodide
MBI		1-methyl-1*H*-benzoimidazol-3-ium iodide
MI		Methylene iodide
τ	[min]	Residence time
t	[***s***]	Time
T	[**°C**]	Temperature

REFERENCES

AHER, S.B., MUSKAWAR, P.N., THENMOZHI, K., AND BHAGAT, P.R. 2014. *European Journal of Medicinal Chemistry 81*, 408–419. http://www.sciencedirect.com/science/article/pii/S0223523414004504.

BOIANI, M., AND GONZALEZ, M. 2005. *MRMC 5*, 4, 409–424.

DRÖGE, T., AND GLORIUS, F. 2010. *Angew. Chem. 122*, 39, 7094–7107.

GRIECO, G., BLACQUE, O., AND BERKE, H. 2015. *Beilstein journal of organic chemistry 11*, 1656–1666.

GUILLENA, G., J RAMÓN, D., AND YUS, M. 2010. *Chemical reviews 110*, 3, 1611–1641.

JACOBSEN, H., CORREA, A., POATER, A., COSTABILE, C., AND CAVALLO, L. 2009. *Coordination Chemistry Reviews 253*, 5-6, 687–703.

OEHNINGER, L., RUBBIANI, R., AND OTT, I. 2013. *Dalton transactions (Cambridge, England : 2003) 42*, 10, 3269–3284.

RUBBIANI, R., CAN, S., KITANOVIC, I., ALBORZINIA, H., STEFANOPOULOU, M., KOKOSCHKA, M., MÖNCHGESANG, S., SHELDRICK, W.S., WÖLFL, S., AND OTT, I. 2011. *Journal of medicinal chemistry 54*, 24, 8646–8657.

SAUK, T., HENKE, L., XIAO, C., HARTIG, D., AND SCHOLL, S. 2019. *Chem. Eng. Technol., in revision*.

PEG-YLATED PARENTERAL NANOEMULSIONS AS PROSPECTIVE CARRIERS FOR ENHANCED BRAIN DELIVERY WITH DIAZEPAM AS A MODEL DRUG – PHYSICOCHEMICAL CHARACTERISATION

Đoković J. [1], Konkel M. [2], Mitrović J. [1], Savic S.M. [3], Watrobska-Swietlikowska, D. [2], Cekić N. [3], Savić S.D. [1]

[1] Department of Pharmaceutical Technology and Cosmetology, University of Belgrade – Faculty of Pharmacy, Vojvode Stepe 450, Belgrade, Serbia

[2] Department of Pharmaceutical Technology, Medical University of Gdansk, Hallera 107, 80-416 Gdansk, Poland

[3] Faculty of Technology, University of Niš, Leskovac 16000, Serbia

e-mail of corresponding author: snezana.savic@pharmacy.bg.ac.rs

ABSTRACT

Parenteral nanoemulsions are regarded as biocompatible drug delivery systems for lypophilic drugs. When it comes to delivering actives to the brain as a target site, prolonged circulation time is desirable. The objective of this study was to conduct physicochemical characterization of PEGylated nanoemulsions as prospective carriers for enhanced brain delivery, using diazepam as a model active substance for brain targeting. Nanoemulsions were prepared by high pressure homogenization method and characterized regarding droplet size, zeta potential, pH, conductivity, viscosity and in vitro release profile. PEG2000-DSPE and PEG5000-DPPE were used for PEGylation. All the formulations were autoclaved and stored at room temperature. After 2 months there were no significant changes in physicochemical parameters in autoclaved formulations which rendered them as good potential templates to incorporate drugs for brain targeted delivery.

Keywords: PEGylated nanoemulsions, diazepam, physicochemical characterization, in vitro release

INTRODUCTION

Nanoemulsions are regarded as biocompatible drug delivery systems which are especially beneficial for parenteral application of water insoluble actives. It is considered that the oil droplets are rapidly removed from the circulation by the components of the mononuclear phagocytic system (MPS) [Hormann, 2016]. When it comes to brain as a target site, prolonged circulation time of oil droplets is beneficial as it allows more time for an active to reach and cross the blood brain barrier. One of the strategies used to prolong the circulation time of parenteral nanoemulsions is coating the surface of oil droplets with polyethyenglicol (PEG) chains. PEG chains provide protection against detections by opsonins from plasma and MPS removal from the circulation by increasing the surface hydrophilicity [Kandadi, 2011]. Diazepam is available on the market as nanoemulsion preparation (Diazelmus, Kabi-Pharmacia, Sweden) and is commonly used benzodiazepam [Đorđević, 2013]. The aim of this study was to develop and characterize PEGylated parenteral nanoemulsions as possible carriers for prospective delivery of actives to the brain, using diazepam as a model active substance.

RESEARCH CONCEPT

Nanoemulsions (non-PEGylated - NPEG and PEGylated) were prepared by high pressure homogenization method, autoclaved and characterized regarding droplet size, zeta potential, pH and conductivity both initially and after 2 months of storage at room temperature. Additionally, viscosity measurements and *in vitro* release study of the formulations were performed.

1. Nanoemulsion preparation and sterilization

Diazepam loaded nanoemulsions (2mg/g) were prepared using high pressure homogenization method

at room temperature. Water and oil phase were prepared separately. Aqueous phase (glycerol, polysorbate 80, highly purified water and 0,1 M NaOH) was added to oil phase (soybean oil, medium chain triglycerides, soybean lecithin, butylhydroxytoluene and diazepam) and homogenized using rotor stator homogenizer (IKA Ultra-Turrax® T25 digital) at 8000 rpm for 3 minutes. Formulations were further homogenized by high-pressure homogenizer (EmulsiFlex-C3, Avestin Inc., Canada) for 9 cycles at 500 bar. PEGylation agents used were PEGylated phospholipids: PEG2000-DSPE (P2) or PEG5000-DPPE (P5), which were added to the aqueous phase at concentration of 0,1% or 0,3% (P2_0.1%, P2_0.3% P5_0.1%, and P5_0.3%). All formulations were sterilized in autoclave at 121°C for 15 minutes.

2. Size and zeta potential measurements

Formulations were characterized regarding the mean droplet size (intensity weighed mean diameter, Z-Ave), droplet size distribution - polydispersity index (PDI) and zeta potential (ZP) by Zetasizer Nano ZS90 (Malvern Instruments Ltd., Worcestershire). In order to confirm the size measurements and check for larger droplets presence laser diffraction measurements were performed using Beckman Coulter LS 13 320 (Beckman Coulter, Inc., Brea, California).

3. Conductivity, pH and viscosity

Conductivity and pH measurements were performed to test the formulations' stability after sterilization and during storage as well as suitability for parenteral application. Viscosity measurements were conducted in order to assess the formulations' syringeability and suitability for parenteral application.

4. *In vitro* release studies

The drug release was studied by dialysis bag method using cellulose membrane with molecular weight cut off of 12000. Dialysis bags with 2 ml of the formulations were placed in 200 ml of the dissolution medium - phosphate buffer pH 7,4 (USP) : methanol = 80:20 (*v/v* %). Samples were drown after 0.083, 0.167, 0.333, 0.67, 1, 2, 4, 8, 12 and 24 hours and analyzed for diazepam content by spectrophotometer at 230 nm. The release profiles were analyzed with different kinetic models: zero order, first order, Higuchi, Baker-Lonsdale, Korsmeyer-Peppas and Hixon-Crowel models (DDSolver packet for Microsoft Excel apication).

RESULTS

The size measurements preformed initially and after 2 months of storage showed that Z-ave was in the range of 180 nm to 220 nm, with PDI below 0,2 for both non-autoclaved and autoclaved samples (**Figure 1**.). Laser diffraction measurements showed that d_{100} was below 1 µm for all samples.

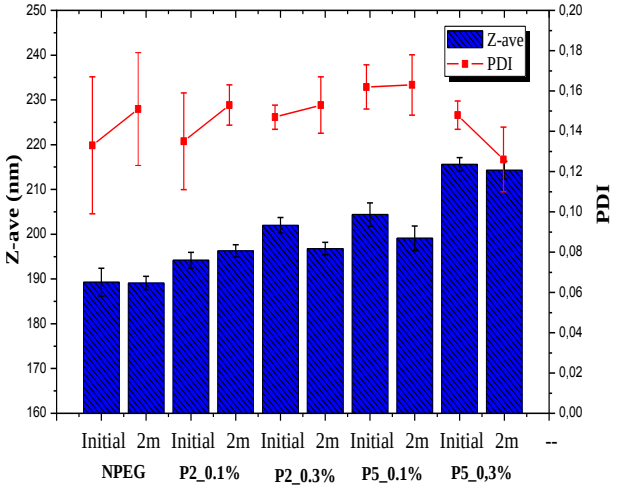

Figure 1. Z-ave and PDI results of the non-autoclaved formulations

Zeta potential for all the samples was between -30 and -50 mV (**Figure 2)**. Non-autoclaved samples had significant changes in pH (decreasing from around 7 to about 5 within 2 months) and conductivity (increasing from around 100 µS/cm to around 400 µS/cm). As for the autoclaved samples, pH and conductivity remained stable at around 7 and 100 µS/cm, respectively. Viscosity was around 5 mPa*s for all samples.

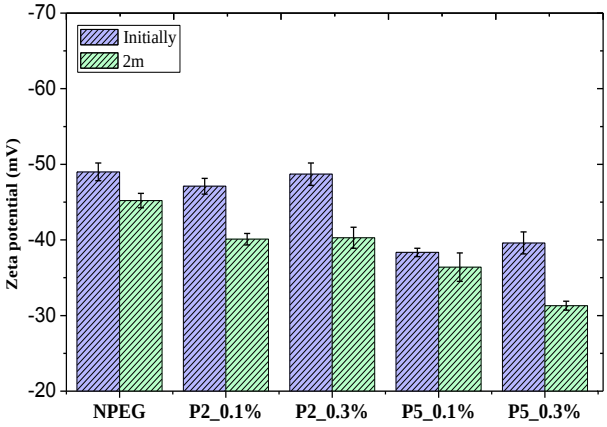

Figure 2. Zeta potential for the non-autoclaved formulations.

The results from in vitro release study are shown on **Figure 3.**

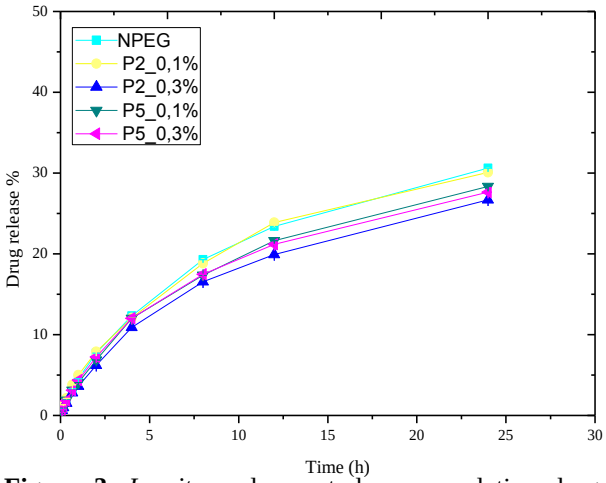

Figure 3. *In vitro* release study – cumulative drug release

DISCUSSION

All the PEGylated formulations had higher droplet size comparing to the non-PEGylated formulation and Z-ave increased with increasing concentration of PEGylated phospholipids. Droplet size was higher when using PEG5000-DPPE compared to PEG2000-DSPE, which can be explained with the longer of PEG chains in PEG5000-DPPE formulations. Nevertheless, the Z-ave was below 500 nm for all the formulations, with no droplets larger than 1 μm detected, which is concordant with USP requirements. PDI remained below 0.2 showing narrow size distribution. Given that the formulations are stabilized with soybean lecithin, zeta potential values at around -40 mV were expected. During storage and autoclaving phospholipids and oils can succumb to hydrolysis, which in turn leads to increased negative zeta potential value. This could be perceived as beneficial given that the higher zeta potential values indicate better stability, but in this case it is a consequence of free fatty acid liberation, which leads to pH value decrease, which in turn promotes further degradation and destabilization in nanoemulsions [Klang, 2011]. Interestingly, in obtained autoclaved nanoemulsions showed better stability in terms of maintaining pH and conductivity values compared to the unsterilized formulations, which requires further insight . Lower absolute zeta potential values can been detected in formulations containing PEG5000-DPPE versus the non-PEGylated and the formulations containing PEG2000-DSPE, probably due to longer PEG chains increasing hydrophilicity on the surface. [Kandadi, 2011]. Interestingly, it appeared that the autoclaved samples showed better stability compared to the non-autoclaved samples regarding pH and conductivity measurements. Low viscosity of the formulations rendered them safe for parenteral use and showed that adding PEGylated phospholipids did not significantly increase the formulations' viscosity.

In the *in vitro* release study it could be observed that the highest release of diazepam was from the non-PEGylated formulation (Figure 3). That release profile was similar with the formulation containing 0,1 % PEG2000-DSPE, suggesting that the used concentration was too low to coat the nanoemulsion droplet surface and slow down the release. The slowest release was observed when using 0,3 % PEG2000-DSPE compared to both the non-PEGylated formulation and the formulations containing PEG5000-DPPE, which could be explained by PEG2000-DSPE forming more rigid packing at the interface comparing to DPPE chains, therefore causing slower release of the incorporated diazepam. This was corroborated by the fact that the Higuchi model, which describes drug release as a diffusion based process founded in the Fick's law was the best fit to describe the profiles (highest R^2, R_{adj}^2 and the lowest AIC - Akaike Information Criterion) [Costa, 2001]. Higuchi dissolution constants were lower for the formulations containing PEGylated phospholipids which indicated that they slow down the diffusion of the diazepam from the droplets.

CONCLUSIONS

Initial physicochemical characterization suggested that investigated nanoemulsions were appropriate for parenteral application. Release profiles showed that the PEGylated formulations could delay the release of the incorporated drugs, which could be beneficial when prolonged release of the active is required. They could be considered as prospective template carriers for the water insoluble actives when prolonged circulation time is desired, for example for brain targeted delivery. However, further investigations are necessary in order to prove pharmacokinetic advantages *in vivo*, like pharmacokinetic study in animal models.

ACKNOWLEDGMENT

This work was supported by the Ministry of Education, Science and Technological development, Republic of Serbia, within the framework of the project TR34031 as well as CEEPUS project CIII-RS-1113-02-1819

Central European Knowledge Alliance for Teaching, Learning and Research in Pharmaceutical Technology (CEKA PharmTech).

REFERENCES

[Hormann, 2016] Hormann K., Zimemer A., 2016, Drug delivery and drug targeting with parenteral lipid nanoemulsions-a review, *J. Control. Release*, Vol. 223, pp. 85-98.

[Kandadi, 2011] Kandadi P., Afzal S. M., Goparaboina S.and Veerabrahma K. ,2011, Brain specific delivery of pegylated indinavir submicron lipid emulsions, *Eur. J. Pharm. Sci.*, Vol 42,pp. 423-432.

[Đorđević, 2013] Đorđević S., Radulović T., Cekić N., Ranđelović D., Savić M., Krajišnik D., Milić J., Savić S., 2013, Experimental design in formulation of diazepam nanoemulsions: physicochemical and pharmacokinetic performances, *J. Pharm. Sci*., Vol. 102, pp. 4159-4172.

[Klang, 2011] Klang, V., Valenta, C., 2011. Lecithin–based nanoemulsions. *J. Drug Del. Sci. Tech*. Vol. 21,pp. 55–76

[Costa, 2001] Costa, P., Sousa Lobo, J.M., 2001. Modeling And Comparison Of Dissolution Profiles. *Eur. J. Pharm. Sci.* Vol. 13, pp.123–133.

PARTICLE BASED CULTIVATION OF *LENTZEA AEROCOLONIGENES* IN MEMBRANE AERATED STIRRED BIOREACTORS FOR INCREASED REBECCAMYCIN PRODUCTION

Kathrin Schrinner[1,3]*, Marcel Schrader[2,3], Jana Niebusch[1], Nadine Wurzler[1], Arno Kwade[2,3], Rainer Krull[1,3]

[1]Institute of Biochemical Engineering, TU Braunschweig, Rebenring 56, 38106 Braunschweig
[2]Institute for Particle Technology, TU Braunschweig, Volkmaroder Str. 5, 38104 Braunschweig
[3]Center of Pharmaceutical Engineering, TU Braunschweig, Franz Liszt Straße 35a, 38106 Braunschweig
*e-mail: k.schrinner@tu-braunschweig.de

ABSTRACT

Filamentous microorganisms represent the majority of natural producers of antibiotics and other active pharmaceutical ingredients (APIs). *Lentzea aerocolonigenes* is a filamentous actinomycete producing the antitumor antibiotic rebeccamycin. The addition of glass beads (100 g/L, Ø = 969 µm) in shake flask cultivations led to a significant increase in rebeccamycin production compared to an unsupplemented cultivation by inducing mechanical stress. To achieve larger amounts of rebeccamycin a scale-up was conducted. A bubble free membrane aeration was chosen to reduce the power input to stirrer and particle induced stress. Glass bead addition (50 g/L, Ø = 969 µm) in this membrane aerated stirred bioreactor increased rebeccamycin concentration compared to an unsupplemented cultivation as well. Moreover it reduced biomass growth on the aeration membrane which is a widespread challenge in membrane aerated bioreactors.

Keywords: membrane aeration, filamentous microorganisms, particle enhanced cultivation, mechanical stress

INTRODUCTION

Lentzea aerocolonigenes, belonging to the filamentous microorganisms, produces the antitumor antibiotic rebeccamycin. The microorganism exhibits a complex morphology ranging from freely dispersed mycelia to dense pellets [Pommerehne et al., 2019]. The morphology is linked to the product formation and can be controlled by e.g., inoculum concentration and viability, pH, medium composition, hydromechanical stress, addition of inorganic salts or particles [Walisko et al., 2015]. Rebeccamycin formation in *L. aerocolonigenes* was increased by the adjustment of mechanical stress induced by glass particles in shake flask scale [Walisko et al., 2017]. Scale up from shake flasks to laboratory scale bioreactors is often linked to increased mechanical stress and since is an important factor to be considered. Membrane aerated bioreactors show a reduced power input since no bubbles are present.

RESEARCH CONCEPT

Cultivations of *L. aerocolonigenes* in shake flask scale were conducted in 250 mL flasks with 4 baffles and 50 mL filling volume. A preculture was inoculated with 1 mL of frozen mycelium and incubated for 2 days at 28 °C and 120 min^{-1}. 300 µL of this preculture were used for inoculation of the main culture. Glass particles were added for adjustment of the induced mechanical stress at the beginning of the cultivation. Different size ranges and concentrations of glass beads were investigated. The flasks were incubated on an orbital shaker at 120 min^{-1} (50 mm amplitude) at 28 °C for 10 days. The growth medium consisted of 4 g/L glucose, 4 g/L yeast extract and 10 g/L mat extract with a pH of 7.2.

A scale up to a stirred bioreactor (Applikon Biotechnology, The Netherlands) with 1.2 L filling volume was performed. Aeration in this bioreactor was conducted via an oxygen permeable silicone tube (wall thickness = 0.2 mm; diameter = 2.9 mm, Reichelt Chemietechnik, Germany). The tube was wound around the installations inside the bioreactor and the end was placed above the liquid to provide additional headspace aeration. The length of the tubing as well as the aeration rate and the stirrer speed were varied. When glass particles were added a mean size of Ø = 969 µm was chosen. Cultivations were inoculated with 7.5 mL of a 2-day preculture and grown at 28 °C for 10 days with daily sampling.

Cell dry weight (CDW) was determined gravimetrically. Substrate and product quantification were conducted as described by [Walisko et al., 2017].

RESULTS AND DISCUSSION

L. aerocolonigenes was first investigated in shake flask scale, where the addition of glass beads showed increased product formation. Different glass bead sizes and concentrations were tested and the optimal rebeccamycin concentration of about 70 mg/L was achieved with a mean glass bead diameter of 969 µm in a concentration of 100 g/L. An unsupplemented control, however, only provided 5 mg/L rebeccamycin (**Fig. 1**).

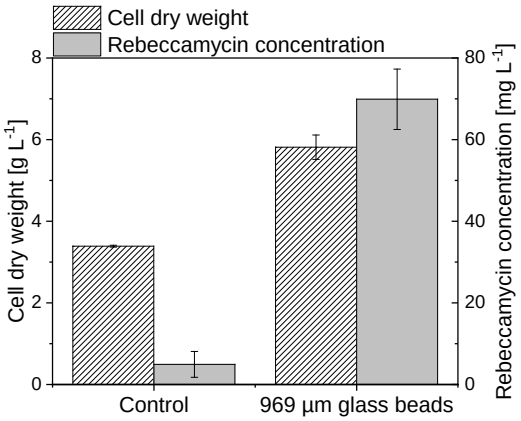

Figure 1: Cell dry weight concentration and rebeccamycin concentration of shake flasks cultivations without and with 100 g L^{-1} glass beads after 10 days of cultivation.

This process should be transferred to bioreactor scale to provide larger amounts of rebeccamycin since larger volumes are used. A certain amount of mechanical stress was beneficial for rebeccamycin production, however, excessive stress decreases product formation [Walisko et al., 2017]. Since conventional aeration in bioreactors creates additional stress, a bubble free membrane aeration was chosen.

A first cultivation without glass beads led to a maximum of 12 mg/L rebeccamycin (**Fig. 2**) which is comparable to an unsupplemented shake flask cultivation. During this cultivation, however, excessive biomass growth on the silicone membrane was observed (**Fig 3**, left). The addition of glass beads reduced the growth of biomass on the silicone tube (**Fig. 3**, right). The moving glass beads lead to a permanent abrasion ensuring an improved oxygen transfer.

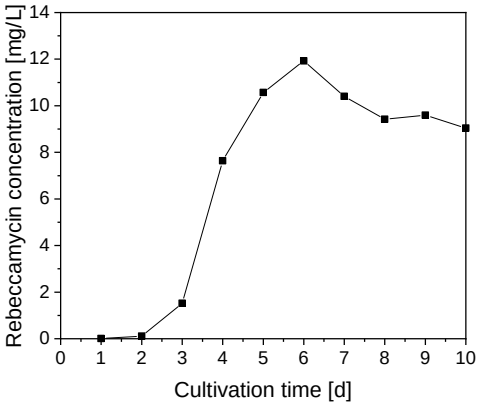

Figure 2: Rebeccamycin concentration of a silicone membrane aerated bioreactor cultivation without glass particles at an agitation rate of 400 min^{-1} and an aeration rate of 0.2 L/min (0.4 L/min during exponential phase).

Figure 3: Biomass growth on silicone membrane without (left, 5 m tube length) and with glass beads (right, 50 g/L, Ø = 969 µm, 2.5 m tube length) added to the cultivation.

Moreover, the cultivation with glass beads resulted in an increased rebeccamycin concentration (**Fig. 4**). With 50 g/L glass beads of 969 µm mean diameter a maximum rebeccamycin concentration of 42 mg/L was provided.

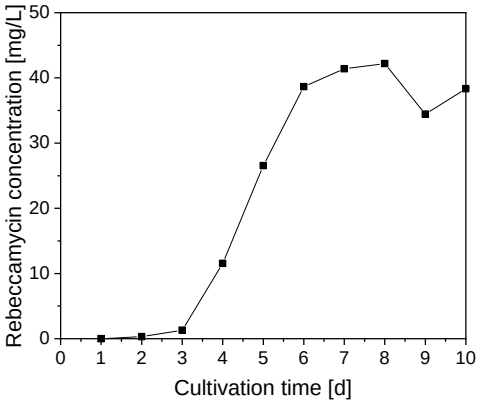

Figure 4: Rebeccamycin concentration of a silicone membrane aerated bioreactor cultivation with glass

particles (50 g/L, Ø = 969 µm) at an agitation rate of 650 min^{-1} and an aeration rate of 0.2 L/min (0.4 L/min during exponential phase).

CONCLUSIONS

Successful cultivations of *L. aerocolonigenes* in a membrane aerated stirred bioreactor were conducted. The use of membrane aeration through a silicone tube reduces the mechanical stress induced on the microorganism and additionally avoids foaming which is often problematic especially for complex media. The in this paper presented combination of membrane aeration and glass bead addition provides further advantages. The increase of product formation by the addition of glass beads as seen in shake flasks could also be observed in bioreactor scale. Furthermore the glass beads decrease the biomass growth on the silicone membrane since they are causing a permanent abrasion. This makes membrane aerated bioreactors a promising cultivation platform, especially for other filamentous microorganisms.

ACKNOWLEDGMENT

The authors gratefully acknowledge financial support from the German Research Foundation (DFG) in the Priority Programme 1934 *DiSPBiotech – Dispersity, structural and phase changes of proteins and biological agglomerates in biotechnological processes* (*KR 1897/6-1).*

REFERENCES

[Pommerehne et al., 2019] Pommerehne, K., Walisko, J., Ebersbach, A., Krull, R., 2019, The antitumor antibiotic rebeccamycin – challenges and advanced approaches in production processes, *Appl. Microbiol. Biotechnol.*, 103, 3627–3636.

[Walisko et al., 2015] Walisko, R., Mönch-Tegeder, J., Blotenberg, J., Wucherpfennig, T., Krull, R., 2015, The taming of the shrew – Controlling the morphology of filamentous eukaryotic and prokaryotic microorganisms, *Adv. Biochem. Eng. Biotechnol*., 149, 1–27.

[Walisko et al., 2017] Walisko, J., Vernen, F., Pommerehne, K., Richter, G., Terfehr, J., Kaden, D., Dähne, L., Holtmann, D., Krull, R., 2017, Particle-based production of antibiotic rebeccamycin with *Lechevalieria aerocolonigenes*, *Process Biochem*, 53, 1–9.

PARAMETER IDENTIFIABILITY OF ARTEMISININ SYNTHESIS USING DESIGN OF EXPERIMENTS

Moritz Schulze[1,2], Susann Triemer[3], René Schenkendorf[1,2,*],

Andreas Seidel-Morgenstern[3,4], Ulrike Krewer[1,2]

1: Institute of Energy and Process Systems Engineering, TU Braunschweig, Germany
2: Center of Pharmaceutical Engineering, TU Braunschweig, Germany
3: Max Planck Institute for Dynamics of Complex Technical Systems, Magdeburg, Germany
4: Otto-von-Guericke-University, Magdeburg, Germany
*r.schenkendorf@tu-braunschweig.de

ABSTRACT

Artemisinin-based combination therapies are recommended by the World Health Organization to treat malaria, one of the most abundant infectious diseases in the world. Recently, a novel production route, which combines the extraction and the catalyzed chemical synthesis, has been shown to be a promising sustainable processing alternative [Triemer, 2018]. To exploit its mechanism, operational settings and limits, mathematical modeling might be beneficial when thorough system insight is required. In a first step, we consider the catalyzed synthesis step from dihydroartemisinic acid to artemisinin, and we show that only a subset of the parameters of the considered model is identifiable with the available sparse data using a singular value decomposition approach. In a second step, within the framework of design of experiments (DoE), we demonstrate the effect of additional experimental data to overcome the non-identifiability problem of the model parameters.

Keywords: parameter identifiability, design of experiments, parameter sensitivities, singular value decomposition, antimalarial artemisinin synthesis

INTRODUCTION

In the case of antimalarial drugs, artemisinin is an essential precursor to several active pharmaceutical ingredients (APIs). Aiming for lower costs, the two-step partial synthesis of dihydroartemisinic acid (DHAA) to artemisinin has gained interest in academia and industry. To improve the production of artemisinin, process systems engineering concepts can be applied. For instance, mathematical process models may predict the best catalysts, solvents, reaction conditions, as well as the overall reactor type and operating conditions. However, when applying model-based process design concepts, the risk of false predictions and misinterpretations depends critically on data quality and uncertainties of the identified model parameters, respectively. Besides a valid process model and informative experimental data, the model parameters have to be theoretically identifiable. In the literature, various identifiability concepts exist, but only some of these methods apply to complex, non-linear process models. In this study, we determine the local parameter sensitivity matrix for a simplified process model of the two-step partial synthesis of DHAA to artemisinin, and we analyze the parameter identifiability of this process model using a singular value decomposition approach [Stigter, 2017]. To improve the parameter identifiability, we also apply a model-based design of experiments (DoE) concept that demonstrates the effect of additional experimental data on the parameter identifiability.

METHODS

Frequently, dynamic processes are described via ordinary or partial differential equation systems, and the model parameters p are identified via numerical optimization methods minimizing the differences between simulation results and experimental data. The parameter identification problem, however, might be ill-posed in the case of non-identifiable model parameters. In DoE and the identifiability analysis, the local parameter sensitivity matrix is an essential measure [Schenkendorf, 2018] and is defined as:

$$\boldsymbol{SM}_{t_k}[\mathbf{i},\mathbf{j}] = \left.\frac{\partial y_i}{\partial p_j}\right|_{t_k},$$

where $\boldsymbol{y_i}$ is the i*th* model response function and $\boldsymbol{p_j}$ the j*th* model parameter. If the sensitivity matrix $\boldsymbol{SM}$ is singular, that is, the matrix is rank deficient, the model parameters cannot be identified properly [Stigter, 2017]. To test the rank of the $\boldsymbol{SM}$, the singular value decomposition can be used:

$$\boldsymbol{SM}(\boldsymbol{t_0}, \dots, \boldsymbol{t_k}, \boldsymbol{p}) = \boldsymbol{u_1}\boldsymbol{\sigma_1}\boldsymbol{v_1^T} + \cdots + \boldsymbol{u_q}\boldsymbol{\sigma_q}\boldsymbol{v_q^T},$$

where $\boldsymbol{\sigma_i}$ are the singular values, $\boldsymbol{u_i}$ are the left-singular vectors, and $\boldsymbol{v_i}$ are the right-singular vectors. Here, zero singular values indicate a lack of identifiability, and the non-zero elements of the corresponding singular vectors $\boldsymbol{v_i}$ reveal the non-identifiable parameter or parameter combinations.

RESULTS

The details of the implemented two-phase process model of the partial synthesis of artemisinin, which has 10 system states and 7 unknown model parameters, can be found in [Triemer, 2016]. Moreover, we assumed that 7 of the 10 system states are measurable. In Fig. 1, the resulting singular values are shown. The singular values $\sigma_i, i \in \{5,6,7\}$ are close to zero, that is, the model parameters are non-identifiable. The related singular vectors $\boldsymbol{v}_i, i \in \{5,6,7\}$ clearly show that only a minor subset $\{\boldsymbol{p}_3, \boldsymbol{p}_6\}$ of the model parameters can be identified in principle; see Fig. 2. In turn, the model parameters $\{\boldsymbol{p}_4, \boldsymbol{p}_5\}$ and the combination of $\boldsymbol{p}_1, \boldsymbol{p}_2$, and $\boldsymbol{p}_7$ are non-identifiable.

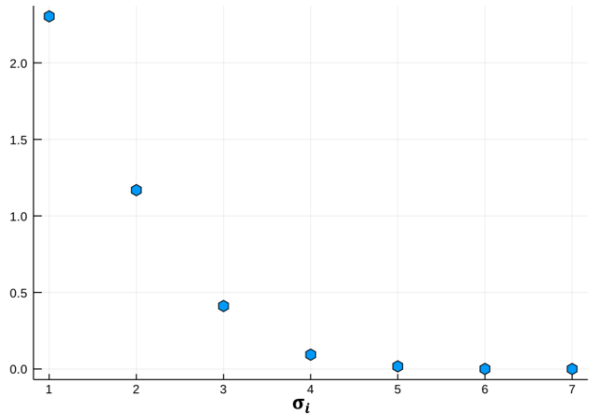

Figure 1: Singular values of the local sensitivity matrix.

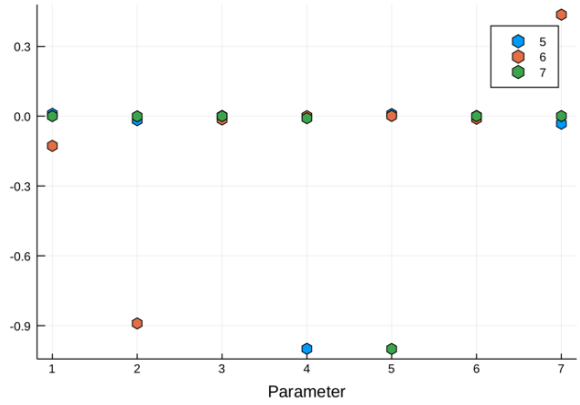

Figure 2: Elements of the right-singular vectors of the singular values $\sigma_i, i \in \{5,6,7\}$.

When applying DoE and increasing the number of experimental data, we observed no improvement regarding the identifiability. Thus, there is a structural lack of parameter identifiability of the studied process model of the partial synthesis of artemisinin.

CONCLUSIONS

We studied the identifiability of a given process model of the partial synthesis of artemisinin. Based on the sensitivity matrix and its singular values, we proved that the model parameters are non-identifiable and that additional experimental data do not result in a proper parameter identification problem. Future work will combine DoE and model reduction techniques to improve the parameter identifiability, leading to reliable model-based process analysis and design results for an optimal artemisinin synthesis.

ACKNOWLEDGMENT

This work was supported by the Max Planck Society and the International Max Planck Research School for Advanced Methods in Process and Systems Engineering.

REFERENCES

[Triemer, 2018] Triemer, S., Gilmore K., Vu, G. T., Seeberger, P. H., and Seidel-Morgenstern, A., 2018, Literally Green Chemical Synthesis of Artemisinin from Plant Extracts, *Angewandte Chemie International Edition*, Vol. 57(19).

[Schenkendorf, 2018] Schenkendorf, R., Xiagzhong, X., Rehbein, M., Scholl S., and Krewer U., 2018, The Impact of Global Sensitivities and Design Measures in Model-Based Optimal Experimental Design, *Processes*, Vol. 6(4).

[Stigter, 2017] Stigter, J. D., Joubert D., and Molenaar, J., 2017, Observability of Complex Systems: Finding the Gap, *Scientific Reports*, Vol. 7(1).

[Triemer, 2016] Triemer, S., 2016, Experimentelle und theoretische Untersuchung der photokatalytischen Oxidation von Dihydroartemisininsäure zu Artemisinin, *Master Thesis*, Otto-von-Guericke Universität, Magdeburg.

PGX TECHNOLOGY: NOVEL TAILOR-MADE AND TUNEABLE DELIVERY SYSTEMS FOR POORLY WATER-SOLUBLE BIOACTIVES

AUTHOR(S); Bernhard Seifried[a], Feral Temelli[b], Donna Vine[b], Ricardo Couto[b], Byron Yepez[a], Emily Wong[a], Paul Moquin[a]

[a)] Ceapro Inc., 7824-51 Avenue, Edmonton, AB, T6E 6W2, CANADA;

[b)] University of Alberta, Department of Agricultural, Food and Nutritional Sciences, Edmonton, CANADA;

E-MAIL: bseifried@ceapro.com

ABSTRACT

The delivery of poorly water-soluble bioactives, including active pharmaceutical ingredients (API) and nutraceutical components is of great interest for existing drugs and new drug developments, cosmetic formulations, functional foods and nutraceuticals. This article presents a novel patented technology called PGX Technology, which utilizes pressurized gas expanded (PGX) liquids to dry, micronize, purify and functionalize water-soluble polymers. PGX Technology can generate open-porous nanostructured polymer carriers composed of one or several water-soluble polymers forming powders, granules, nano-fibrils, aerogels and exfoliated nano-composites with specific surface areas (SSA) ranging from tens to several hundred m^2/g. Such mesoporous water-soluble carrier systems can be impregnated with a bioactive by means of adsorptive precipitation, utilizing supercritical carbon dioxide, leading to the uniform deposition of nano-scale particles (<120 nm) throughout the porous matrix, forming a bioactive-polymer complex, for example coenzyme Q10 on β-glucan (CoQ10-iBG). A nano-dispersion of CoQ10 is formed when such CoQ10-iBG complex is dissolved in water, which is stable over 6 months at room temperature. The bioavailability of the CoQ10-iBG complex tested in rats compared favorably with a positive control (CoQ10 in triolein) and a commercial CoQ10-cyclodextrin complex.

Keywords: gas expanded liquid, biopolymer nano-fibers, nano-dispersion, solid dosage form

INTRODUCTION

Novel strategies for the formulation and processing of poorly water-soluble bioactives and drugs range from lipid-based colloidal drug delivery systems (DDS) to drug nanosuspensions and innovative solid dosage forms such as orodispersible films (ODFs) or electrospun fiber mats as drug carriers [Göke, 2018]. The generation of drug nanosuspensions can be achieved by either bottom-up or top-down methods. Top-down methods usually start from larger drug particles, which are then reduced in size by applying mechanical shear, force or cavitation treatment. Top-down methods employ milling techniques, such as wet milling, colloid milling, jet milling or high-pressure homogenization methods, such as micro-fluidization or a piston gap technique [Chin, 2014; Wais, 2016]. In a bottom-up method the drug is typically dissolved first in a suitable solvent and then precipitated by changing solubility, which can be achieved in several ways, such as the addition of an antisolvent. In such antisolvent precipitation processes the method of addition and mixing of the antisolvent to the solution becomes critical and can be achieved by means of rapid mixing devices, ranging from simple stirrers to rotating fixed beds, multi inlet vortex mixers and confined liquid impinging jets to reach highly turbulent and fast mixing thereby controlling supersaturation and nucleation [Chan, 2011]. Processing techniques using supercritical fluids (SCF) to produce drug nanoparticles/nanocrystals have also been developed, which take advantage of the highly tunable solvent properties of SCFs [Padrela, 2018]. The SCF in such process can be utilized as an antisolvent to cause precipitation out of a solution, a solvent for the solute or as an additive to facilitate atomization and drying [Padrela, 2018; Tabernero, 2012]. Moreover, SCF processes were developed for particle formation of polymers to be used as carrier delivery systems [Yeo, 2005]. For polymer processing, the SCF can be dissolved in a polymer melt and aid in melting point

reduction and atomization, such as in the "Particle formation from gas-saturated solution" (PGSS) process, leading to highly porous polymer particles and agglomerates [Yeo, 2005].

Pressurized Gas eXpanded (PGX) liquid Technology has been developed at the University of Alberta [Seifried, 2010], is patented in the US, Europe and Canada [Temelli & Seifried, 2016 and 2018] and has been scaled-up to demo-scale at Ceapro Inc. [Seifried, 2019]. This platform technology can purify and dry aqueous solutions or slurries of polymers into open-porous nano-structured particles and fibrils utilizing a PGX fluid composed of supercritical carbon dioxide ($SCCO_2$) and anhydrous ethanol at mild operating conditions of 40°C and 100 bar as drying fluid. With the PGX Technology, single and multiple polymers can be processed by simply blending polymer solutions or suspensions to generate exfoliated nano-composites. As well, the water-soluble polymers can be further modified by cross-linking during the PGX process, allowing generation of tailor-made and tunable delivery systems.

The first objective of this work is to present various polymers processed by PGX Technology into open-porous particles, fibrils and nano-composites with large specific surface area (SSA). The next objective is to demonstrate that such open-porous PGX biopolymer carriers can be loaded with a bioactive forming novel bioactive impregnated polymer complexes termed "**i**mpregnated **P**olymer comple**X**" (iPX) by means of adsorptive precipitation utilizing $SCCO_2$ [Gurikov, 2018]. Specifically, PGX processed oat β-glucan was loaded with the bioactive Coenzyme Q10 (CoQ10), a poorly bioavailable lipophilic substance with antioxidant activity. The new complex termed CoQ10-iBG is compared to a commercial CoQ10-cyclodextrin complex in terms of water dispersibility and physical nanosuspension stability. Finally, a pilot study demonstrating the intestinal bioavailability of CoQ10 was performed to determine the direct in-vivo intestinal bioavailability of CoQ10 from the CoQ10-iBG complex compared to a standard food grade and commercial crystalline CoQ10 formulations using an intestinal-lymph cannulated rodent model.

RESEARCH CONCEPT

Generation of polymer carrier: PGX Technology involves the spraying of an aqueous solution or slurry of polymer into a pre-pressurized collection chamber, together with a PGX fluid, composed of $SCCO_2$ and a water-soluble co-solvent/antisolvent (i.e. ethanol, acetone or isopropanol) by means of a coaxial nozzle. At the processing conditions, the PGX fluid and aqueous phase become completely miscible thereby eliminating interfacial tension and capillary forces leading to rapid precipitation of the polymer and quick removal of the water. Thus, open-porous and unique nanoscale morphologies can be generated.

Loading of bioactive onto polymer carrier: The porous polymer carrier generated by PGX is then subjected to an adsorptive precipitation process utilizing $SCCO_2$ to load a bioactive or drug onto the matrix [Gurikov, 2018]. In this process, the bioactive is essentially solubilized at elevated pressure and suitable temperature in $SCCO_2$ and passed through a bed of porous polymer carrier previously prepared using the PGX Technology. During this step, the SCCO2 with the dissolved bioactive or drug can penetrate the entire carrier matrix deep into the porous structure, where it can interact with the polymer matrix, leading to adsorption of the drug on the polymer. Furthermore, by modulating the pressure during the adsorptive precipitation process a sudden change of solute solubility in the $SCCO_2$ solution can be rapidly induced, leading to precipitation of nano-scale deposits of the bioactive throughout the matrix [Gurikov, 2018]. For this study, an open-porous polymer carrier was generated by PGX Technology from oat β-glucan (BG) and then loaded with CoQ10 by means of adsorptive precipitation as described and characterized elsewhere [Liu, 2018; Couto, 2018].

Helium Ion Microscopy: For imaging the nanoscale features of the various PGX-processed polymers and impregnated CoQ10-iBG complex a Helium ion microscopy (HiM) analysis was performed on a Zeiss Orion NanoFab Helium Ion Microscope (Ostalbkreis, BW, Germany). Secondary Electron (SE) images were collected at 30 kV accelerating voltage and 1.5 pA beam current. An electron flood gun was utilized to neutralize positive charges accumulated on the sample surfaces, which enables direct imaging of insulating materials.

Stability of aqueous CoQ10 dispersions: Aqueous dispersions of the hydrophobic bioactive CoQ10 were prepared by dissolving either a commercial CoQ10-γ-cyclodextrin (CoQ10-CD) complex (CAVAMAX®, containing 20% w/w of CoQ10) or the CoQ10-iBG complex loaded with 8% w/w of CoQ10 in about 250mL of reverse osmosis (RO) water aiming at a CoQ10 concentration of 0.4 mg/mL by slowly dispersing the

powder into pre-heated RO water at 40°C in beakers and mixing with a magnetic stirrer. The beakers were then covered with parafilm and left to cool to room temperature on the lab bench. The dispersions were left at room temperature under a dark box to prevent light exposure and observed up to 6 months.

Bioavailability Study: The study design and experimental protocol for the intestinal bioavailability of CoQ10 from different formulations is shown in Figure 1.

CoQ10 formulations: The bioavailability of CoQ10 was tested using four formulations: i) 3% w/w CoQ10-iBG (n=3) pilot test, ii) 8% w/w CoQ10-iBG (n=9), iii) 20% w/w CoQ10-CD product (n=6) and iv) Food grade CoQ10 in triolein (n=6). Each formulation (i-iii) was prepared by dispersing the sample in deionized distilled water heating and mixing in a water bath at 45°C for 35 min and cooling to room temperature (~23°C). Since the food grade crystalline CoQ10 is insoluble in water, it was prepared in triolein (1mL), which represents a positive control for absorption of this lipophilic nutrient. Each formulation of CoQ10 was administered intra-gastrically at a dose of ≈10 mg/kg body weight based on CoQ10 bioavailability studies in animal and rodent models [Hatanaka, 2008; Barakat, 2013].

Intestinal bioavailability: The intestinal bioavailability of CoQ10 from the CoQ10-iBG complex and standard formulations was evaluated using surgical cannulation of the stomach and intestinal mesenteric lymphatic vessel in a rodent model, which is a direct measure of the absorption of lipophilic nutrients and compounds, as previously described [Wang, 2012]. Intestinal lymph was collected into tubes containing EDTA and stored at -80°C for HPLC analyses.

HPLC Analysis of Ubiquinones: HPLC methods were established by modifying previously described methods for CoQ9 and CoQ10 [Schulz, 2006; Tarry-Adkins, 2016; Boitier, 1998; Mosca, 2002]. The phylloquinone Vitamin K was used as an internal standard and the quantitation of CoQ9 and CoQ10 was performed using commercial standards to identify and detect these ubiquinones in intestinal lymph samples. In brief, total lymph ubiquinone (CoQ9 and CoQ10) was oxidized with 1,4-benzoquinone, and extracted with 1-propanol and then analyzed by reverse-phase HPLC (Agilent Poroshell 120, 4.6x100 mm) with UV detection at 275 nm. Peak areas were analyzed, and CoQ9 and CoQ10 were quantified using vitamin K as an internal standard (1mg/200 mL sample). Validation of the HPLC protocol was based on linear calibration curves of each standard and 99-100% recovery of the standards; vitamin K, CoQ9 and CoQ10 (Thermo Fisher Scientific, DC chemicals, Sigma-Aldrich).

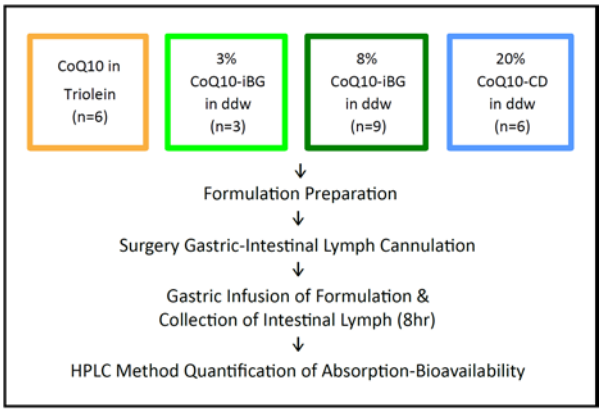

Figure 1: Study design and experimental protocol for determining the bioavailability of CoQ10 formulations.

Bioavailability and Pharmacokinetics: % Total absorption of CoQ10, CoQ10 area under the curve (CoQ10-AUC), maximum concentration (cMax) were determined as previously described [Barakat, 2013; Wang, 2012]. % Absorption was adjusted per volume of lymph and per hour of collection to reflect pharmacokinetics of lymph absorption-bioavailability [Wang, 2012; Barakat, 2013].

RESULTS

To demonstrate the capabilities of PGX Technology, several biopolymers were processed into open-porous structures, which can be impregnated with drugs or bioactives and utilized as bioactive delivery systems. Some examples are illustrated in Figure 2, showing PGX processed corn starch, pectin, sodium alginate, and an alginate-pectin exfoliated composite.

The PGX processed oat β-glucan is displayed in Figure 3(A) illustrating the open-porous structure. The BG carrier was impregnated to generate the CoQ10-iBG complex with spherical nanocrystals of CoQ10 with an average size of about 92 nm (Figure 3(B)).

The stability of CoQ10 dispersions in water at room temperature is illustrated in Figure 4 after about 18 hours (left image) and after 6 months (right image). The CoQ10-iBG complex dispersion remained stable for more than 6 months at room temperature.

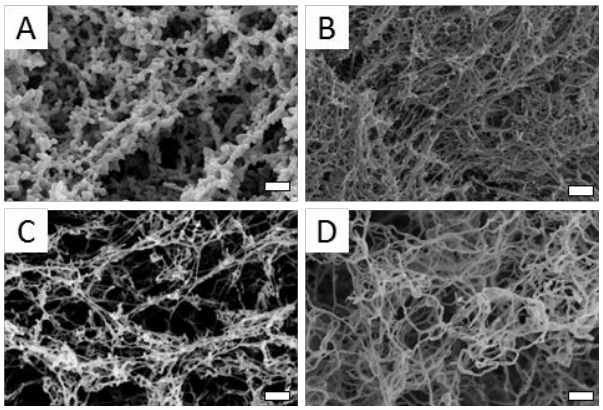

Figure 2: HiM images of (A) PGX processed corn starch, (B) pectin, (C) sodium alginate, and (D) alginate-pectin nano-composite. Scale bar length: 200 nm.

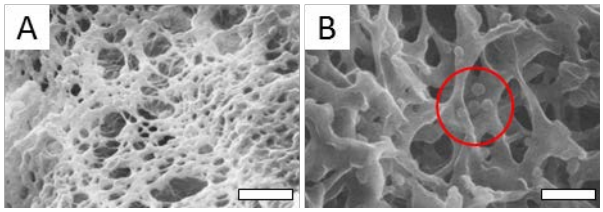

Figure 3: HiM images of (A) open-porous polymer carrier generated by PGX Technology from oat β-glucan, and (B) CoQ10-iBG complex with nanocrystals of CoQ10 inside red circle (source: [Liu 2018]). Scale bar length: 500 nm.

Figure 4: Stability of CoQ10 dispersions in water, majority of commercial CoQ10-CD (left beaker) precipitated in 18.35 hrs (left image), whereas the CoQ10-iBG complex (right beaker) was stable for more than 6 months (right image).

Bioavailability of CoQ10 formulations: The results of the bioavailability study are shown in Table 1.

Table 1: CoQ10 bioavailability results for the different formulations used in the rodent model.

	CoQ10-triolein	*3% CoQ10-iBG*	*8% CoQ10-iBG*	*20% CoQ10-CD*
% Total Abs.	2.43 ±1.01	1.71 ±0.93	4.06 ±2.12	3.27 ±2.06
c_{Max} *(mg/ml)*	53.10 ±6.23	27.54 ±7.21	63.82 ±31.04	56.97 ±24.38
CoQ10-AUC (mg/ml)	67.23 ±35.42	55.63 ±33.53	136.90 ±73.32	133.3 ±65.82

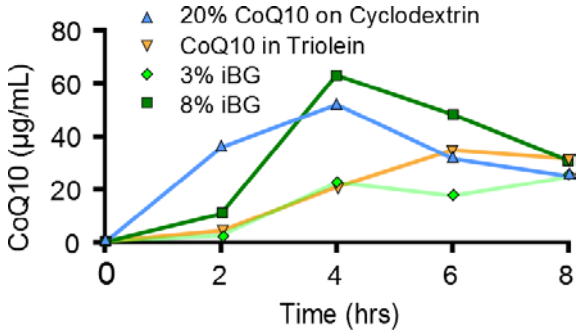

Figure 5: Absorption kinetics of CoQ10 formulations.

DISCUSSION

The CoQ10 area under curve (CoQ10-AUC) was >50% higher for both the 8% CoQ10-iBG and 20% CoQ10-CD formulations compared to the 3% CoQ10-iBG and Food CoQ10 in triolein formulations (Table 1). The data show that both BG and cyclodextrin formulations increase the absorption of the lipophilic nutrient CoQ10; however, the kinetic profile was different with the 8% CoQ10-iBG formulation having a delayed maximal absorption compared to the 20% CoQ10-CD (Figure 5). This may reflect overall faster digestion, including gastric emptying of the 20% CoQ10-CD compared to the 8% CoQ10-iBG formulation most likely due to the higher viscosity of the β-glucan. Due to the fine particles of CoQ10 deposited on the BG carrier the bioavailability could be enhanced as well, which would agree with a previous study where CoQ10 nanocrystals with 80 nm diameter had a 7.3-fold increased bioavailability compared to a coarse suspension of the bulk drug [Sun, 2012].

CONCLUSIONS

This work demonstrates the capabilities of PGX Technology to generate tailor-made and tunable bioactive carrier/delivery systems from water-soluble biopolymers. Such biopolymers can be impregnated with lipophilic bioactives utilizing $SCCO_2$ assisted adsorptive precipitation forming novel iPX formulations. Resulting iPX are water dispersible and form stable nanodispersions, which, in the case of CoQ10, were shown to be more bioavailable. Use of other polymers, polymer combinations, and cross-linked polymers can lead to improved delivery and release profiles of drugs/bioactives, which is our ongoing investigation.

ACKNOWLEDGMENT

The authors thank Audric Moses for HPLC method development and analyses.

REFERENCES

[Boitier, 1998] Boitier, E., Degoul, F., Desguerre, I., Charpentier, C., François, D., Ponsot, G., Diry, M., Rustin, P., Marsac, C., 1998, A case of mitochondrial encephalomyopathy associated with a muscle coenzyme Q10 deficiency. *J. Neuro. Sci.*, 156:41-46.

[Mosca, 2002] Littarru, G.P., Mosca, F., Fattorini, D., Bompadre, S., Battino, M., 2002, Assay of Coenzyme Q10 in Plasma by a Single Dilution Step. *Analytical Biochemistry*, 305:49-54.

[Schulz, 2006] Schulz, C., Obermüller-Jevic, U.C., Hasselwander, O., Bernhardt, J., Biesalski, H. K., 2006, Comparison of the relative bioavailability of different coenzyme Q10 formulations with a novel solubilizate (SoluTM Q10). *Int. J. Food Sci. and Nutr.*, 57:546-555.

[Hatanaka, 2008] Hatanaka, J., Kimura, Y., Lai-Fu, Z., Onoue, S., Yamada, S., 2008, Physicochemical and pharmacokinetic characterization of water-soluble CoenzymeQ10 formulations. *Int. J. Pharm.*, 363(1), 112–117.

[Seifried, 2010] Seifried, B., 2010, Physicochemical Properties and Microencapsulation Process Development for Fish Oil Using Supercritical Carbon Dioxide, Ph.D. Thesis, University of Alberta.

[Chan, 2011] Chan, H.-K., Kwok, P.C.L., 2011, Production methods for nanodrug particles using the bottom-up approach. *Adv. Drug Delivery Rev.*, 63(6), 406–416.

[Sun, 2012] Sun, J., Wang, F., Sui, Y., She, Z., Zhai, W., Wang, C., Deng, Y., 2012, Effect of particle size on solubility, dissolution rate, and oral bioavailability: evaluation using coenzyme Q10 as naked nanocrystals, *Int. J. Nanomedicine*., 2012; 7: 5733–5744.

[Tabernero, 2012] Tabernero, A., Martín del Valle, E.M., Galán, M.A., 2012, Supercritical fluids for pharmaceutical particle engineering: Methods, basic fundamentals and modelling. *Chem. Eng. Process*., 60:9-25.

[Wang, 2012] Wang, Y., Vine, D.F., 2012, The intestinal bioavailability of vaccenic acid and activation of peroxisome proliferator-activated receptor-alpha and -gamma in a rodent model of dyslipidemia and the metabolic syndrome. *Mol. Nutr. Food. Res.*, 56:1234-1246.

[Barakat, 2013] Barakat, A., Shegokar, R., Dittgen, M., Müller R. H., 2013, Coenzyme Q10 oral bioavailability: effect of formulation type. *J. Pharm. Invest.*, 43:431-451.

[Chin, 2014] Lim Chin, W. W., Parmentier, J., Widzinski, M., Tan, E. H.,Gokhale, R., 2014, A Brief Literature and Patent Review of Nanosuspensions to a Final Drug Product. *J. Pharm. Sci.*, 103(10), 2980–2999.

[Wais, 2016] Wais, U., Jackson, A. W., He, T., Zhang, H., 2016, Nanoformulation and encapsulation approaches for poorly water-soluble drug nanoparticles. *Nanoscale*, 8(4), 1746–1769.

[Temelli & Seifried, 2016] Temelli, F., Seifried, B., 2016, Supercritical fluid treatment of high molecular weight biopolymers. U.S. Patent No. 9,249, 266.

[Tarry-Adkins, 2016] Tarry-Adkins, J.L., Fernandez-Twinn, D.S., Hargreaves, I. P., Neergheen, V., Aiken, C.E., Martin-Gronert, M.S., McConnell, J.M., Ozanne, S.E. ,2016, Coenzyme Q10 prevents hepatic fibrosis, inflammation, and oxidative stress in a male rat model of poor maternal nutrition and accelerated postnatal growth. *Am. J. Clin. Nutr.*, 103(2), 579–588.

[Couto, 2018] Couto, R., Seifried, B., Yépez, B., Moquin, P., & Temelli, F. (2017). Adsorptive precipitation of co-enzyme Q10 on PGX-processed β-glucan powder. *J. of Supercrit. Fluids*, 141, 157-165.

[Göke, 2018] Göke, K., Lorenz, T., Repanas, A., Schneider, F., Steiner, D., Baumann, K., Bunjes H., Dietzel, A., Finke, J.H., Glasmacher, B., Kwade, A., 2018, Novel strategies for the formulation and processing of poorly water-soluble drugs. *Eur. J. Pharm. Biopharm.*, 126, 40–56.

[Gurikov, 2018] Gurikov, P.; Smirnova, I. Amorphization of Drugs by Adsorptive Precipitation from Supercritical Solutions: A Review. *J. Supercrit. Fluids*, 132, 105–125.

[Liu, 2018] Liu, N., Couto, R., Seifried, B., Moquin, P., Delgado, L., & Temelli, F. (2018). Characterization of oat beta-glucan and coenzyme Q10-loaded beta-glucan powders generated by the pressurized gas-expanded liquid (PGX) technology. *Food Res. Int.*, 106, 354-362.

[Temelli & Seifried, 2018] Temelli, F., Seifried, B., 2018, Supercritical fluid treatment of high molecular weight biopolymers. European Patent EP 2 553 000 B1.

[Padrela, 2018] Padrela, L., Rodrigues, M.A., Duarte, A., Dias, A. M. A., Braga, M.E.M., de Sousa, H.C., 2018, Supercritical carbon dioxide-based technologies for the production of drug nanoparticles/nanocrystals – A comprehensive review. *Adv. Drug Deliv. Rev.*, 131:22-78.

[Seifried, 2019] PGX Technology Brochure available on webpage: https://www.ceapro.com/technologies/pgx (accessed on 2019-Jun-18).

DESIGN AND PROCESSING OF SOLID DISPERSIONS IN PHARMACEUTICAL INDUSTRY

Carsten Timpe

F. Hoffmann La Roche AG, CH-4070 Basel, Switzerland

ABSTRACT

Solid dispersions have already been described over more than 50 years ago in scientific literature to improve solubility of poorly water soluble drugs. With the increasing number of new poorly soluble drug candidates discovered at early industrial stages, the knowledge about these metastable amorphous systems has significantly improved over the decades. While in the early days of solid dispersions pharmaceutical companies were rather very reluctant to invest in corresponding manufacturing technologies, nowadays a significant number of market drug products has been developed based upon this not novel drug delivery principle. The presentation will give an overview about properties of solid dispersions, industrial screening and manufacturing methods and the biopharmaceutical implications.

Keywords: Solid dispersion, amorphous, solubility, metastable, drug delivery

INTRODUCTION

With the dramatic increase in poorly soluble drug candidates (Biopharmaceutical Classes I and IV) from drug discovery organisations in industrial drug development, scientists had to look for innovative approaches to improve their aqueous and in-vivo solubilities. Beside salt formation, particle size reduction (e.g. milling, micro- or nano-nizing), formation of Cyclodextrin complexes or incorporation of poorly soluble drug candidates in microemulsion systems (SEDDS, SMEDDS), the destruction of the crystal lattice in a suitable matrix and thus formation of a metastable amorphous system or solid dispersion has in the meantime turned out to become one of the most attractive approaches in industrial drug development.

RESEARCH CONCEPT

Delivery principle

The interest in solid dispersions has started in the 1960s already and a first definition was given by Chiou and Riegelmann: " A solid dispersion is a dispersion of one or more active ingredients in an inert carrier or matrix by the melting (fusion), solvent, or the melting-solvent method [Chiou, Riegelmann, 1971]. With regards to the metastable nature of these ideally amorphous systems, the question that researchers had to solve was always the physical stability, preventing recrystallization of try at least to delay such an event until the end of the shelf-life of a marketed drug product. Such a stabilization could be a solubility, thermodynamically based concept or the formation of a solid dispersion where the dispersed molecules of the poorly soluble drug candidates are kinetically immobilized, e.g. by adjusting high glass transition temperatures for the solid dispersion using the principles described by the Gordon-Taylor equation with w1 and w2 representing the weight fractions e.g. of drug and matrix/polymer and Tg1 and Tg2 their corresponding glass transition temperatures (Tg is then the glass transition temperature of the solid dispersion).

Gordon-Taylor equation

Equation 1

$$Tg = \frac{w_1 Tg_1 + K w_2 Tg_2}{w_1 + K w_2}$$

Nowadays solid dispersions are divided into 3 different categories or generations – starting in the early daysof the 1st generation with crystalline carriers (e.g. Urea, Fructose), moving later to polymeric carrier based (2nd generation) and then more recently to those of the 3rd generation including surface active carrier types.

Screening approaches

Details about different types of amorphous systems will be discussed during the presentation and screening concepts discussed (e.g. solubility in liquids, use of Hansen solubility parameters, DSC technique, other methods). Supportive modern analytical technologies will be briefly mentioned (e.g. SEM, TEM; micro Raman technique [Karavas, Georgarakis, Docoslis, Bikiaris, 2007]., solid stage NMR

Manufacturing technologies

Over the past decades a couple of different manufacturing technologies have been applied. Generally the most prominent approaches are either based upon melting (e.g. hot melt-extrusion HME) or solvent based (e.g. spray drying, spray granulation). During the presentation further technical details and a scale-up experiment will be discussed..

Biophamaceutical aspects

An increase in aqueous solubility by forming a solid dispersion can improve drug absorption and thus the bioavailability of a poorly soluble drug significantly. Nevertheless it needs to be considered that vertain drugs have a high tendency to crush out or precipitate once the solid dispersion reaches the gastrointestinal tract. Therefore formulation scientists need to test solid dispersion prototype formulations also with regards to their precipitation robustness. Addition of surfactant-type carriers might improve the robustness significantly. Also such aspects have to be routinely screened nowadays,

RESULTS

The examples provided during the presentation will demonstrate how to develop solid dispersions by screening the right formulations and selecting the right manufacturing technology at an industrial scale including scaling-up and

DISCUSSION

The presentation explains the evolution of solid dispersion formuations over the last 50 years and how it is possible nowadays to develop stable and better up-scalable solid dispersions than ever before.

CONCLUSIONS

Solid dispersions are an attractive modern approach to deliver poorly soluble (“brickstone”) drugs successfully in an industrial environment. This has led to the market introduction of multiple products helping to significantly improve patients` lives.

ACKNOWLEDGMENT

I would like to thank all the great scientists from which I learned a lot about solid dispersions over the years at Lilly, Novartis and Roche

NOMENCLATURE

SEDDS	self-emulsifying drug delivery system
SMEDDS	self-microemulsifying drug delivery system
SEM	scanning electron microscopy
TEM	transmission electron microscopy
Tg	glass transition temperature
W1, w2	weight fraction

REFERENCES

[Chiou, Riegelmann, 1971] W.L. Chiou and S. Riegelman, J. Pharm. Sci., 1971, 60, 1281-1302.

[Karavas, Georgarakis, Docoslis, Bikiaris, 2007]. Evangelos Karavas, Manolis Georgarakis, Aristides Docoslis, Dimitrios Bikiaris, Int. J. Pharmaceutics 340 (2007) 76–83